NASA CR-
141892

A GAS FLOW INDICATOR FOR PORTABLE LIFE SUPPORT SYSTEMS

by

R. L. Bass, III

E. C. Schroeder

FINAL TECHNICAL REPORT
Contract No. NAS9-13575
SwRI Project No. 02-3713

Prepared for

National Aeronautics and Space Administration
Lyndon B. Johnson Space Center
Houston, Texas 77058

May 1975

SOUTHWEST RESEARCH INSTITUTE
SAN ANTONIO   CORPUS CHRISTI   HOUSTON

A GAS FLOW INDICATOR FOR PORTABLE LIFE SUPPORT SYSTEMS

by
R. L. Bass, III
E. C. Schroeder

FINAL TECHNICAL REPORT
Contract No. NAS9-13575
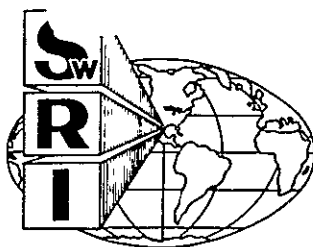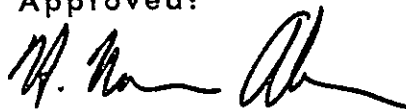SwRI Project No. 02-3713

Prepared for

National Aeronautics and Space Administration
Lyndon B. Johnson Space Center
Houston, Texas 77058

May 1975

Approved:

H. Norman Abramson
Vice President, Engineering Sciences

ABSTRACT

A three-part program has been conducted to develop a Gas Flow Indicator (GFI) to monitor ventilation flow in a portable life support system. The first program phase identified concepts which could potentially meet the GFI requirements. In the second phase, a working breadboard GFI, based on the concept of a pressure sensing diaphragm-aneroid assembly connected to a venturi, was constructed and tested. Extensive testing of the breadboard GFI indicated that the design would meet all NASA requirements including eliminating problems experienced with the ventilation flow sensor used in the Apollo program. In the third program phase, an optimized GFI was designed by utilizing test data obtained on the breadboard unit. A prototype unit was constructed using prototype materials and fabrication techniques with several major components manufactured by outside vendors. Performance tests indicated that the prototype GFI met or exceeded all requirements.

TABLE OF CONTENTS

TABLE OF CONTENTS (Contd.)

LIST OF FIGURES

LIST OF FIGURES (Contd.)

LIST OF TABLES

I. INTRODUCTION

This report describes all work performed by Southwest Research Institute in the development of a gas flow indicator (GFI) for portable life support systems (PLSS). The work was conducted under Contract No. NAS9-13575, for the Lyndon B. Johnson Space Center of the National Aeronautics and Space Administration, with Mr. Steve Martin serving as the NASA Technical Monitor.

The objectives of this project were to perform the engineering design, development, and testing of a gas flow indicator (GFI). The GFI is to be used in a portable life support system (PLSS) during extravehicular activities (EVA) associated with future space programs. The GFI will monitor the ventilation loop flow to an astronaut's space suit and actuate an autible warning circuit when the flow drops below a critical level. A summary of the desired features and specifications for the GFI are given below.

GFI Specification Summary

Critical Flow Rate	5 ± 0.3 actual cubic ft per minute (acfm) (142 ± 9.5 actual liters per minute (alm))
Alarm Actuation Flow Rate	5.3 to 4.7 acfm (150 to 133 alm), 0.25 sec max. actuation time
Alarm Deactuation Flow Rate	5.3 acfm (150 alm), 0.50 sec max. deactuation time
Normal Operating Pressure	3.8 ± 0.15 psia (0.27 ± 0.01 kgf/cm^2)
Operating Pressure Range	3.5 to 15 psia (0.25 to 1.05 kgf/cm^2)
Gas Compositions	Pure O_2 Air - N_2/O_2 mixture CO_2 Content - 0 to 15 mm of mercury Moisture Content - 0 to 100% relative humidity
Temperature	35 to 130°F (Normal Range 50 to 80°F) (2 to 54°C (Normal Range 10 to 27°C))

Electrical Requirements	Supply Voltage - 15.5 to 20.5 volts d.c. Max. Current - 50 milliamps
	   - open 100 Ω min. impedance
	Switch
	      - closed 100 Ω max. impedance @ 10 ma

Size   0.75" (1.91 cm) inlet and outlet hose
                              connections

Pressure Drop   0.30" (0.76 cm) H_2O maximum at

$w = 8.50 \pm 0.1$ pph (O_2)
$(3.9 \pm 0.05$ kgf/hr (O_2))

$P = 3.8 \pm 0.1$ psia
$(0.27 \pm 0.007$ kgf/cm^2)

$T = 70 \pm 2°F$ $(21 \pm 1°C)$

General GFI Requirements

- The meter must operate over a wide range of pressures, temperatures, and with different gas constituents.

- Pressure drop through the meter must be maintained at a minimum.

- The meter must be capable of repeated use with no inflight maintenance and a minimum of ground maintenance and check-out between flights.

- The meter should present no potential safety hazards to the life support system.

The GFI development program was conducted in three phases which consisted of:

(1) Concept studies

(2) Breadboard development

(3) Prototype development.

The results of the work in each of these phases are discussed in subsequent chapters of this report.

2

II. CONCEPT STUDIES

II. 1   Background

Several flow metering concepts were evaluated to determine the best methods to meet the GFI requirements. Prior to evaluating the concepts the most important aspects of selecting a GFI concept were discussed with the NASA Technical Monitor. These discussions revealed that one of the main problems with the GFI's used on the Apollo Program was the repeated maintenance and recalibrations required because of condensed moisture and other particulate matter present in the gas flow. In view of this, a major emphasis in the concept studies and subsequent GFI development was directed at providing a GFI with operational characteristics insensitive to moisture and other flow contaminants.

The wide range of flow temperature, pressure, and gas composition specifications and their effects on instrument operation were also discussed. For example, three possible GFI operational characteristics are:

(GFI - 1)   an instrument with output inherently a direct function of flow rate and independent of gas temperature, pressure and composition,

(GFI - 2)   an instrument with response versus flow rate affected by temperature, pressure and gas composition but compensated either electronically or mechanically so final output is dependent only on flow rate, and

(GFI - 3)   an instrument with response versus flow rate dependent on gas pressure, temperature and composition and with final output not compensated for these variables.

GFI-1 would be the most attractive; however, if the variation in output with flow properties of GFI-3 could be established and a reliable and repeatable calibration obtained for each condition then this type of instrument would be acceptable if it had other desirable features such as low maintenance and power requirements.

Other aspects of GFI operation were also established. The normal operating flow rate and pressure of the GFI were initially set at $Q = 6$ acfm (170 alm) and 8 psia (0.56 kgf/cm^2). Early in the program the normal operating pressure was changed to 3.8 psia (0.27 kgf/cm^2) but this did not affect the concept evaluations. It was established that the maximum flow

rate is 7 acfm (198 alm). Also, during checkout the GFI operates at 23 psia (1.62 kgf/cm^2) at a flow rate of 4.5 acfm (127 alm). In addition, normal steady-state operating temperature will be between 50 and 80°F (10 to 27°C).

II.2   Concepts Evaluated

Based on the background information and the GFI specifications, the following GFI concepts were selected for detailed evaluations.

1. Heated Tracer GFI

2. Vortex Shedding Meter (VSM) GFI

3. Turbine Meter GFI

4. Differential Pressure GFI
   a. Pitot Static
   b. Orifice
   c. Venturi

A description of the operational characteristics of these concepts and the details of how they can be implemented to meet the GFI requirements are given in Appendices A through D. The detailed engineering calculations presented in these Appendices were used as the basis for evaluating each concept.

II.3   Evaluation Criteria

The GFI concepts were evaluated with respect to the following criteria:

Evaluation Category	Weighting Factor
Operational characteristics	3
Electronic complexity	2
Mechanical complexity	1
Reliability	3
Power requirements	1
Expected life	2
Maintenance	2
Size (volume and envelope)	1
Weight	2
Cost	1
Development risk	3
Development lead time	1
Impact on PLSS	1

For each of these categories, the concept was rated on scale from zero to 10, with 10 being the best rating. In addition, weighting factors were applied to each of the categories. These weighting factors were set by the NASA Technical Monitor. Weighting factors of 3 and 1 are representative of the most and least important categories, respectively. The final value in a category is given by the rating per category times the weighting factor.

For some of the categories, the evaluations could be based on engineering calculations while for others a subjective evaluation had to be applied. For example, weight, size and power requirements could be accurately estimated while questions of reliability, development risk, and development lead time required a more subjective evaluation.

II.4   Concept Evaluation and Ranking

The results of the GFI concept evaluations are summarized in Table I. An attempt was made to keep the evaluations as unbiased as possible. This was accomplished by having four project engineers rate each concept independently. The numbers presented in Table I represent the composite averages from the four individual ratings. Table II summarizes the concept comparisons with respect to estimated size, weight, power, and pressure drop. Additional comments about each of the concepts in each evaluation category are given below.

Heated Tracer GFI

- Operational Characteristics -- Since the heated tracer GFI is inherently independent of environmental factors, it gets a high rating in the operational characteristics category. Its final rating in this category is 8.

- Electronic Complexity -- The heated tracer GFI is very complex electronically because of the electrical requirements to produce and detect the heated tracer. The heated tracer GFI get a rating of 2 for electronic complexity.

- Mechanical Complexity -- The heated tracer GFI is mechanically simple since it has no moving parts and is essentially a flow tube. Its mechanical complexity rating is 8.

- Reliability -- The extremely delicate source and detector probes make this technique subject to poor reliability, and its rating in this category is 2.

5

TABLE I. GFI CONCEPT EVALUATION SUMMARY

	Evaluation Criteria													
Weighting Factor	3	2	1	3	1	2	2	1	2	1	3	1	1	
Concept	Good Operational Characteristics	Low Electronic Complexity	Low Mechanical Complexity	High Reliability	Low Power Requirements	Long Expected Life	Low Maintenance	Small Size (Volume & Envelope)	Light Weight	Low Cost	Low Development Risk	Short Development Lead Time	Minimal Impact on PLSS	TOTALS
Heated Tracer	24	4	8	6	3	6	8	5	14	5	9	3	3	98
V S M	24	10	8	15	5	10	10	7	16	6	15	5	4	135
Turbine	21	12	5	21	6	8	8	8	18	4	24	8	6	149
Uncompensated Venturi	6	18	7	24	9	16	16	7	18	8	24	8	8	169
Mechanically Comp. Venturi	18	18	3	21	9	14	12	7	16	5	18	5	8	154
Electrically Comp. Venturi	15	8	6	15	4	10	10	4	10	5	15	6	5	113
Total Pressure	9	8	6	9	4	10	10	4	10	5	15	6	5	101
Orifice	3	8	6	6	4	10	10	4	10	5	9	3	5	83

Maximum Rating/Category = 10 points
Minimum Rating/Category = 0 points
Final Value/Category = Rating/Category x Weighting Factor

TABLE II.

GFI CONCEPT COMPARISONS -
ESTIMATED SIZE, WEIGHT, POWER AND PRESSURE DROP

Concept	Weight (kgf)	Volume (cm^3)	Envelope (cm)	Power (watts)	Pressure Drop (cm H$_2$O)
Heated Tracer	0.454	500	23 x 9.0 x 5.5	1.5 to 2.0	0.68
VSM	0.341	325	15 x 6.5 x 5	0.5 to 1.0	0.08
Turbine Meter	0.227	250	10 x 10 x 7.5	0.5	0.64
Venturi . Uncompensated	0.227	400	19 x 12.5 x 5	~ 0	0.58
. Mech. Compensated	0.341	325	19 x 12.5 x 5	~ 0	0.58
. Elect. Compensated	0.636	650	20.5 x 10 x 7.5	1.0	0.58
Total Pressure	0.636	650	12.5 x 10 x 7.5	1.0	0.43
Orifice	0.636	650	12.5 x 10 x 7.5	1.0	0.64
Apollo GFI	0.454	225	14 x 7.5 x 4.0	1.0	0.64

7

- Power Requirements -- The complex electronic circuitry requires larger power than other methods, and the final rating in this category is 3.

- Expected Life -- The expected life of the heated tracer GFI is low because of the delicate probes and complex electronics, and its rating in this category is 3.

- Maintenance -- Maintenance on the heated tracer GFI will probably entail periodic replacement of source or detector wires and electronic components. Its final maintenance rating is 4.

- Size -- The volume of the heated tracer GFI package is relatively small; however, its unusual length makes it less attractive, and its final rating is 5.

- Weight -- The estimated weight of the heated tracer GFI is 0.454 kgf, and its rating in this category is 7.

- Cost -- The mechanical simplicity of this technique results in a relatively low production cost compared to the other methods, and its final rating in this category is 5.

- Development Risks -- Uncertainties in the electronics, probe life and reliability of this technique make it a high development risk, and its overall rating in this category is 3.

- Development Lead Time -- The same factors affecting development risk imply that this technique must have a long development lead time, and its final rating in this category is 3.

- Impact on PLSS -- The high temperature source wire of the heated tracer GFI could pose a safety problem in the oxygen environment. In addition, its power requirements and delicate probes could also create an impact on the PLSS. Its final rating in this category is 3.

In summary, the heated tracer GFI is an attractive method since it is inherently independent of atmospheric conditions, and the possibility exists for obtaining an instrument with one output characteristic over all

8

operating specifications. However, it appears doubtful that the extremely small detector and source wires could be expected to perform reliably without maintenance in a flow stream containing particulates and moisture. In addition, its high power requirements and the need for additional development risks and lead time make this technique less attractive. It ranks 7th out of the eight concepts studied.

Turbine Meter GFI

The turbine meter was evaluated, in part, on reference material (Reference B-3) supplied by Quantum Dynamics, since they produce a turbine meter which has the potential of meeting the GFI requirements.

- Operational Characteristics -- The turbine meter is basically independent of gas properties in the specified operating range. Environmental factors could affect bearing drag characteristics. Rating is 7.

- Electronic Complexity -- The turbine meter system is intermediate in electronic complexity between a mechanically actuated contact switch and an electronically compensating system. Rating is 6.

- Mechanical Complexity -- The turbine meter is not complex with regard to the total number of parts required. However, the necessary mechanical parts do require precision construction. Rating is 5.

- Reliability -- The turbine meter should be quite reliable as long as large solids are kept away from the turbine wheel. Based on this assumption and the fact that the electronics are relatively simple, the rating is 7.

- Power Requirement -- Power requirements are low with respect to the heated tracer, VSM or electronically compensated venturi but high compared to the mechanical switch in the uncompensated venturi. Rating is 6.

- Expected Life -- The expected life of the turbine meter appears adequate for any anticipated mission cycle but is limited by the turbine shaft bearings. Rating is 4.

- Maintenance -- Maintenance would consist of replacement of the turbine shaft and bearings after approximately 500 to 600 hours of operation (dry bearings). Bearing

- replacement could be a precision operation, but normal cleaning and recalibration would be relatively simple. Rating is 4.

- Size -- The turbine meter would be slightly smaller, mechanically and electronically, than other concepts. Rating is 8.

- Weight -- The turbine meter would be slightly lighter mechanically and electronically than other concepts. Rating is 9.

- Cost -- The mechanical precision required in the construction and assembly of the turbine meter would result in a relatively high production cost. Rating is 4.

- Development Risks -- Development risk is low since an existing meter is available which can be used with moderate redesign, and the required electronics is relatively simple. Rating is 8.

- Development Lead Time -- Lead time would be low since the GFI would be an adaptation of existing technology. Rating is 8.

- Impact on PLSS -- Impact would be moderate with regard to power consumption and pressure drop. Safety, as distinct from reliability, would be high. Rating is 6.

In summary, the turbine meter is an attractive concept since currently available meters appear to meet most of the GFI specifications. The primary drawback to the turbine meter is a potential calibration change due to bearing wear; however, this will probably not be a problem during a mission cycle. It ranks 3rd out of the eight concepts.

Vortex Shedding Meter (VSM) GFI

- Operational Characteristics - The VSM is insensitive to temperature, pressure, and absolute viscosity over a wide operating range. It is sensitive to geometrical changes which could arise from corrosion, water or film build up. Its final rating in this category is 8.

10

- Electronic Complexity - The most complicated part of the VSM will be an adequate electronic circuit to sense high frequency vortex shedding. Therefore the rating in this category is 5.

- Mechanical Complexity - The VSM is very simple mechanically. It consists of a cylinder mounted on the diameter of a tube. This cylinder may be removed for periodic inspection. It may be necessary to install some upstream straightening vanes. The rating is 8.

- Reliability - Assuming the sensor is operated within its specified environment, the VSM's reliability is directly a function of the electronics reliability. The rating is 5.

- Power Requirements - The present design calls for a thermistor operated in a self-heated mode. Its dissipation constant is typically .2 mW/$^{\circ}$C. Power required for the sensor is small, therefore sufficient power is available for the signal conditioning and logic circuits. The rating is 5.

- Expected Life - The VSM is a rugged device mechanically, however, the sensors and electronics could reduce its expected life. The rating is 5.

- Maintenance - The thermistor should be checked on a periodic basis. It may be necessary to replace the sensor. The rating is 5.

- Size - The VSM could be fabricated such that the volume required would be approximately the same as the existing meter. The rating is 7.

- Weight - Estimated weight is 0.341 kgf. The rating is 8.

- Cost - Fabrication of mechanical parts is simple, but the electronic part is somewhat complicated. Rating is 6.

- Development Risk - Vortex shedding is a well-known phenomena, and the meter can be made to function rather easily. The most difficult problem to solve is the development of a sensing technique. The rating is 5.

11

- Development Lead Time - Most of the elements required for the successful development of the VSM are within the state-of-the-art. The major part of the lead time will be the optimization of the sensing technique. The rating is 5.

- Impact on PLSS - The major safety problem is that of exposing a potential spark in an oxygen environment; however, if the flow surfaces are very clean, rapid oxidation is unlikely. The circuitry required will be more complicated than that of the present system and could require more power. The rating is 4.

In summary, the VSM is an attractive concept since its output characteristics are essentially independent of P, T and gas composition. Its primary drawback is electronic complexity, power and development risk and lead time. It ranks 4th out of the eight concepts.

Differential Pressure GFI

The differential pressure method can be implemented to provide five different concepts for the GFI application. These five concepts include (1) an uncompensated venturi, (2) an electrically compensated venturi, (3) a mechanically compensated venturi, (4) a total pressure probe, and (5) a flow orifice. Since the differential pressure of a venturi, orifice, or total pressure probe is affected by temperature, static pressure, and gas composition, these techniques must be compensated if an output independent of these flow parameters is required. The five differential pressure concepts represent various options of compensated or uncompensated techniques.

(1) Uncompensated Venturi GFI

- Operational Characteristics -- The uncompensated venturi is extremely sensitive to pressure variations; and temperature variations can also affect the GFI operation. If the operating environmental range is within the design tolerances, then the instrument will function properly; otherwise, a separate calibration is required. Its operational characteristics are therefore rated 2.

- Electronic Complexity -- There are no electronics required other than a direct circuit to the alarm which is activated by a pressure switch. Its rating is 9 for this category.

12

- Mechanical Complexity -- The only active mechanical component is the differential pressure switch. Hence, it is rated 7 in mechanical complexity.

- Reliability -- In the environmental range for which it is designed its improvement over the Apollo GFI indicates it can be quite reliable. Its rating in reliability is 8.

- Power Requirements -- The power required to operate this concept is only that needed to actuate the alarm, and it is rated 9

- Expected Life -- The expected life of the uncompensated venturi should be relatively long. The only component which may require replacement is the switch contact points. The rating in this category is 8.

- Maintenance -- Some maintenance will probably be required over a long period of time to calibrate the pressure switch. This should be relatively minor, and it can be rated 8 in maintenance.

- Size -- The diaphram of the pressure switch can be of a small design, therfore the volume occupied (400 cm^3) by the uncompensated sensor is relatively small. Hence, it is rated 7.

- Weight -- The uncompensated venturi meter will have a very small weight, consisting totally of actual venturi weight plus the pressure switch weight. The total weight will be approximately 0.227 kgf; the unit has a rating of 9.

- Cost -- The uncompensated venturi will be relatively inexpensive since no electronic parts are necessary. The only expensive item is the fabrication of the venturi and pressure switch; the rating in cost is 8.

- Development Risks -- Due to the relative simplicity of this method, the development risks are minimal. The rating in this category is 8.

- Development Lead Time -- The time required to develop this GFI concept will be relatively short. Hence, the rating is 8.

13

- <u>Impact on PLSS</u> -- The power requirements are nil, therefore no demands will be made on the PLSS in this area. Also, there is no disturbance of the gas composition or temperature due to the venturi. Impact on PLSS is minor and the rating in this category is <u>8</u>.

In summary, the concept is extremely simple; however, it is very sensitive to environmental changes and therefore might prove undesirable, especially should the environmental conditions exceed the design limits. It ranks first out of the eight concepts.

(2) <u>Electrically Compensated Venturi</u>

- <u>Operational Characteristics</u> -- Due to the venturi's sensitivity to environmental conditions (pressure and temperature), its operational characteristics are not as ideal as an instrument which does not require compensation for these variations. Hence, its final rating in this category is <u>5</u> for an electronically compensated instrument.

- <u>Electronic Complexity</u> -- The compensated venturi is considerably more complex than an uncompensated model or a mechanically compensated version. The electronics involved are less complex than required of a heated tracer GFI. It is rated 4 in this category.

- <u>Mechanical Complexity</u> -- The electronically compensated venturi is mechanically simple since it has no moving parts. The only mechanical problems that might develop are related to the pressure transducers used to sense the differential pressure. Hence, the GFI is rated 6 in this category.

- <u>Reliability</u> -- With proper design, the basic operation should be reliable; however, due to possible drift in the pressure transducer signals, the reliability is decreased. It has been rated <u>5</u> in this category.

- <u>Power Requirements</u> -- The total power required to drive the transducers and signal conditioning equipment is very near or may be above the limits set by the specifications. Hence, this unit must be rated <u>4</u> in this category.

14

- Expected Life -- The expected life of the electronically compensated venturi is questionable due to the pressure transducing equipment. It is believed, however, that these components are relatively durable and this GFI concept can be rated 5 in this category.

- Maintenance. -- The pressure transducers may require considerable recalibrations and periodic check outs or possible replacement. The same applies to the signal conditioning circuitry. Hence, this concept is rated 5 for maintenance.

- Size -- The volume of the electronically compensated venturi is relatively large due to the differential pressure transducer volume and the electronic package. This unit is rated 4.

- Weight -- The estimated weight of the electronically compensated venturi is 0.636 kgf, and it is rated 5 in this category.

- Cost -- The electronics and the detailed machining of the interior will make the concept relatively expensive to produce. It is therefore rated 5 in this category.

- Development Risks -- Because the pressure transducing instrumentation required is commercially available, the biggest risk involves the development of the signal conditioning circuit. The overall rating in this area is 5.

- Development Lead Time -- The development lead time for this concept will be relatively short since the electronics required is already commercailly available. Hence, the development lead time rating is 6.

- Impact on PLSS -- It is conceivable that the power requirements needed for this instrument could cause changes in PLSS design; thus it is rated 5.

In summary, this concept rates high in mechanical complexity, and development lead time. Due to the small differential pressures which must be sensed, the differential pressure transducer required must have a large diaphragm and hence higher volume and weight. The electronic complexity is moderate; the power requirements are borderline. The electrically compensated venturi is ranked 5th out of eight concepts.

15

(3) Mechanically Compensated Venturi

• Operational Characteristics -- The operational charac-
teristics of a mechanically compensated venturi are
similar to the electronically compensated venturi.
However, since the mechanical compensation technique
makes this unit a totally mechanical system, the opera-
tional characteristics should be rated above that of an
electronically compensated model. The final rating in
this category is 6.

• Electronic Complexity -- The only electronics required
is the circuit to the alarm which is activated when the
switch is closed. The rating in this category is 9.

• Mechanical Complexity -- This concept is considerably
complex mechanically and will require detailed design
of the flexible components. Its final rating in this
category is 3.

• Reliability -- Once a complete and working GFI of this
type has been developed, it should prove very reliable
due to the absence of complex electronics. However, it
must be kept relatively clean to insure that there are no
malfunctions due to friction created at any of the pivot
points. Its final rating is 7.

• Power Requirements -- The power requirements are
minimal due to the absence of electronics. The final
rating in this category is 9.

• Expected Life -- The expected life of this concept should
be relatively long. The final rating is 7.

• Maintenance -- Due to the mechanical complexity of
this concept, routine maintenance may be required to
clean the instrument and inspect all the seals. The
rating in this category is 6.

• Size -- The volume of the mechanically compensated
venturi GFI is ~ 325 cm^3. This GFI will fit in an
envelope of 19 X 12.5 X 5 cm. The rating in this cate-
gory is 7.

- Weight -- The weight of the mechanically compensated venturi GFI will be approximately 0.341 kgf, assuming the material to be aluminum. The rating is 8.

- Cost -- The mechanically compensated venturi will be fabricated from relatively inexpensive parts. It will, however, cost approximately the same as the electronically compensated venturi. Its rating is 5.

- Development Risks -- This concept represents a novel system which is a somewhat greater risk than electronic compensation. The final rating in this category is 6.

- Development Lead Time -- The time required to accomplish the detailed mechanical design will also exceed the time and effort required for the electronically compensated model. The rating in this category is 5.

- Impact on PLSS -- This concept should have relatively little effect on the PLSS. Its rating in this category is 8.

In summary, this concept along with the uncompensated venturi appears to be the most desirable of the three venturi methods. Electronic complexity and power requirements are nonexistent, and the weight and volume are less than the electronic unit. Since considerable detailed design work will be required in advance, the development lead time and risk are somewhat higher than the uncompensated and electronically compensated venturi. It ranks second out of the eight concepts.

(4) Total Pressure Probe, and

(5) Orifice Meter GFI

The total pressure concept and the orifice meter concept operate on the same principle as the electronically compensated venturi meter. Therefore, except for the categories of operational characteristics and reliability, the electronically compensated orifice and total pressure meter rate the same as the electronically compensated venturi meter. In addition, due to the large variation in orifice discharge coefficient, the orifice meter is rated lower in development risk and lead times. The orifice and total pressure meters are rated in these categories below:

Total Pressure

Operational Characteristics -- Due to the flow interference created by the total head probe in the small diameter line, the operational characteristics of this system cannot

17

be rated high. Also, the sensitivity to environmental conditions is quite pronounced; hence its rating is 3.

- Reliability -- This instrument cannot be considered too reliable due to the problems described above in the operational characteristics. Its final rating in this category is 3.

Orifice Meter

- Operational Characteristics -- The extremely large variation of the discharge coefficient with Reynolds number makes any type of compensation scheme difficult at best. In general, this makes the concept totally unacceptable. Hence, its rating in this category is 1.

- Reliability -- The reasons explained above for the poor operational characteristics make this an unreliable concept. Hence, it is rated 2 in this category.

- Development Risks -- Are also rated a low 3 for the same reasons

- Development Lead Time -- Is also rated 3 due to the problems with discharge coefficent.

In summary, the total pressure and flow orifice methods are less attractive than the venturi concepts, and they rank 6th and 8th, respectively.

II. 5 Concept Selection

The concept evaluations indicated that the uncompensated and mechanically compensated venturi (ranked 1 and 2) were the most promising GFI concepts. Since an existing turbine meter (ranked 3) appeared to meet most of the GFI specifications, the turbine meter was also considered as an alternate concept. It was recommended that a breadboard mechanically compensated venturi GFI (MCV-GFI) be designed and tested. In the event that the mechanical compensator did not perform to GFI requirements, the breadboard unit could be modified to produce an uncompensated venturi GFI with minimum effort. It was also recommended that concurrent with the breadboard design of the MCV-GFI, the turbine meter be performance-tested and, based on the results, either the turbine meter or the MCV be developed into a working breadboard GFI.

18

The performance test with turbine meter are discussed in Appendix E. The results of these tests revealed that the turbine meter was prone to operational failures resulting from particulates lodging in the rotor. Also, the power required to convert the unit to the GFI application exceeded the specified maximum of 1.0 watt. Therefore, all breadboard efforts were concentrated on the mechanically compensated venturi concept.

III. BREADBOARD DEVELOPMENT

III. 1 Mechanically Compensated Venturi (MCV) Operational Characteristics

The MCV-GFI concept is based on using a pressure sensing diaphragm-aneroid assembly connected to a venturi tube (Figure 1). The pressure differential (P_1-P_2) acts on the diaphragm to make or break the switch contacts located inside the evacuated bellows. By proper sizing of the diaphragm and bellows areas, a unit can be designed to break the switch contacts independent of flow static pressure (pressure compensation). Other variations in flow parameters (temperature and gas composition) result in negligible errors for the ranges given in the GFI specifications. Bi-metallic temperature compensating strips can also be incorporated, however, for mechanical temperature compensation if required.

A force balance on the mechanical compensator (Figure 2) yields

$$(P_1-P_2) A_D = (P_2-P_i) A_B + K_B X + K_p X_p \qquad (1)$$

For an evacuated bellows $(P_i = 0)$ at the alarm point $(x = 0)$

$$\frac{\Delta P}{P_2} = \frac{P_1-P_2}{P_2} = \frac{A_B}{A_D} + \frac{K_p X_p}{P_2 A_D} \qquad\qquad (2)$$

The relation between flow rate, Q, and pressure drop, ΔP, for the venturi is given by

$$Q = \frac{A_2}{\sqrt{1 - (A_2/A_1)^2}} \sqrt{\frac{2g\, RT\, (P_1-P_2)}{P_2}} \qquad (3)$$

Solving for $\Delta P/P_2$ yields

$$\frac{\Delta P}{P_2} = \frac{Q^2}{C^2} \frac{\left(1 - (A_2/A_1)^2\right)}{2A_2\, g\, RT} = \frac{\overline{K}Q^2}{C^2} \qquad (4)$$

Equation (4) indicates that at a given flow rate the ratio of $\Delta P/P_2$ remains constant as long as no changes in temperature, gas composition or venturi discharge coefficient, C, occur. This implies that at the alarm Q, the ratio of $\Delta P/P_2$ is a constant regardless of the static pressure.

20

MOUNTED PARALLEL TO VENTURI
AXIS ON FINAL DESIGN

DIAPHRAGM

SUPPORT PLATE

PRESSURE SENSING BELLOWS
(EVACUATED)

ELECTRICAL
LEADS

ELECTRICAL CONTACT AND AXIAL
GUIDE MOUNTED INSIDE BELLOWS

P_1

P_2

d_1

d_2
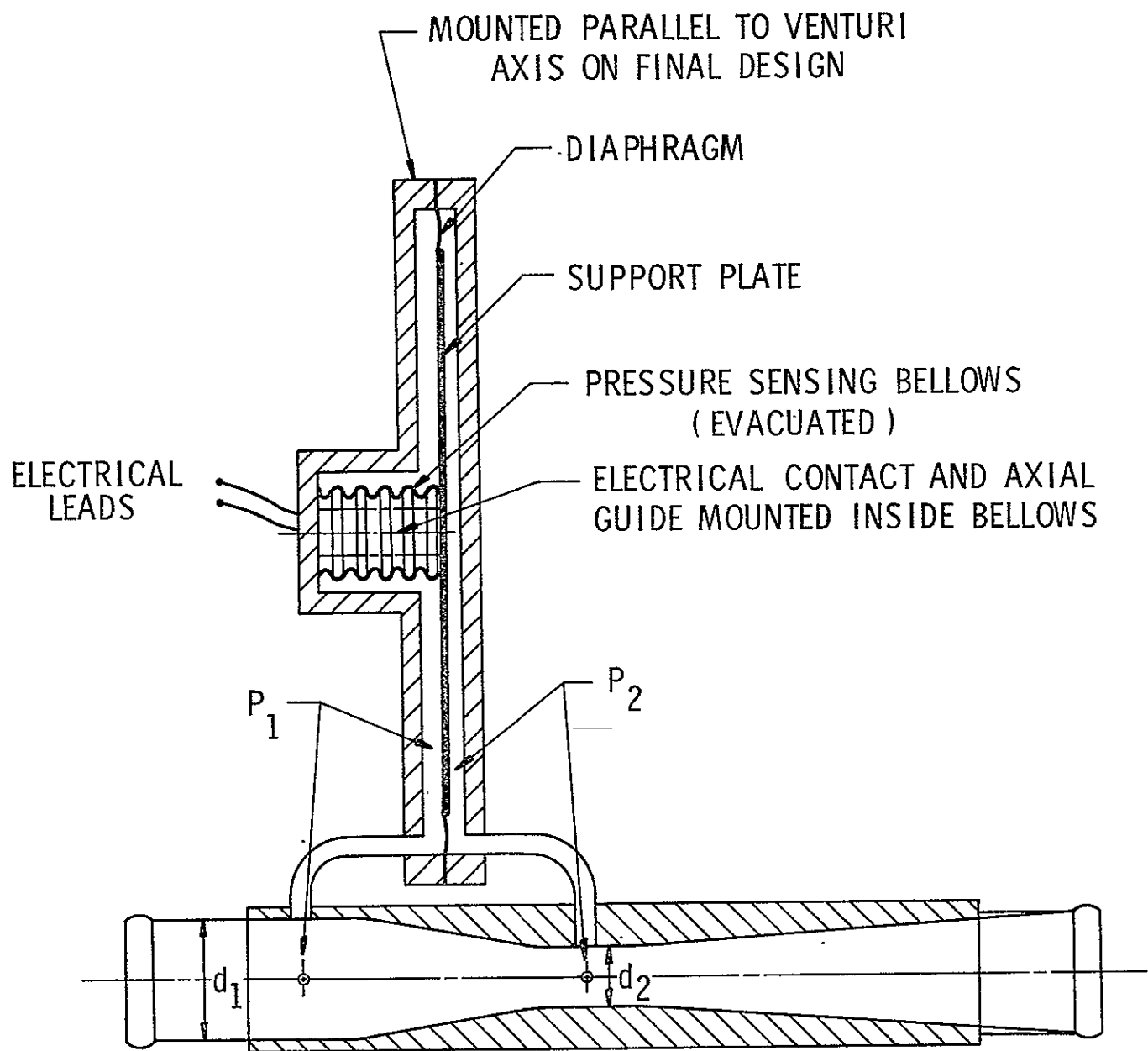
Figure 1. Mechanically Compensated Venturi Schematic

A_D − Diaphragm Area
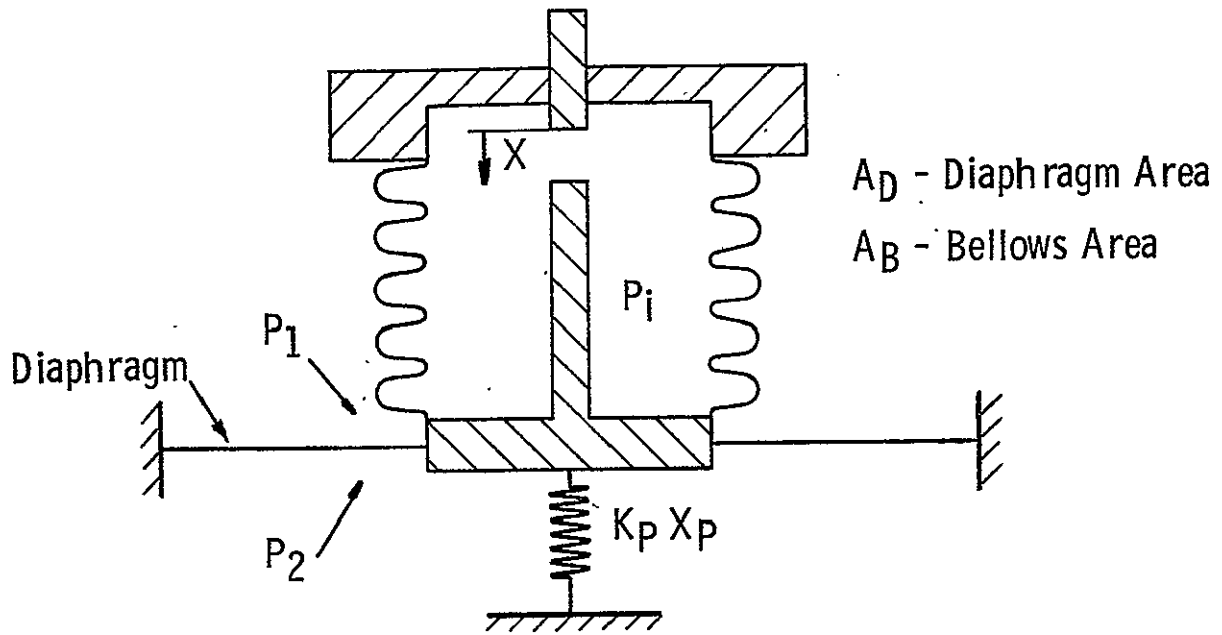
A_B − Bellows Area

Diaphragm Force	$(P_1 - P_2)\, A_D$	↓
Bellows Vacuum	$(P_2 - P_i)\, A_B$	↑
Bellows Elasticity	$K_B X$	↑
Preload	$K_P X_P$	↑ ↓

Figure 2. Mechanical Compensator Force Balance

Substituting Equation (4) into Equation (2), yields

$$Q^2 = \frac{C^2}{\overline{K}} \left[\frac{A_B}{A_D} + \frac{K_p X_p}{P_2 A_D} \right] \tag{5}$$

which represents the compensator design equation at the alarm flow rate.

III. 2   Breadboard MCV Design

III. 2. 1   Initial Design Considerations

The MCV Breadboard was initially designed with the assumption that no preload adjustment spring would be used and that the bellows would be assembled so the electrical contacts are just touching when the bellows is at its free length. At this condition a force balance on the bellows is given by

$$P_2 A_B = (P_1 - P_2) A_D \tag{6}$$

where A_D and A_B are the effective diaphragm and bellows areas, respectively. Therefore, the diaphragm area is

$$A_D = A_B \frac{P_2}{(P_1 - P_2)} \tag{7}$$

When the flow rate increases above the alarm value, $(P_1 - P_2)$ increases, and the bellows expands to separate the contacts. At flow rates below the alarm rate, $(P_1 - P_2)$ decreases with the net bellows force maintaining the electrical contact. For no preload (from Equation (5)),

$$Q^2 = \frac{C^2}{\overline{K}} \left[\frac{A_B}{A_D} \right] \tag{8}$$

Errors due to variations in T and R for the anticipated operating temperature range $(10 \leq T \leq 27^\circ C)$ and for changing from O_2 to air were determined. If the GFI is designed to operate in O_2 at $22^\circ C$, then the actual alarm rate will be

$$\frac{Q_a}{Q_d} = \sqrt{\frac{T_a}{T_d}} \tag{9}$$

or $0.979 \leq Q_a \leq 1.007\, Q_d$ for $10 \leq T \leq 27^\circ C$

where subscripts a and d represent actual and design conditions. If air is used, then the error band is

$$\frac{Q_a}{Q_d} = \sqrt{\frac{T_a R_a}{T_d R_d}} = \sqrt{\frac{T_a}{T_d} \frac{53.3}{48.3}} \tag{10}$$

or $\quad 1.03 < Q_a < 1.06 \, Q_d \quad$ for $\quad 10 < T < 27°C$

Therefore, no compensation for temperature is required since Q_a remains within the specified $\pm 6\%$ of Q_d with either air or O_2. Additional errors can be introduced by variations in C with Reynolds number, Re. However, this source of error can be minimized by choosing the design C at the Re corresponding to the normal operating pressure.

III.2.2 Sizing Considerations

The diaphragm size for the breadboard MCV was based on the required pressure drop characteristics. The GFI specification[*] on pressure drop was originally

$$\Delta P_{loss} = 0.25" \, H_2O \, (0.635 \text{ cm } H_2O) \ @$$

$$P = 3.8 \text{ psia } (0.27 \text{ kgf/cm}^2)$$

$$T = 70°F \, (21°C)$$

$$\dot{w} = 8.65 \text{ pph } (O_2) \, (3.97 \text{ kgf/hr})$$

$$Q = 6.73 \text{ acfm } (191 \text{ alm})$$

Typical losses for a well-designed venturi were assumed to be $\sim 12\%$ of P_1-P_2; therefore, at the specified operating conditions

$$\Delta P = P_1 - P_2 = \frac{\Delta P_{loss}}{.12} = 2.08" \, H_2O \, (5.28 \text{ cm } H_2O) \tag{11}$$

At 5 acfm (142 alm) at 3.8 psi (0.27 kgf/cm^2) and 65°F (18°C), the venturi ΔP is given by

$$\Delta P = 2.08 \times \left(\frac{5}{6.73}\right)^2 \left(\frac{530}{525}\right) = 1.17" \, H_2O \, (2.95 \text{ cm } H_2O) \tag{12}$$

---

[*] This specification was changed to 0.30" H_2O (0.76 cm H_2O) later in the program.

24

A practical bellows size for this application is ~0.5" (1.27 cm) O.D. with 0.125 in.^{2} (0.806 cm^2) effective area, A_B. The effective diaphragm diameter is, from Equation (7)

$$d_{D_e} = \sqrt{\frac{4}{\pi} \frac{P_2}{\Delta P} \cdot A_B} = \sqrt{\frac{4 \times .125 \times 3.8 \times 27.7}{\pi \, 1.16}} \qquad (13)$$

or $\quad d_{D_e} = 3.8$ in. (9.65 cm).

The actual overall diaphragm diameter required to provide A_D is $d_d = 4.08$ in. (104 cm) and is dependent on the housing and support plate diameter. These initial sizing calculations were based on a hypothetical venturi with a 12% loss factor. To finalize the breadboard design, a venturi was constructed and its pressure drop and loss characteristics measured at the alarm Q. Concurrent with the venturi tests, compensator design and material options were evaluated. A flow chart depicting the design optimization scheme is shown in Figure 3.

III. 2. 3 Compensator Design

The primary component of the MCV-GFI is the mechanical compensation unit. Details of the initial breadboard compensator design are shown in Figure 4. For clarity, this schematic is drawn with a scale of 2 to 1. All compensator components are shown on this diagram. The materials and fabrication techniques for the experimental breadboard GFI and those projected for a prototype GFI are presented in Table III. Nickel as opposed to stainless steel bellows were evaluated. Stainless steel is more corrosion resistant; however, nickel bellows are easier to fabricate, and the repeatability of small bellows characteristics is better with nickel than with stainless steel. Therefore, the breadboard GFI was built utilizing nickel bellows.

The differences in fabrication techniques and materials between the breadboard GFI and the final prototype unit are shown in Table III. The breadboard venturi tube and compensator housing were made from lucite in order to observe the effects of moisture on the GFI operational characteristics. The differences in fabrication techniques between the breadboard and prototype units were to allow more flexibility with the experimental model in order that the design could be optimized during the test stages. In either case, the fabrication techniques are within the current state-of-the-art, and no special problems were foreseen for either breadboard or prototype units.

It is noted that the bellows would be electron beam welded to the end fittings in a prototype model. The initial development model did not

25

```
        ┌─────────────────────────┐
        │      Build  Venturi      │
        └─────────────────────────┘
                    │
                    ▽
        ┌─────────────────────────┐
        │    Determine  Venturi    │
        │   ΔP  vs  Q  @  P &T      │
        └─────────────────────────┘
                    │
                    ▽
        ┌─────────────────────────┐
        │        Optimize          │
        │     Venturi  Design      │
        └─────────────────────────┘
                    │
                    ▽
        ┌─────────────────────────┐
        │    Build  Bellows /      │
        │    Switch  Assembly      │
        └─────────────────────────┘
                    │
                    ▽
      ┌───────────────────────────────┐
      │  Determine  Bellows / Switch   │
      │   Characteristics  vs  ΔP/P    │
      └───────────────────────────────┘
                    │
                    ▽
      ┌───────────────────────────────┐
      │   Optimize  Bellows / Switch   │
      │      Diaphragm  Design         │
      └───────────────────────────────┘
                    │
                    ▽
    ┌───────────────────────────────────┐
    │  Assemble  Complete  Mechanically  │
    │    Compensated  Venturi-GFI        │
    └───────────────────────────────────┘
                    │
                    ▽
    ┌───────────────────────────────────┐
    │   Flow  Tests  Complete  System    │
    └───────────────────────────────────┘
```
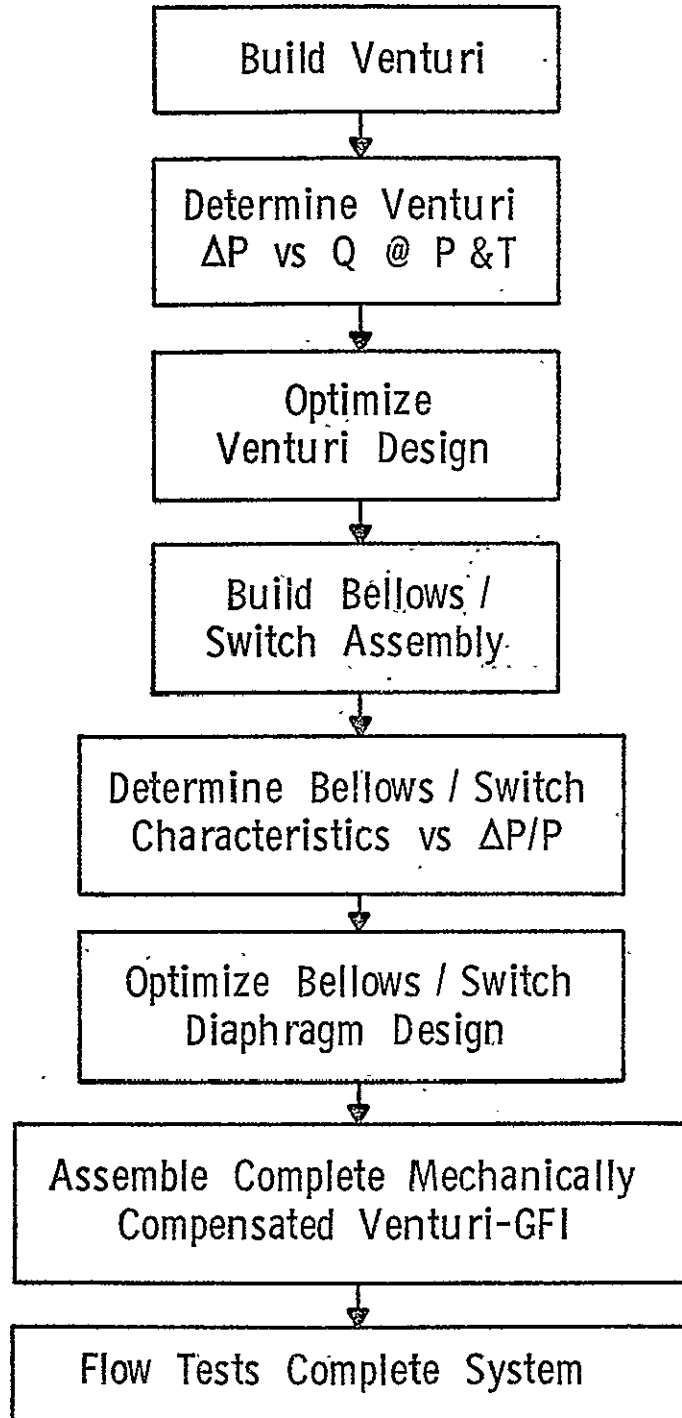
Figure 3. Design Optimization Scheme

TO VACUUM PUMP — ELECTRICAL LEADS

CAP

HIGH PRESSURE PORT

O-RING

BELLOWS

BELLOWS SUPPORT ASSEMBLY

GUIDE ASSEMBLY

HOUSING

RING

P_1

P_2

DIAPHRAGM PLATE

COVER

O-RING

DIAPHRAGM

LOW PRESSURE PORT
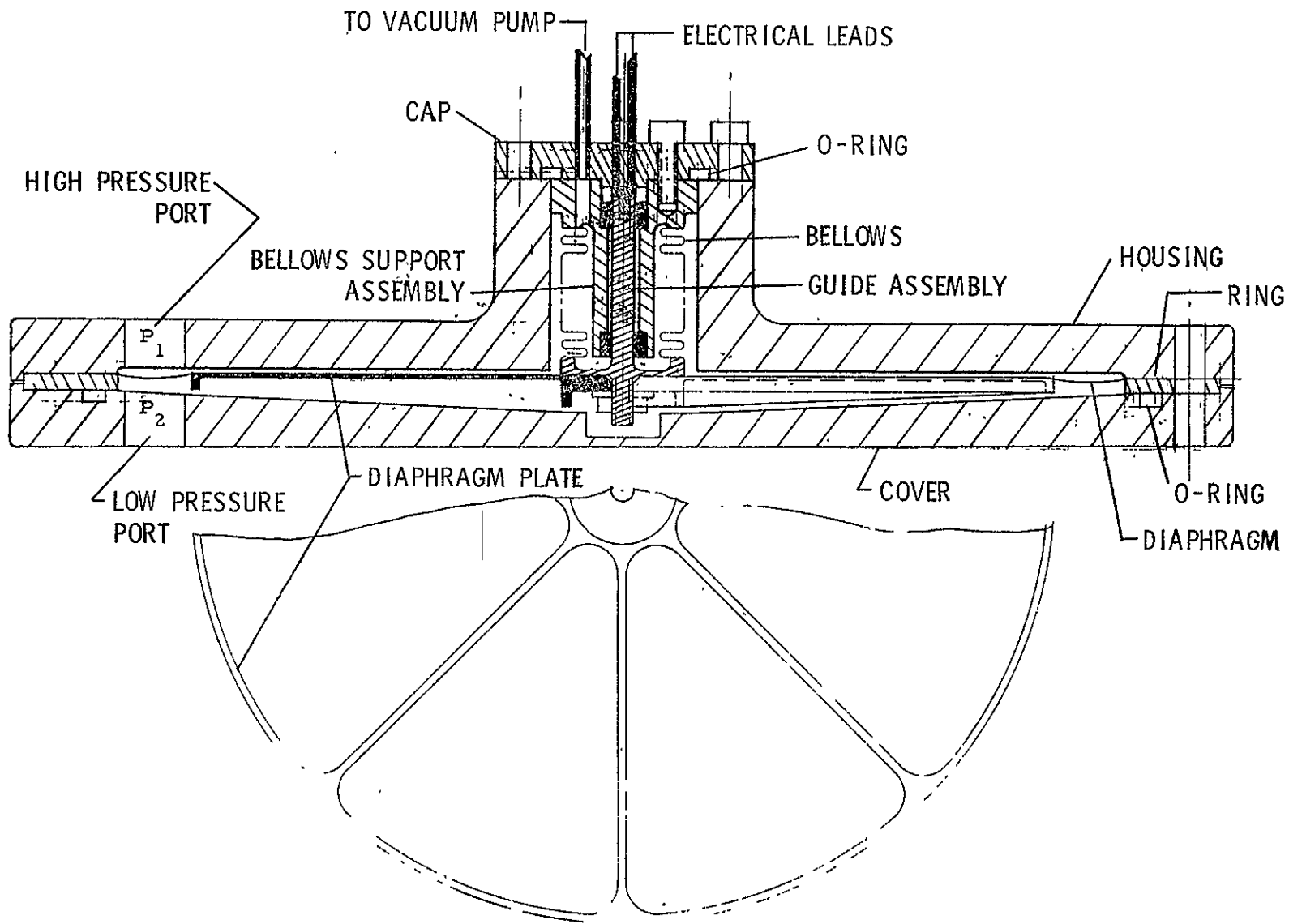
Figure 4. Details of Breadboard Compensator (Initial Design)

TABLE III. MECHANICALLY COMPENSATED VENTURI COMPONENT LIST

Component	Material		Fabrication Technique	
	Breadboard	Prototype	Breadboard	Prototype
Venturi	Nickel	Nickel	Electro-deposited	
Housing	Lucite	Aluminum	Machined	
Cover	Lucite	Aluminum	Machined	
Cap	SST		Machined	
Bellows Support Assembly	SST & Teflon	SST & Sapphire	Machined	
Diaphragm Plate	Aluminum		Machined	
Ring	Aluminum		Machined	
Guide Assembly	SST, Epoxy, & Paliney 7	SST & Paliney 7	Machined	
Bellows	Nickel	SST	Electro-deposited	Welded
Diaphragm	Dacron Reinforced Silicone Rubber		Hand-Made	Molded
Evacuated Bellows Assembly	---		Epoxy	Electron Beam Welded

incorporate electron beam welding in the fabrication stage. Initially, the bellows was epoxyed to the end fittings. In addition, a pressure port on the support cap was used to evacuate the bellows in the breadboard testing. This allowed the flexibility of disassembling the bellows so modifications could be made to the components internal to the bellows (such as the teflon support bushings).

The bellows' response characteristics are critical in determining the operational characteristics of the compensator. Tests were performed on a commercially available bellows to determine predictability and repeatability of the bellows' response to pressure loading. A schematic of the test setup is shown in Figure 5. The test bellows had a 0.5" (1.27 cm) O.D. with a 0.125 in.^{2} (0.806 cm^2) effective area (A_B) which was the bellows size chosen for sizing the breadboard diaphragm. The bellows test involved evacuating the bellows interior to simulate static pressure levels (P_2) between 3.5 and 15 psia (0.25 to 1.05 kgf/cm^2). In addition, small weights were hung from the base of the bellows to simulate the venturi differential pressure (P_1-P_2) loading on the diaphragm. An Ohm meter was hooked to the electrical contacts, and for a given static pressure level, the weight required to remove electrical contact was measured. Test results are shown in Figure 5. The solid line represents the predicted response based on the manufacturer's publised effective area. The circles represent actual data points measured in the testing. At all pressure levels the data is in excellent agreement with the anticipated response curve, and repeatability from loading and unloading the bellows is also good. This showed that characteristics-of-an off-the-shelf bellows are predictable and repeatable such that no special bellows design or fabrication technique will be necessary in a final prototype unit. Also, a bellows with a lower spring rate than the one tested would give additional sensitivity and would provide a more accurate compensator. Bellows with approximately 1/3 the spring rate of the one used for these tests were used in the breadboard MCV-GFI.

The alarm switch and the effect of the loss of vacuum on switch operation was evaluated as part of the compensator design effort. Several possibilities regarding the location and design of the alarm switch were considered. The use of a microswitch located below the diaphragm in the lower cover plate was considered as an alternative to the design shown on Figure 4. This design has the advantage of removing the bellows internal switch arrangement which will simplify evacuating and sealing the bellows and reduce the chance of a vacuum leak. The outside switch has the disadvantage of placing the switch out of the vacuum in the moisture-laden environment. The use of an external mounted microswitch proved unfeasible since the combination of both low switch activation force and travel, required with the compensator design, was unobtainable. Therefore, the
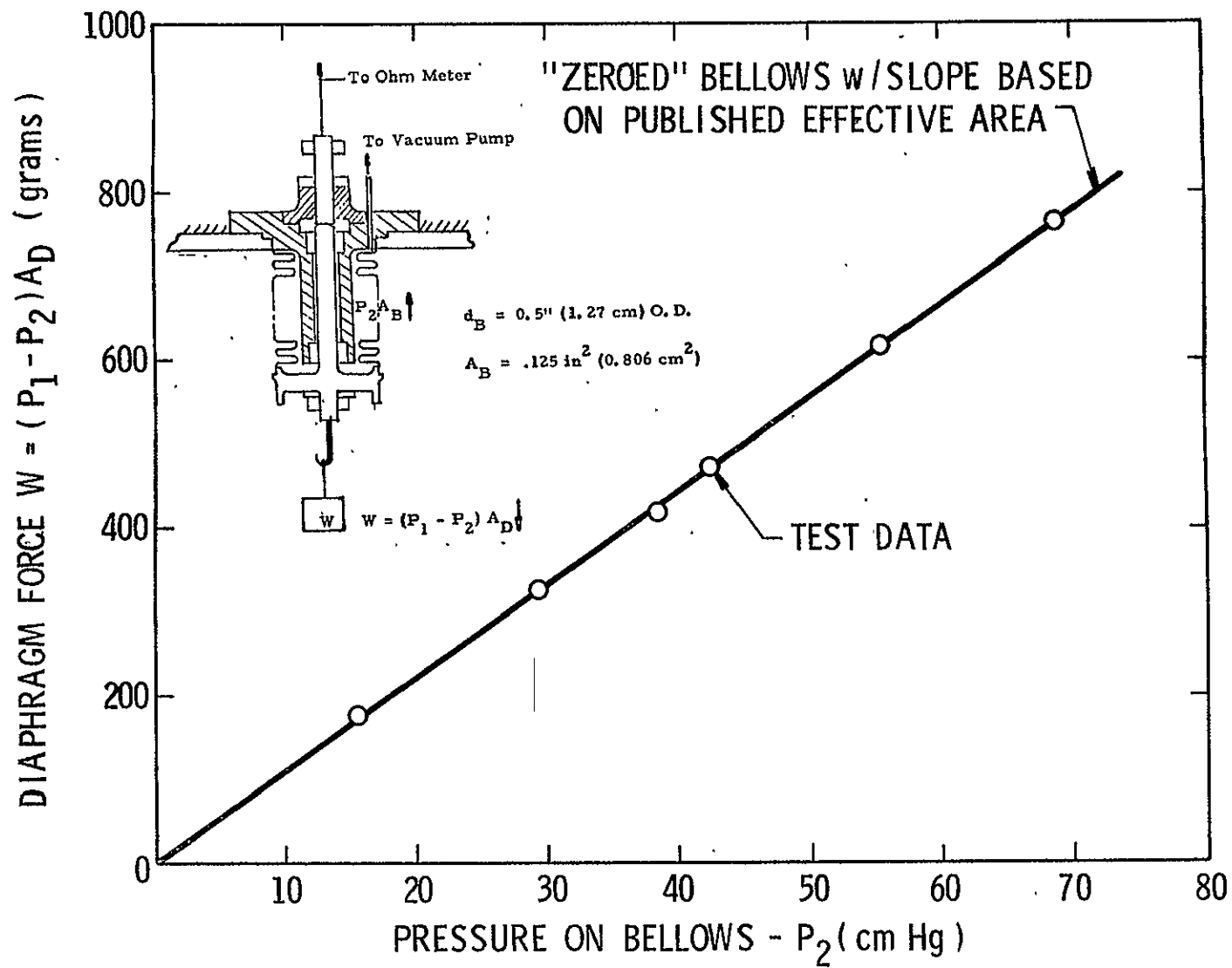
Figure 5. Test Bellows Response Characteristics

internal switch arrangement was chosen as the best design. The leak rates of commercially available bellows and glass insulated electrical feed-through connectors were examined to estimate the life of the internal switch design. Based on manufacturers' claims, a properly constructed bellows-switch arrangement would be reliable for the required life of the unit. Additional thought was also given to the switch contact materials to insure that the switch would activate when the contacts touch. The potential loss of electrical contact from surface film build-up was reduced by using Paliney 7, a gold/silver/platinum alloy developed for similar switching operations.
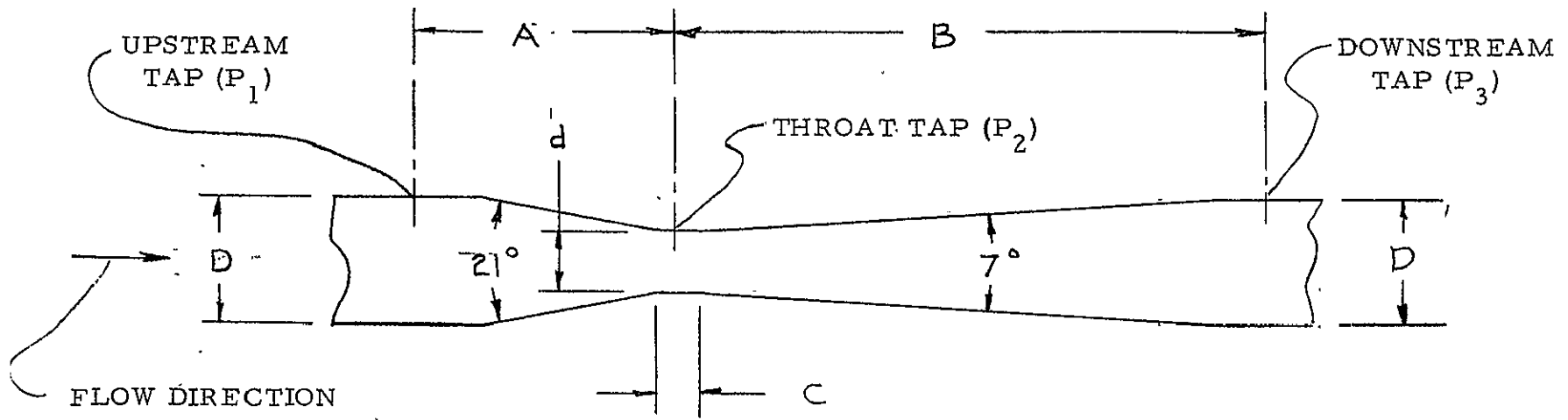
III. 2. 4 Venturi Tests

A venturi tube was cast to design specifications using a commercially available plastic (Clear-Cast) to provide the pressure drop characteristics utilized for sizing the diaphragm/bellows. Pressure loss and pressure drop data for the "Clear-Case" GFI venturi tube were recorded so that compensator diaphragm sizes could be finalized. In addition, similar data for the Rosemount GFI* were recorded for comparison. A description of the test facility utilized to provide the required flow conditions is given in Appendix F.

Figure 6 shows pertinent Rosemount and GFI-1 venturi dimensions and pressure measuring locations. Pressure loss data for both the Rosemount and the GFI-1 venturi tubes are summarized in Table IV. The results reveal that the Rosemount meter has a higher pressure loss than anticipated, 0.31 versus 0.25" H_2O (0.79 versus 0.64 cm H_2O). The pressure loss for the initial GFI venturi design (GFI-1) was measured at 0.42" H_2O (1.07 cm H_2O). This pressure loss was higher than anticipated from the sizing calculations. This resulted from increased losses at lower static pressures as shown on Figure 7. Both the Rosemount and the GFI-1 meter exhibit about a 30% loss coefficient at a static pressure of 3.8 psia (0.27 kgf/cm^2) and a flow rate of 5 acfm (142 alm). The initial design assumption of 12% was obtained from the literature. This value is good at atmospheric pressure where Reynolds numbers are high. At the lower pressure, decreasing Reynolds numbers create increased losses.

The GFI-1 venturi tube was made with a slightly larger throat diameter than needed to obtain the required pressure drop of 1.17" H_2O (2.97 cm H_2O) for a 4.08 in. (10.4 cm) diameter diaphragm. The first model was cast with a slightly larger throat since a second model could be easily obtained by machining the existing aluminum core. The GFI-2, indicated in

---

*The Rosemount venturi was used with the Apollo vent flow sensor (GFI).

FIGURE 6. VENTURI DIMENSIONS, inches (cm)

	A	B	C	D	d
Rosemount	1.0	3.9	.10	.680	.383
	(2.54)	(9.91)	(.254)	(1.73)	(.973)
GFI-1	1.75	3.65	.25	.742	.372
	(4.45)	(9.27)	(.635)	(1.88)	(.945)

TABLE IV. VENTURI COMPARISON

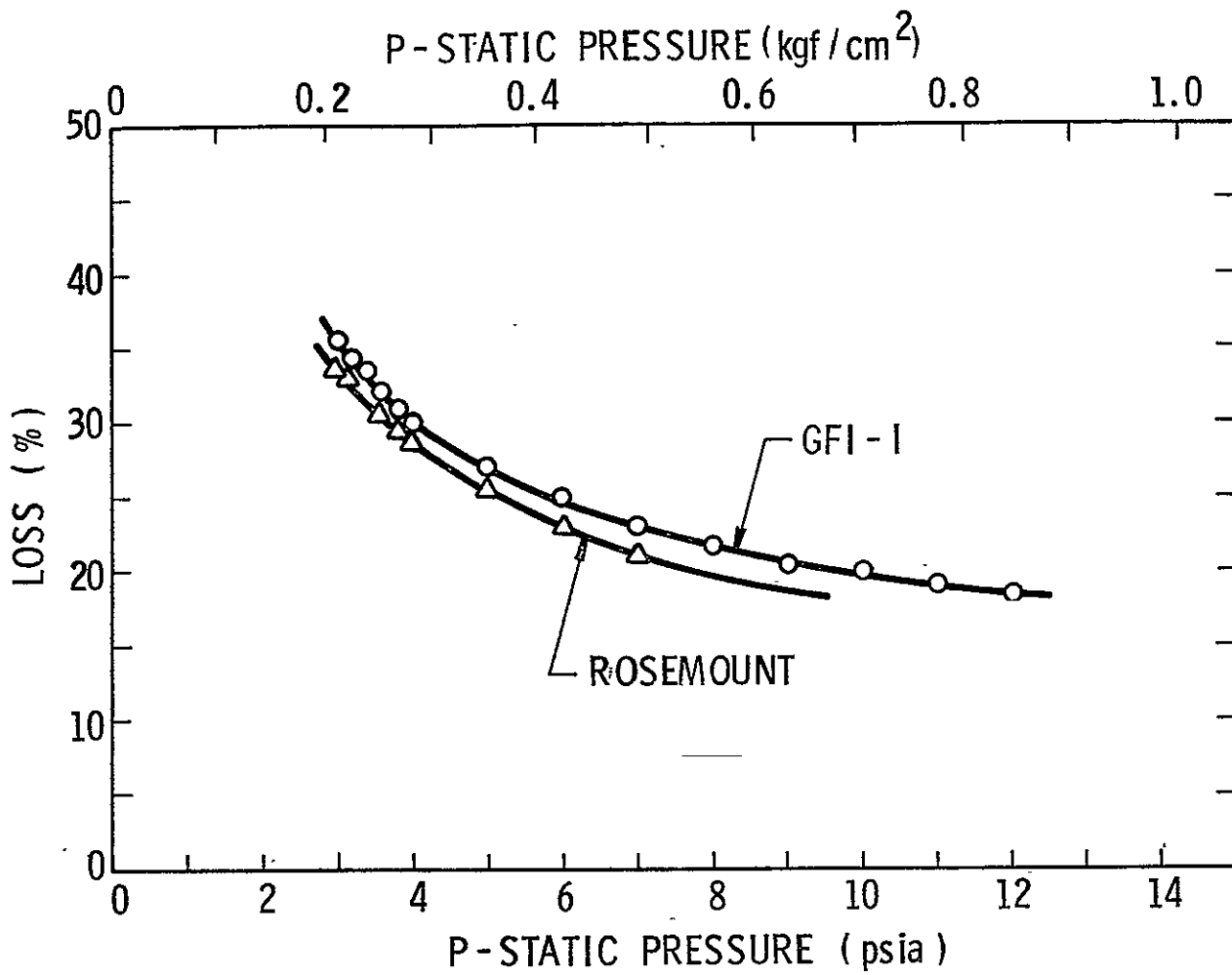| Venturi	ΔP_{1-3} Pressure Loss P = 3.8 psia (0.27 kgf/cm^2) Q = 6.73 acfm O_2 (191 alm O_2)	ΔP_{1-2} Pressure Drop P = 3.8 psia (0.27 kgf/cm^2) Q = 5 acfm O_2 (142 alm O_2)	Required Diaphragm Diameter
Rosemount	0.31" H_2O (0.79 cm)	0.76" H_2O (1.93 cm)	4.95" (12.6 cm)
GFI-1	0.42" H_2O (1.07 cm)	0.89" H_2O (2.26 cm)	4.57" (11.6 cm)
GFI-2	0.53" H_2O (1.35 cm)	1.17" H_2O (2.97 cm)	4.08" (10.4 cm)

Figure 7. Venturi Loss Characteristics @ 5 acfm (142 alm)

Table IV, shows pressure loss characteristics for a venturi that would provide the original design ΔP characteristics and diaphragm sizes. By comparison, the GFI-1 would require a 4.57 in. (11.6 cm) diameter diaphragm because of the smaller ΔP_{1-2}.

Pressure loss measurements for the Rosemount and GFI-1 venturi tubes were discussed with NASA personnel to establish a realistic final pressure loss specification. As a result of these discussions, the pressure loss specification was finalized as follows:

$$\Delta P_{loss} = 0.3'' H_2O \ (0.76 \text{ cm } H_2O) \ @$$

$$P = 3.8 \text{ psia } (0.27 \text{ kgf/cm}^2)$$

$$T = 70°F \ (21°C)$$

$$\dot{w} = 8.5 \text{ pph of } O_2 \ (3.9 \text{ kgf/hr})$$

Since the Rosemount venturi tube used with the Apollo GFI met the specification, the Rosemount venturi, in combination with the mechanical compensator previously designed for the larger ΔP venturi tube, was chosen. This allowed maintaining a reasonable compensator size of $d_d = 4.08''$ (10.4 cm) as well as utilizing the breadboard design sizes and drawings previously established. To make the GFI trigger at the required alarm rate with the small compensator, a diaphragm preload adjustment (see Equation (5)) was required. This preload adjustment allowed the smaller diaphragm size to be used with the Rosemount venturi tube and in addition had the advantage of providing an adjustment of the alarm triggering level at any static pressure. This resulted in more flexibility in setting the alarm rate than the original design which fixed the alarm flow rate once the unit was assembled.

Additional pressure drop measurements were made on the Rosemount tube to determine ΔP versus static pressure characteristics for establishing linearity and sizing the compensator preload spring. The results (Figure 8) indicate a good linear ΔP-P_{O_2} characteristic. Based on these pressure measurements, the required preload adjustment, X, covers a reasonable range of 0.10 to 0.67 in. (0.254 to 1.70 cm) with a 1.27 lb/in. (0.23 kgf/cm) spring for the required range of static pressures.

III.2.5   Breadboard MCV-GFI

Figure 9 shows the schematic of the final breadboard compensator design. The design components are identical to those previously presented in Figure 4 with the exception of the preload adjustment. Since the
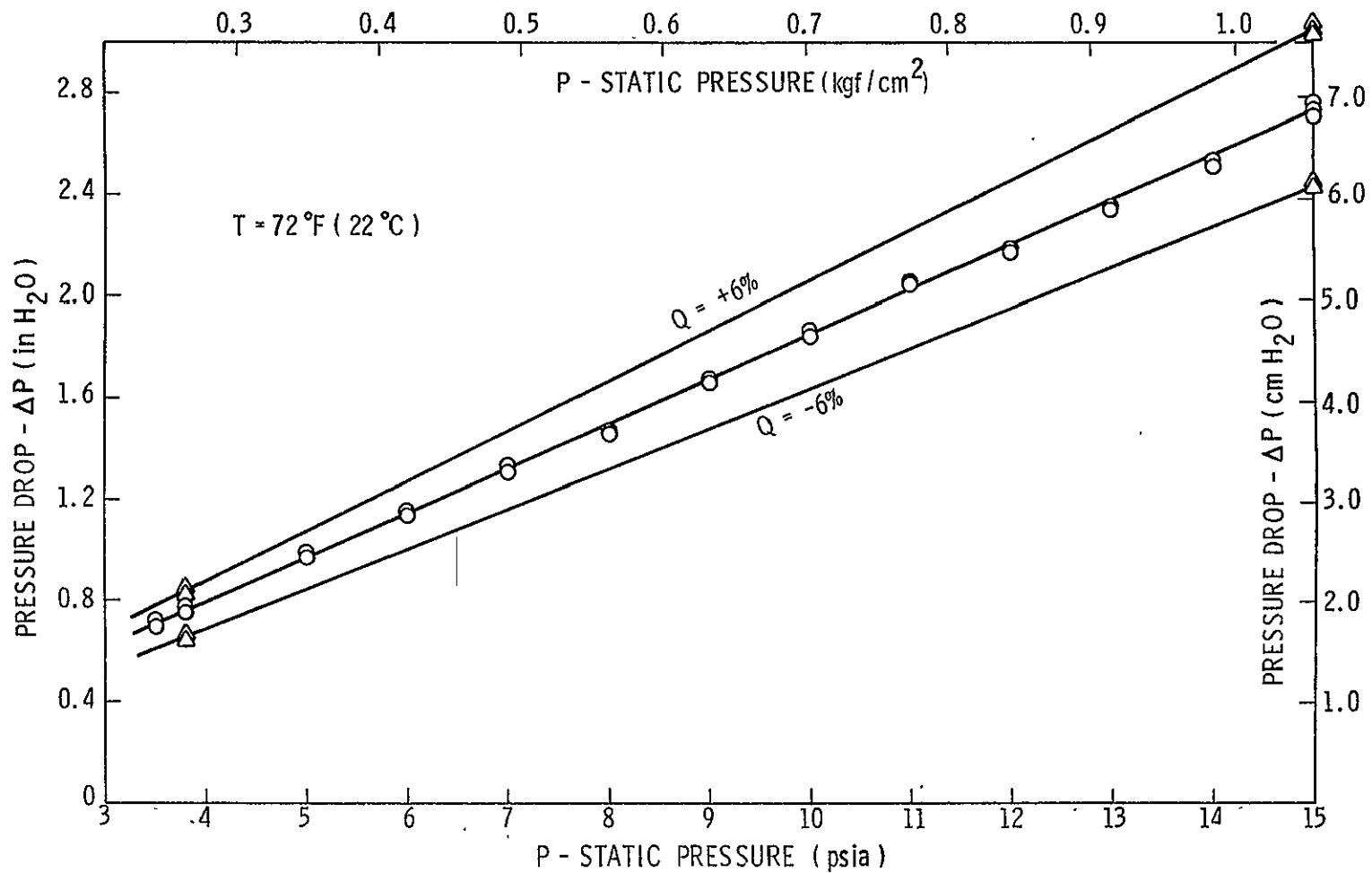
Figure 8. ΔP vs P for Rosemount Tube - Q = 5.0 acfm (142 alm), O_2

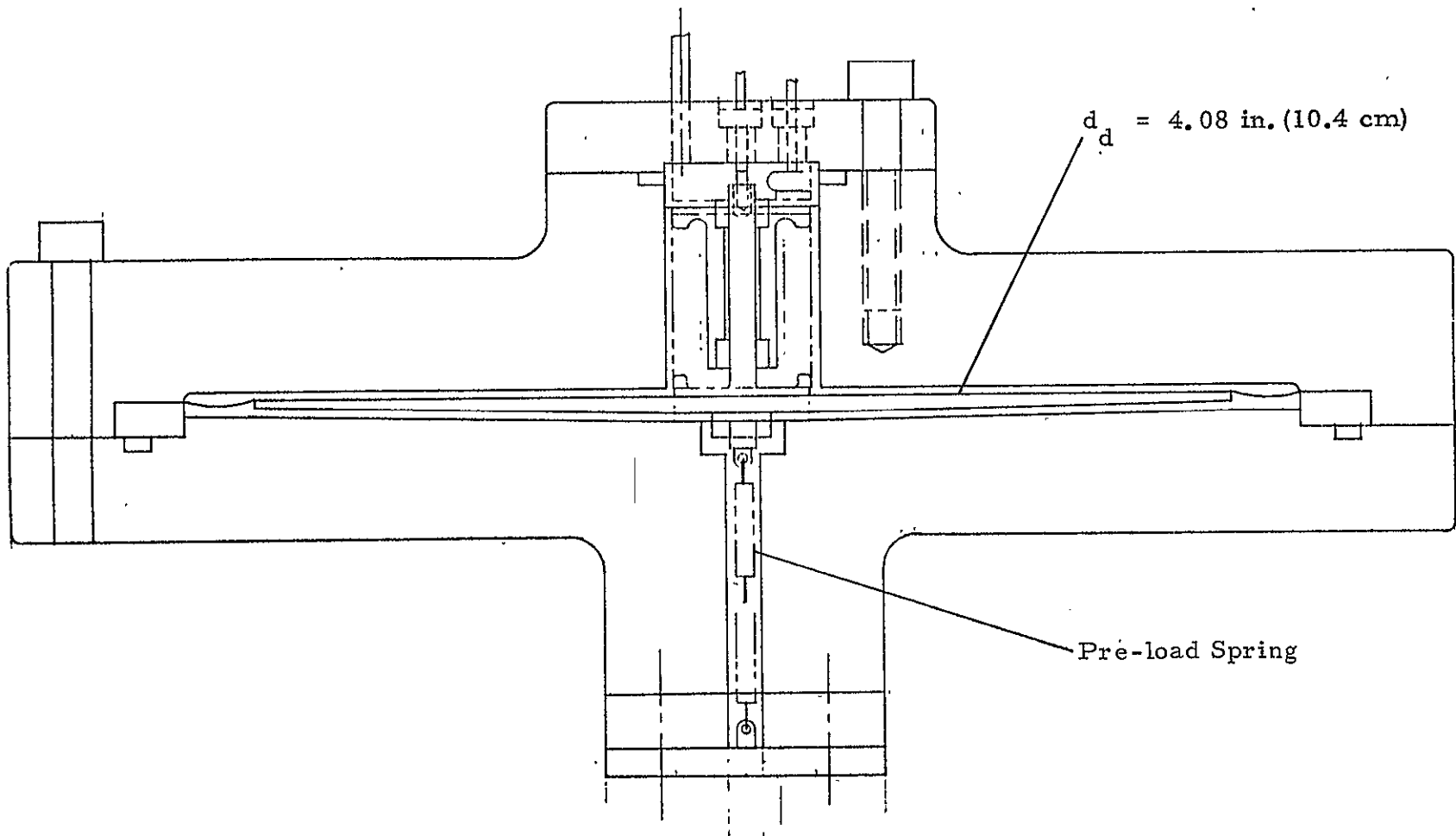d_d = 4.08 in. (10.4 cm)

Pre-load Spring

FIGURE 9. BREADBOARD COMPENSATOR WITH PRE-LOAD ADJUSTMENT

compensator diaphragm diameter was maintained at the previous design value of 4.08 in. (10.4 cm), no resizing of compensator components was required.

The breadboard MCV-GFI was fabricated with the components and techniques indicated in Table III. Figure 10 shows a view of the assembled unit and Figure 11 the disassembled unit with all component parts visible.

III.3 Breadboard Performance Tests

III.3.1 Test Plan

The test plan for the breadboard GFI is presented in Table V. All tests were conducted with the facility and procedures described in Appendix F.

III.3.2 Check-out Tests

Initial check-out flow testing was performed to observe switch operation and to determine triggering repeatability. The switch was sub-jected to the GFI specification voltage and current of 16.8 volts and 25 milliamps, respectively. By increasing and decreasing the GFI flow rate, the switch was allowed to make and break contact, and no problems were experienced with switch stickage or arcing at the specification voltage and current. In fact, repeatability of the switch triggering point was good for repeated test runs. However, a small hysteresis, $\pm 6\%$ at 3.8 psia (0.27 kgf/cm^2), in the alarm trigger point was recorded. When approaching the trigger point from high flow rates (decreasing flow rate), the alarm would trigger at a different point than with increasing flow rate. The triggering point at either increasing or decreasing flow rate was very repeatable. The $\pm 6\%$ hysteresis was attributed to the stiffness of the diaphragm material and the friction in the bellows/switch guide pin bearings. It was anticipated that the majority of this hysteresis was caused by the stiffness of the dia-phragm material. The $\pm 6\%$ error due to hysteresis occurred with a flow static pressure of 3.8 psia (0.27 kgf/cm^2). Operating at higher static pres-sures will result in a smaller error since the differential pressure acting on the diaphragm will be larger while the resistance due to diaphragm stiffness and bearing friction remain constant. To eliminate the hysteresis error, a more flexible diaphragm material was incorporated into the com-pensator and flow testing repeated. With the more flexible diaphragm material, essentially no hysteresis was recorded at any system static pres-sure. With the more flexible diaphragm, the GFI switch activated at the pre-set alarm flow rate with either increasing or decreasing flow rate.
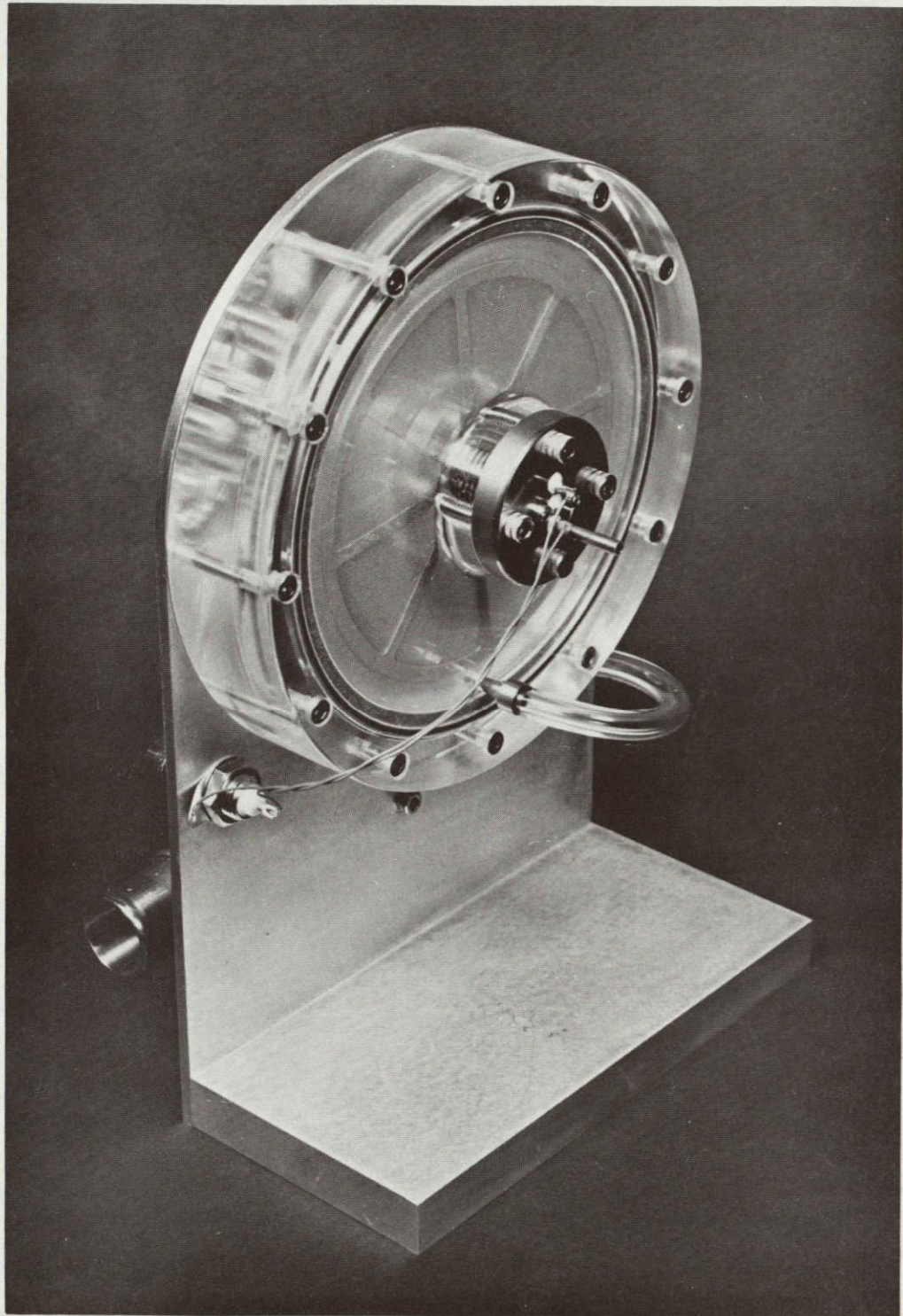
FIGURE 10.   ASSEMBLED BREADBOARD GFI
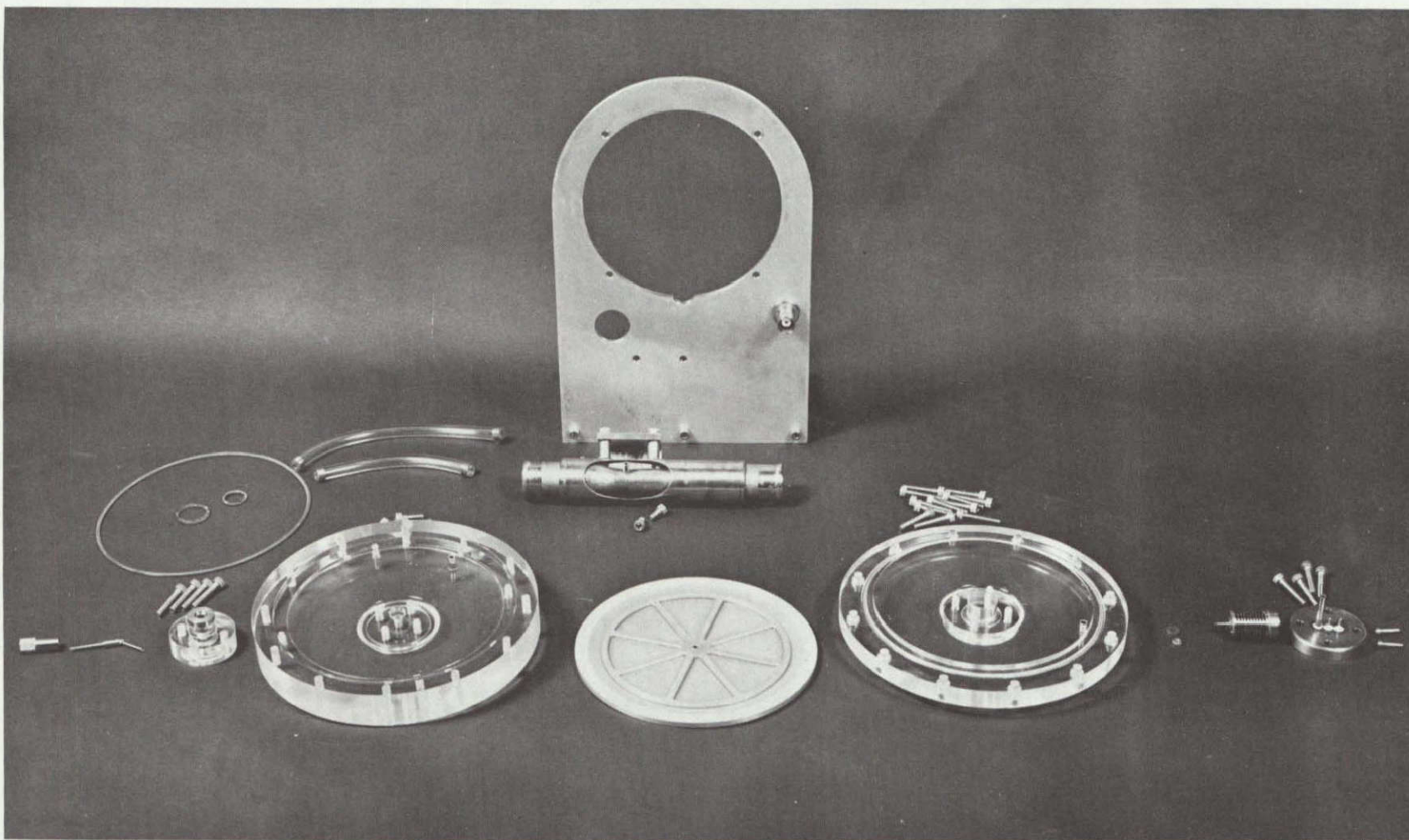
FIGURE 11.   DISASSEMBLED BREADBOARD GFI

TABLE V. BREADBOARD TEST PLAN AND PROCEDURES

Operational:

(1)   Shakedown and check-out

(2)   Determine the preload required at 3.8 psia (0.27 kgf/cm^2), 5 acfm (142 alm) O_2

(3)   Determine the flow rate required to operate the switch at pressures between 3 and 15 psia ($0.27 \leq P \leq 1.05$ kgf/cm^2)

(4)   From (3) above, determine the preload required for check-out with air at 15 psia, 5 acfm (1.05 kgf/cm^2, 142 alm)

(5)   Determine the meter repeatability and hysteresis at various pressures

(6)   Determine meter position sensitivity at 1-g at various pressures

(7)   Perform the 100% humidity test and determine the effect of accumulated moisture in the meter housing

(8)   Determine switch response.

Environmental:

(1)   Determine shock and vibration effects within the limits of breadboard construction

(2)   Subject simulated parts to materials salt spray tests

(3)   Subject meter to temperatures between -45°F and 160°F (-43°C and 71°C) and recheck operational characteristics.

Structural:

(1)   Subject meter to the proof pressure test and recheck operation

(2)   Subject the meter housing to the burst pressure test.

III. 3. 3   Flow Tests

Figure 12 shows the flow rate required to activate the switch versus system static pressure with the compensator preload spring set so the alarm will activate at 5 acfm (142 alm) at 3.8 psia (0.27 kgf/cm^2). The alarm rate at other flow static pressures varies from 4.4 to 6.7 acfm (125 to 190 alm) for $3 \leq P \leq 15$ psia ($0.21 \leq P \leq 1.05$ kgf/cm^2), respectively. By re-setting the preload adjustment, the GFI can be set to trigger at 5 acfm (142 alm) at any system static pressure. The results shown on Figure 12 were obtained with both increasing and decreasing flow rates indicating no hysteresis.

Actual C_D versus Reynolds number measurements were recorded (Figure 13) with the Rosemount venturi tube. The predicted alarm rate using the measured discharge coefficient, C_D, is shown on Figure 12. Since the discharge coefficient changes with static pressure (i.e., Reynolds number) a slight error exists in predicting the actual activation flow rate by assuming $C_D = 0.942$, the value at 3.8 psia (0.27 kgf/cm^2). Using the actual measured C_D's allows an accurate prediction of the alarm flow rate for any static pressure. This ability to accurately predict alarm Q for any flow condition allows confidence in predicted performance for optimized designs. The measured venturi differential pressure, at the activation or the alarm flow rate, versus sytem static pressure (Figure 8) and the measured C_D was extremely beneficial in optimizing bellows and diaphragm sizes for the prototype.

III. 3. 4   Position Sensitivity Tests

Flow tests were performed with the GFI placed in various positions to determine its sensitivity to orientation. The meter was placed with the diaphragm horizontal, vertical, and at numerous other positions between horizontal and vertical. The alarm triggering rate, recorded at 3.8 psia (0.27 kgf/cm^2) at all meter positions remained within 6% of 5 acfm (142 alm) indicating that no appreciable sensitivity to orientation existed. Because of larger pressure forces acting on the diaphragm, position sensitivity will be reduced at higher system static pressures. Also, in zero gravity, no position sensitivity will occur. The test results show that the breadboard GFI design is insensitive to orientation within the accepted alarm triggering accuracy.

III. 3. 5   Switch Response Tests

The response of the breadboard GFI switch was determined by placing a solenoid valve between the two venturi pressure ports such that pressure could be suddenly equalized on both sides of the compensator diaphragm.
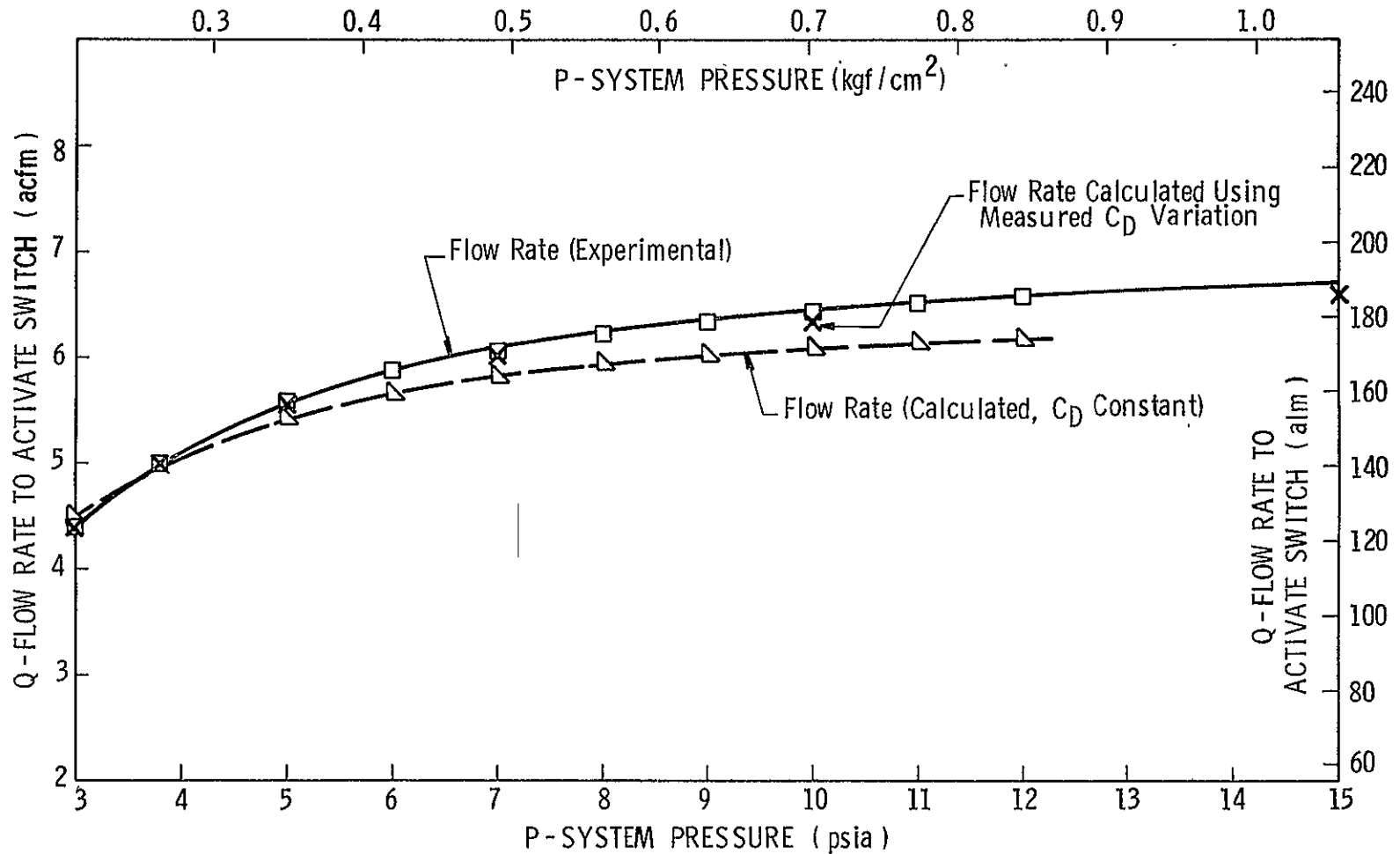
Figure 12. Breadboard GFI Performance Characteristics with O_2
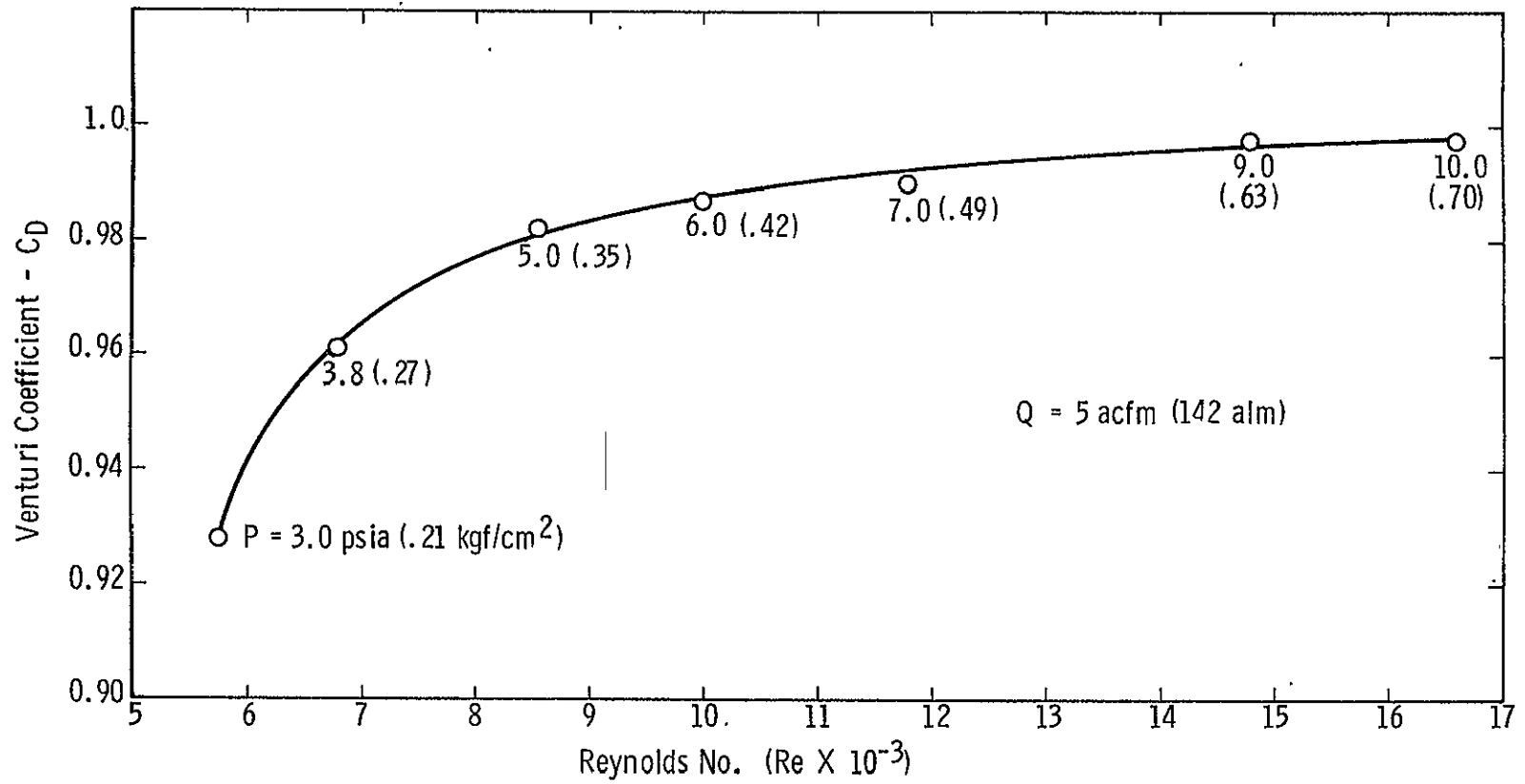
43

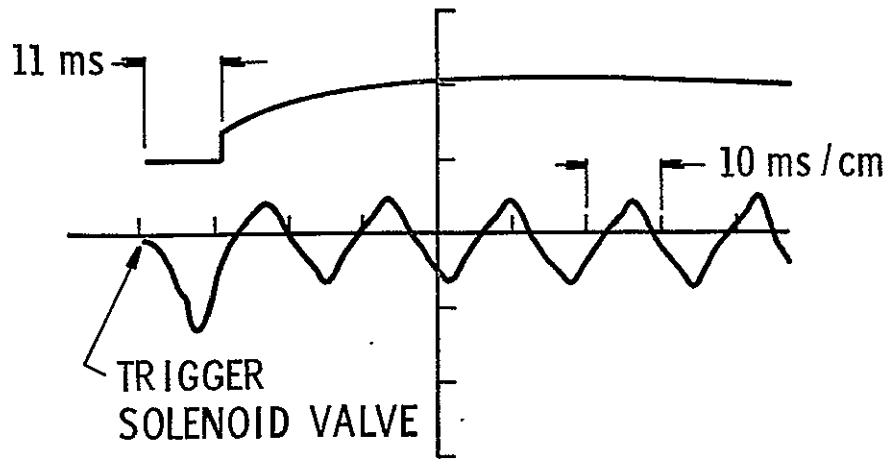Figure 13. Discharge Coefficient versus Re (Rosemount Venturi)

This simulated a rapid drop in flow rate from the normal operating condition of 6 acfm (170 alm) to zero flow. The measured response was therefore the sum of the electrical response of the switch contacts plus the mechanical and fluid response of the air volume/diaphragm/bellows combination. The oscillographs shown in Figure 14 indicate a maximum switch activation (deactivation) time of 11 ms. Since this value includes the time required for the solenoid valve to completely open, the response measurement represents a conservative number. Therefore, the switch response is well within the specified 250 ms.
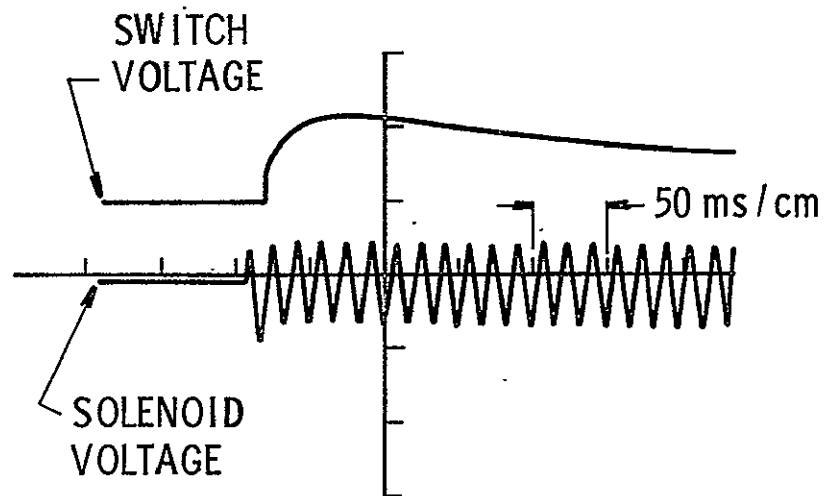
III. 3. 6   Vibration Tests

A vibration test was performed on the breadboard GFI to determine if the switch could be activated under normal flow conditions by high vibration levels. The meter was set at a normal flow rate of 6 acfm (170 alm) at the operating pressure and temperature of 3.8 psia (0.27 kgf/cm^2) and 75°F (24°C), respectively. The GFI was placed on an electromechanical shaker with the diaphragm oriented horizontally (a worst case condition). The meter was vibrated harmonically at 20 Hz from 0 to 10 g. No triggering of the alarm was observed during this testing. Additional tests were performed at a flow rate of 5.3 acfm (150 alm) nearer the alarm value, and no triggering of the alarm was observed up to a level of 5 g's. Switch sensitivity to shock was evaluated by hitting the mechanical compensator with a screw driver. Again, no triggering of the switch was observed with the meter operating at the normal flow rate. This testing demonstrated that the breadboard GFI compensator-switch design was not affected by normal-use vibrations.

III. 3. 7   High Humidity Tests

The alarm activation point was recorded with 100% humidity air flow. During this testing moisture condensed inside the compensator housing and in the pressure port lines. The recorded activation point was unchanged from the dry air testing. Tests were also conducted with the diaphragm cavity completely filled with water by placing the compensator in a vertical position. As the flow pressure was applied to the diaphragm and the bellows expanded, water was forced out of the low pressure port as the volume decreased and increased on the low and high pressure side of the compensator, respectively. This resulted in a differential water head across the diaphragm which changed the switch triggering point because of the hydrostatic pressure difference. However, equalizing the amount of water on both sides of the diaphragm resulted in returning the trigger point to the specified 5 acfm (142 alm). The problems with hydrostatic pressure affecting the GFI performance will obviously not occur in zero gravity. In addition, it is highly unlikely that water would condense and completely fill

11 ms

10 ms / cm

TRIGGER
SOLENOID VALVE

(a)   10 ms / cm

SWITCH
VOLTAGE

50 ms / cm

SOLENOID
VOLTAGE

(b)   50 ms / cm

Figure 14. Breadboard GFI Switch Response
@ 3.8 psia (0.27 kgf / cm^2)

46

the compensator housing. However, even when large droplets of water were present in the compensator, the meter performance was unaffected. Therefore, the high humidity tests showed that the breadboard GFI's operation was not affected by moisture.

III. 3.8 Salt Fog Tests

Salt fog tests per MIL STD 810B - Method 509 were conducted with a 5% sodium chloride solution for 48 hours. GFI materials subjected to this test included (1) the diaphragm material bonded to an anodized aluminum plate and (2) an electro-deposited sulphur-free nickel bellows identical to the one used in the breadboard GFI. The results of this testing revealed no degradation in the bond between the diaphragm material and anodized aluminum or the materials themselves. Examination of the nickel bellows with a microscope showed no degradation of the bellows surface. Some slight discoloration was noted, however, in areas where the bellows contacted the support tray. This probably resulted from a chemical reaction between dissimilar metals which was accelerated by the salt spray. No such problem can occur with the breadboard GFI design.

III. 3.9 Proof Pressure Tests

Proof pressure testing was conducted at the required 1.5 X the maximum operational static pressure (22.5 psia, 1.59 kgf/cm^2). The alarm triggering point at 3.8 psia (0.27 kgf/cm^2), 5 acfm (142 alm) was checked prior to and after subjecting the meter to the proof pressure. No change in the alarm triggering point was observed. It was concluded that pressurizing the meter to 22.5 psia (1.58 kgf/cm^2) did not affect its performance.

III. 3.10 Life Cyclic Tests

It is estimated that approximately 5000 switching cycles could occur in the life of a GFI. A life cycle test was conducted for 10,000 cycles to determine if repeated switching would affect meter performance. The breadboard GFI was placed in the test facility with the flow adjusted such that a large ΔP (3.4" H_2O, 8.6 cm H_2O) occurred across the meter diaphragm. This is a much larger ΔP than will be experienced for any of the required operational conditions. Therefore, an overloading of the switch contacts occurred on each cycling of the switch. Tests were performed with a solenoid valve such that the pressure could be equalized on both sides of the diaphragm as described for the switch response tests. The solenoid was switched in 10 sec intervals; such that for 5 seconds the GFI switch was on and for 5 seconds the GFI switch was off. The tests were conducted over a 30-hour period to provide the 10,000 cycles. By testing in this manner the switch contacts and the entire diaphragm/bellows

switch assembly were cycled for the full 10,000 times. The tests were performed during the 10,000 cycles at the maximum current and voltage of 25 milliamps and 16.8 volts respectively. At the end of the testing the switch was rechecked at a low current and voltage of 5 milliamps, and 5 volts, and the switch also performed accurately at the low current and voltage. No degradation in performance occurred over the 10,000 cycles, and the breadboard GFI continued to perform accurately after the cyclic testing. These tests indicated that the mechanical compensator and switch assembly should have an expected life well beyond that required in the GFI specification.

III. 3. 11 Burst Pressure and Environmental Temperature Tests

The breadboard compensator housings were constructed from plexiglass. Therefore, burst pressure or environmental temperature testing would have been meaningless. As a result, these tests were deferred until the prototype testing. ·

III. 4 Breadboard GFI Conclusions

The results of the breadboard MCV-GFI development indicated that a prototype MCV-GFI could be produced meeting all NASA GFI requirements. The experience and data generated during the breadboard development was utilized to provide an optimized prototype GFI design.

IV. PROTOTYPE DEVELOPMENT

IV.1   Prototype Sizing Considerations

Flow data obtained on the Rosemount venturi tube was used for sizing the prototype bellows/diaphragm combination to provide an optimum GFI design. The optimum GFI was designed to provide full pressure compensation while maintaining a minimum size.

The smallest practical size for the prototype compensator was fixed by the bellows diameter. The minimum acceptable diameter was chosen as $d_B - 0.25$ inch (0.635 cm). For this bellows diameter, the diaphragm and preload spring were sized by using the actual $\Delta P/P$ values measured on the venturi. To size the components, the design equations

$$Q^2 = \frac{C^2}{\overline{K}} \left[\frac{A_B}{A_D} + \frac{K_p X_p}{P_2 A_D} \right] \tag{14}$$

and

$$\frac{Q^2 \overline{K}}{C^2} = \frac{\Delta P}{P_2} \tag{15}$$

were utilized. By measuring $\Delta P/P_2$ versus P_2 at Q_{alarm}, for O_2 at the design temperature, the variations in the discharge coefficient, C, were taken into account. The measured (ΔP vs P_2) were shown in Figure 8. Using the values at 3.8 and 15.0 psia (0.27 and 1.02 kgf/cm^2), results in two simultaneous equations,

$$\Delta P_{3.8} \, A_D = 3.8 \, A_B + F_P$$

$$\Delta P_{15} \, A_D = 15.0 \, A_B + F_P.$$

which are solved to determine A_D and the preload force F_P. The resulting prototype sizes are:

Diaphragm effective diameter	3.13" (7.95 cm)
Diaphragm overall diameter	3.33" (8.46 cm)
Bellows effective diameter	0.250" (0.635 cm)
Preload spring force	0.0245 lb (11.5 gm)

It is noted that the preload spring is in compression since the preload force was assumed positive in the direction of bellows compression in the force balance equation.

The calculated alarm rates for these sizes versus static pressure, are shown in Figure 15. The predicted alarm rates in Figure 15 are based on measured $\Delta P/P$ values. The results reveal the desired static pressure compensation characteristics. The design is based on O_2 at 72°F (22°C). The variations in Q_{alarm} at other temperatures and with air were discussed in Section III.2.1. For the normal operating temperature range, $50 < T < 80°F$ ($10 < T < 27°C$), the alarm rate remains within $\pm 6\%$ of 5 acfm (142 alm). To return the alarm to 5 acfm (142 alm) for these or other flow conditions, the preload setting can be changed. At a given static pressure, the preload force adjustment can also be used to change the alarm triggering point, to a value other than 5 acfm (142 alm).

IV.2   Prototype Design Considerations

The prototype design incorporated several features which represented a significant improvement over the breadboard design. In addition, the prototype design was based on utilizing prototype materials and fabrication techniques. Therefore, as part of the design, vendors for producing primary compensator components were established.

IV.2.1   Prototype Switch Design

An alternate design (Figure 16) was devised for electrically insulating the bellows switch from the main GFI body. This method was considered far superior to the original method used with the breadboard GFI. The prototype method requires only 1 glass feedthrough, and the wiring and insulation inside the bellows to connect the pin-mounted contact to the glass feedthrough is eliminated. The prototype design should improve the performance, reliability, cost and life of the unit by simplifying the overall switch design. Since the primary contact design does not differ from the breadboard unit, the switching performance should be equivalent.

IV.2.2   Vendor Selection

Potential vendors were contacted to discuss fabrication of compensator components in four basic areas:

(1)   The compensator diaphragm

(2)   The electrical glass feedthroughs

(3)   The bellows-aneroid assembly

(4)   The sapphire bearings.

As a result of these discussions, prototype designs were finalized and fabrication techniques and materials were chosen. Vendors were also selected to provide the diaphragms, glass feedthroughs, bearings, and aneroid assemblies.
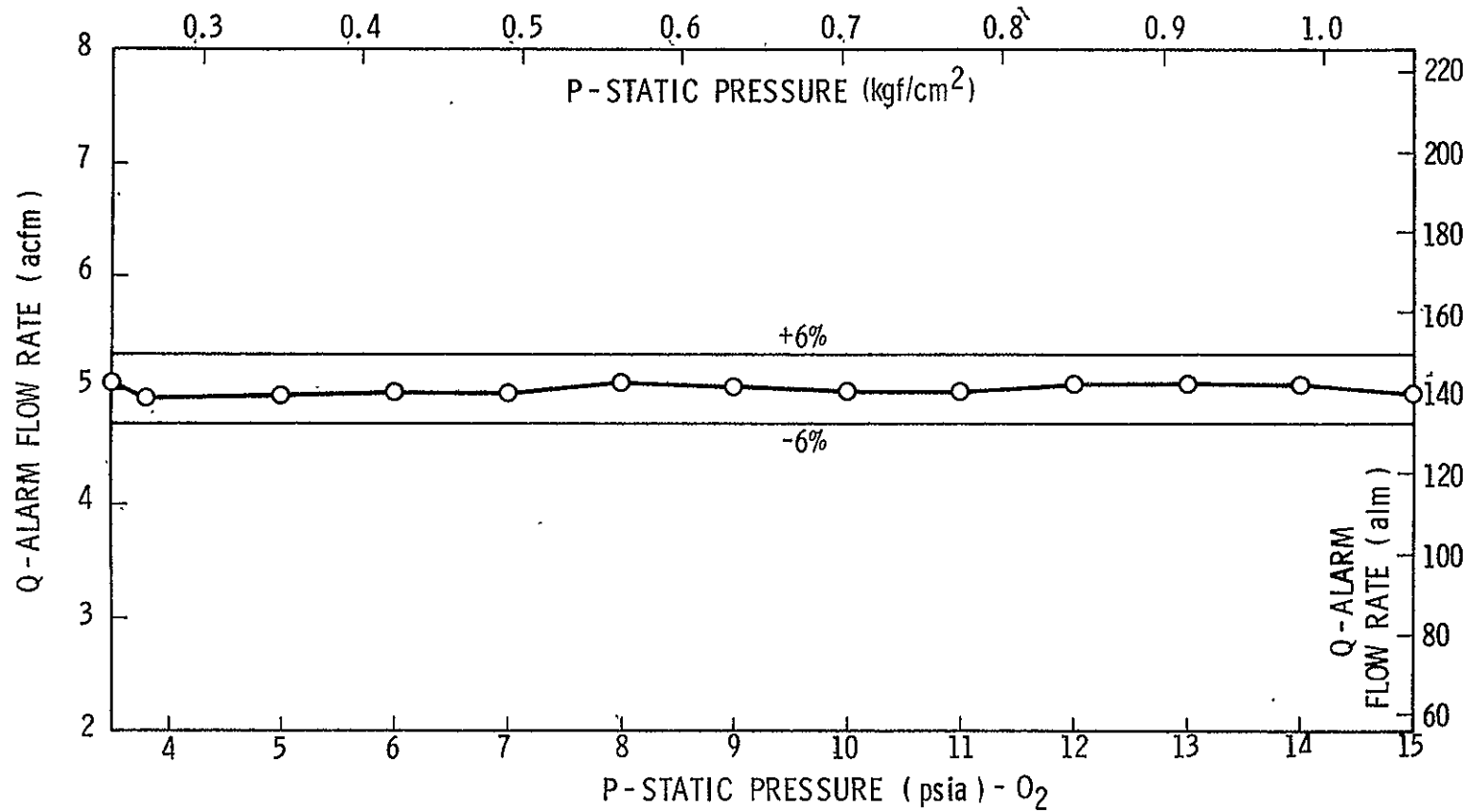
50

Figure 15.   Calculated Prototype Alarm Rate Based on Experimental ΔP vs P Measurements
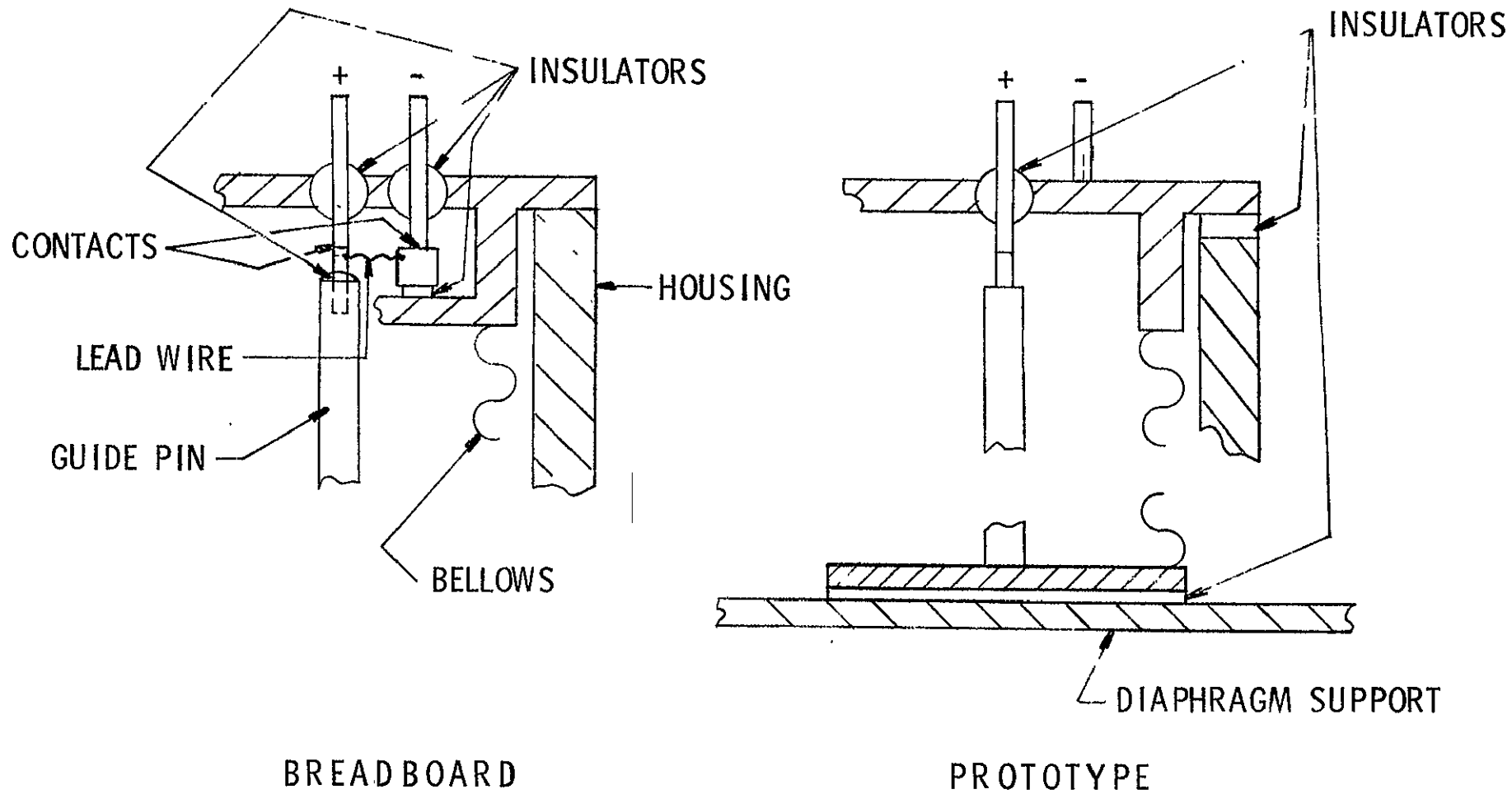
Figure 16. Breadboard and Prototype Switch Designs

52

IV. 2. 3 Prototype Design

Figure 17 shows the overall dimensions of the prototype GFI and Figure 18, an assembly drawing of the compensator, identifies all component parts. The final weight of the prototype GFI is 392 grams. Table VI summarizes the materials and fabrication techniques for the prototype GFI. Photographs of the prototype GFI, assembled and disassembled, are shown in Figures 19 and 20, respectively.

The developmental prototype GFI represents a final design which can be produced into multiple units. In addition, with a few minor exceptions, the fabrication and assembly of the developmental prototype unit was representative of that required of multiple units. The top cap of the developmental prototype unit was not evacuated nor were the electrical leads soldered to the cap feedthrough. This was done to allow NASA personnel to disassemble the unit for future inspections and evaluations.

As a result of the prototype development, several minor improvements to the prototype design were apparent. These were discussed with the NASA Technical Monitor and include:

(1) The weight (392 grams) of the GFI, although well within requirements, could easily be reduced further by removing material from the housing and from the venturi mounting bracket. The housings should also be cast for multiple unit production.

(2) The weight of the lower bellows fitting could be reduced by using a smaller sapphire bearing, and by utilizing a retaining ring in place of the nut which holds the diaphragm assembly in place. This weight reduction, in conjunction with a lighter diaphragm plate, would further decrease the position and acceleration sensitivity of the unit. The use of a retaining ring is considered to be the single most significant improvement, since it would simplify construction, reduce cost, and improve performance.

(3) The preload spring adjustment screw and the inner and outer thrust washers should be made from a hardening grade of stainless steel. All contact surfaces on these parts, as well as the Belleville washer and retaining ring, should be highly finished. These changes are recommended to prevent galling of the contact surfaces.

(4) Improved venturi electrodepositing methods and diaphragm production techniques should also be established prior to multiple unit production.

IV. 3 Prototype Test Results

IV. 3. 1 Prototype Test Plan

The test plan for the prototype GFI is presented in Table VII. The testing of the prototype GFI was essentially a repeat of the tests conducted

Dia.
4.30
(10.92)

1.2
(3.05)

5.30
(13.46)

2.64
(6.69)

0.75 Dia.
(1.91).

2.44
(6.20)
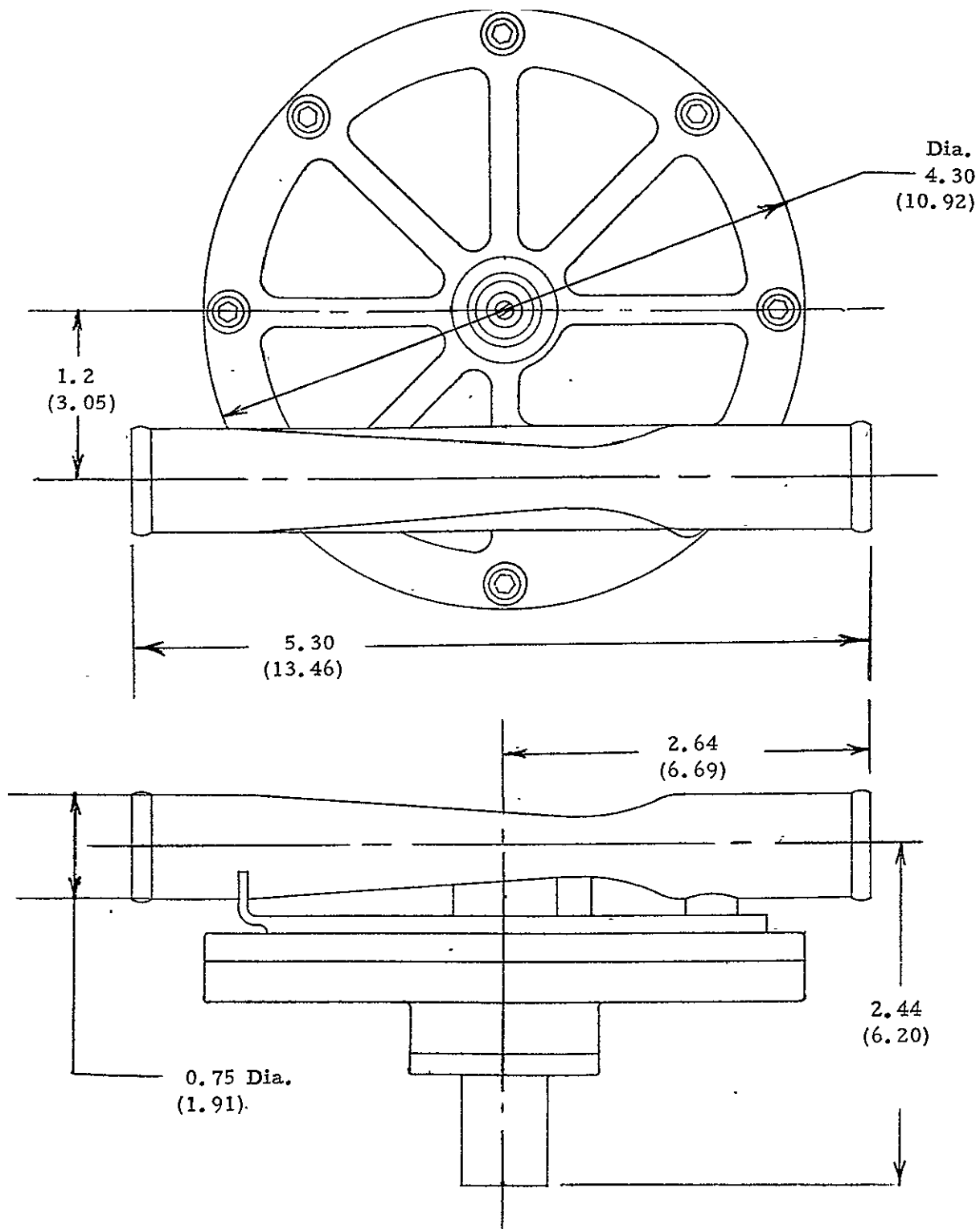
Figure 17. Overall Prototype GFI Dimensions
inches (cm)

-29   Krytox 240AC
-28   SST Safety Wire
-27   Spring
-26   "Torr Seal"
-25   TFE Tube
-24   End Seal
-23   Thread Insert
-22   Socket Hd Screw
-21   Socket Hd Screw
-20   Washer
-19   Seal
-18   "O" Ring
-17   "O" Ring
-16   Insulator
-15   Insulator

-14   Insulator
-13   Washer
-12   Nut
-11   Belleville Spring Washer
-10   Thrust Washer-Inner
-9   Thrust Washer-Outer
-8   Truarc Retaining Ring
-7   Cap
-6   Housing
-5   Cover
-4   Venturi Bracket & Assy.
-3   Aneroid Assy.
-2   Diaphragm Assy.
-1   Spring Adjustment Assy.

Seal Joints with Solder

29 Apply to all Rubbing Surfaces
28 Safety Wire Adjustment Screw and All Screw Heads
26 Apply to Threads Imme-diately Before Assembly

FIGURE 18.   GFI ASSEMBLY DRAWING OF COMPENSATOR

55

TABLE VI

PROTOTYPE GFI

MATERIALS AND FABRICATION TECHNIQUES

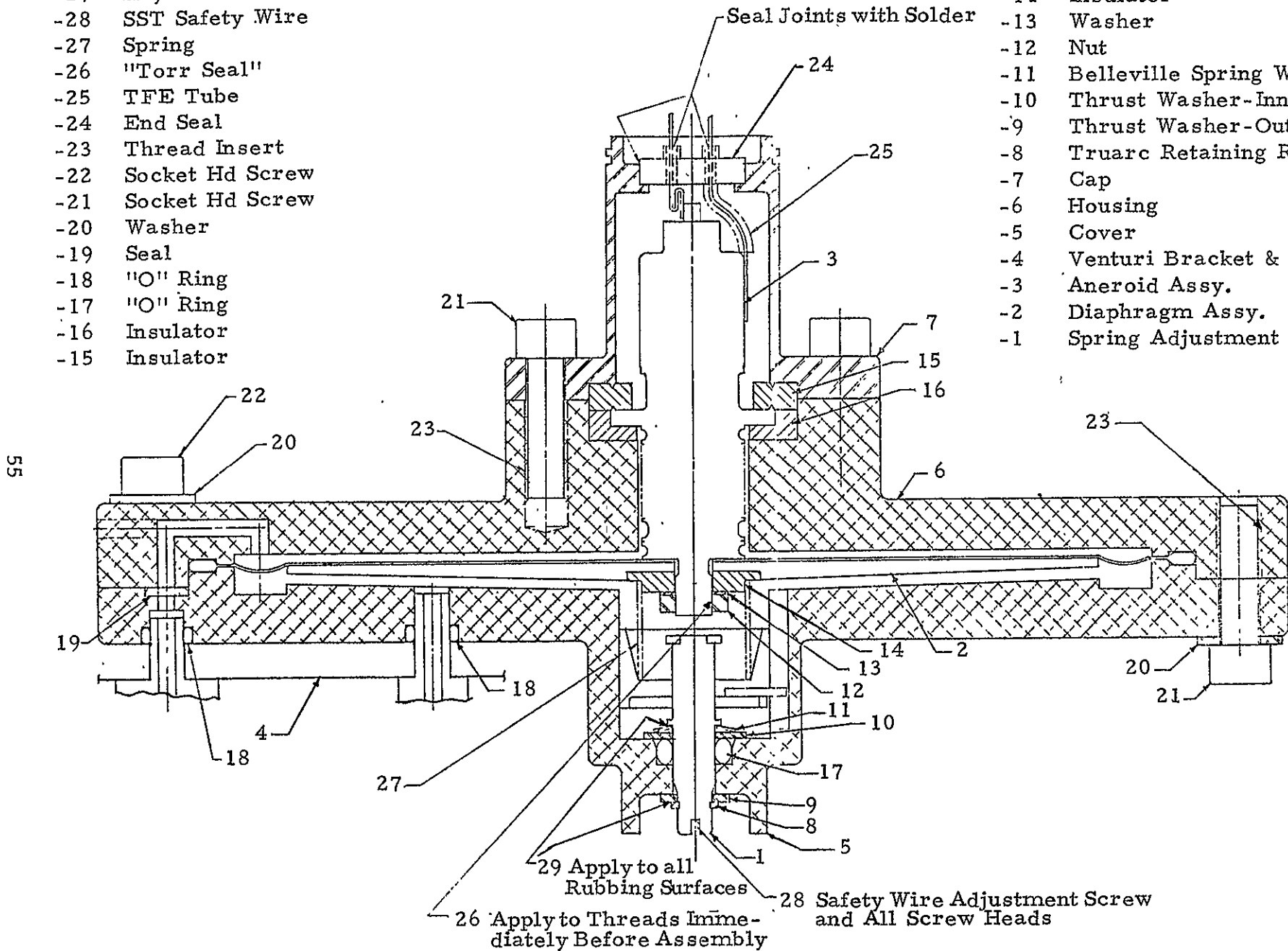| Component or Assembly	Material	Fabrication Technique
Venturi Assy:		
Tube	Nickel	Electrodeposited
Pressure port connectors	Nickel 200	Standard Machining
Bracket	304 Stainless	Standard Machining
		Components assembled by brazing.
Aneroid Bellows Assy:		
Bellows	AM 350 Stainless	Formed & T. I. G. welded
Bellows end fittings	AM 355 Stainless	Standard Machining & E. D. M.
Electrical contacts	Pd, Pt, Ag, Au, Cu, Zn alloy, (Paliney 7)	Purchased
Bearings	Single crystal sapphire	Purchased
Special electrical feedthrough	Kovar & glass	Standard Machining, glass to metal sealing by vendor
		Major components assembled by T. I. G. and electron beam welding. Contacts fastened by electron beam brazing
Main Housing Assy's:		
Housings	6061-T6 Aluminum	Standard Machining and Welding, Anodizing
Thread inserts	Stainless steel	Purchased
		Components assembled by T. I. G. welding and with standard thread insert tools

TABLE VI (Contd.)

PROTOTYPE GFI

MATERIALS AND FABRICATION TECHNIQUES

Component or Assembly	Material	Fabrication Technique
Electrical Connector Assy: Housing Std. Dual Lead Feed-through	347 Stainless Carbon steel glass	Standard Machining Purchased, nickel-plated and hot solder dipped Components assembled by soft solder
Diaphragm Assy: Diaphragm Support plate	Silicon rubber and Dacron 6061-T6 Aluminum	Molded Standard Machining, anodized Components bonded with Dow-Corning RTV 3140 or 732
Preload Spring	18-8 Stainless	Purchased, passivated
Preload Adjustment Assy: Adjustment screw Adjustment sleeve Guide tang Adjustment stop sleeve	304 Stainless	Standard Machining Components assembled by brazing and electron beam welding
Retainer (adjustment screw)	420 Stainless	Purchased
Belleville washers (adjustment screw)	302 Stainless	Purchased

TABLE VI (Contd.)

PROTOTYPE GFI

MATERIALS AND FABRICATION TECHNIQUES

| Component or Assembly	Material	Fabrication Technique
"O" Rings	Teflon	Purchased
Screws and Nuts	303 Stainless	Purchased
Bellows Insulators	Kel-F	Standard Machining
Diaphragm Plate Insulator	Kel-F	Standard Machining
Dished Washer (diaphragm to bellows screw)	304 Stainless	Standard Machining
Safety Wire	Stainless	Purchased
Misc. Assembly:		Electrical leads from dual lead feedthrough to special bellows feedthrough connected by spot welding or soft solder. Adjustment screw and all exposed fastening screws to be safety-wired by standard techniques.
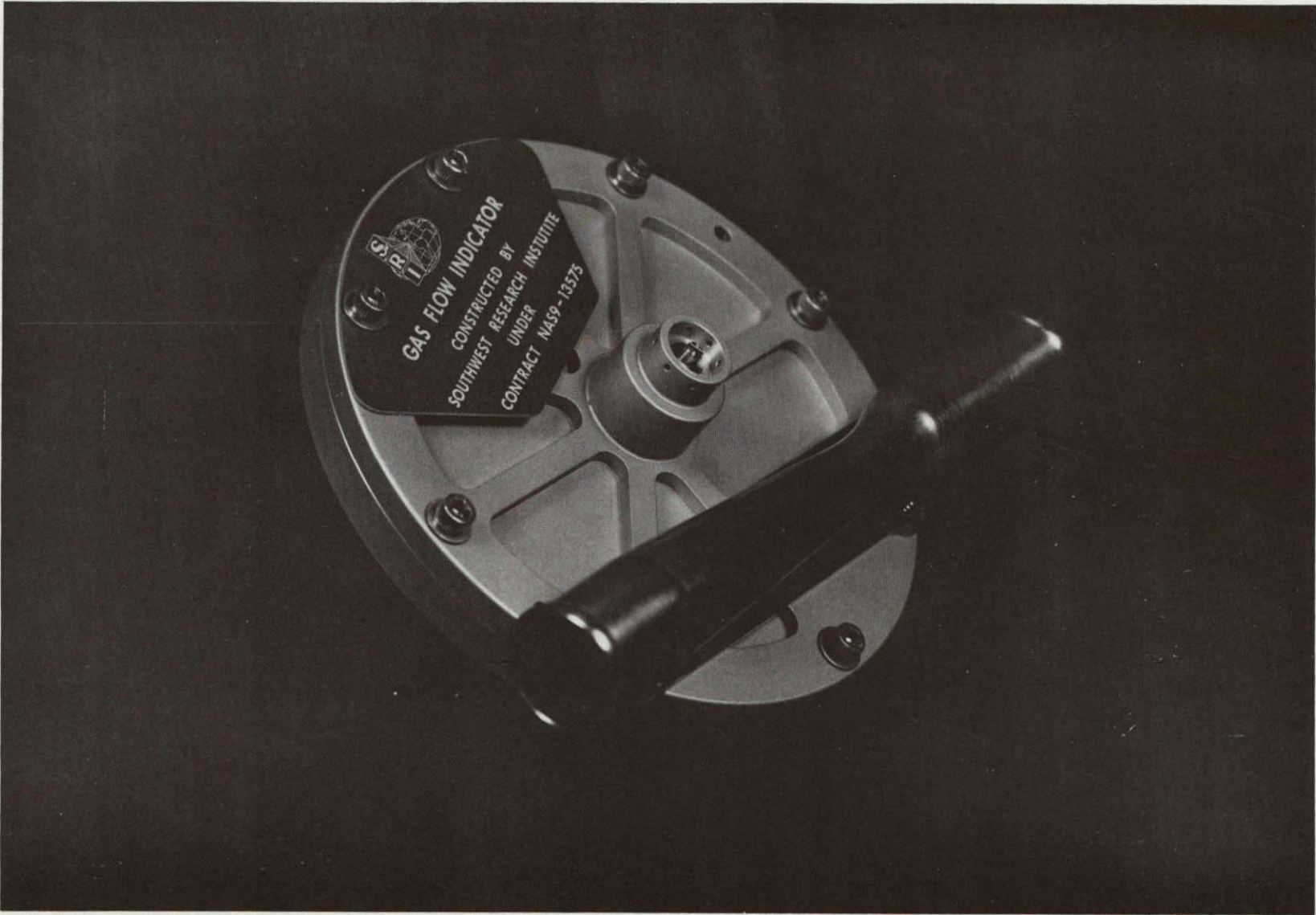
Figure 19. Assembled Prototype GFI
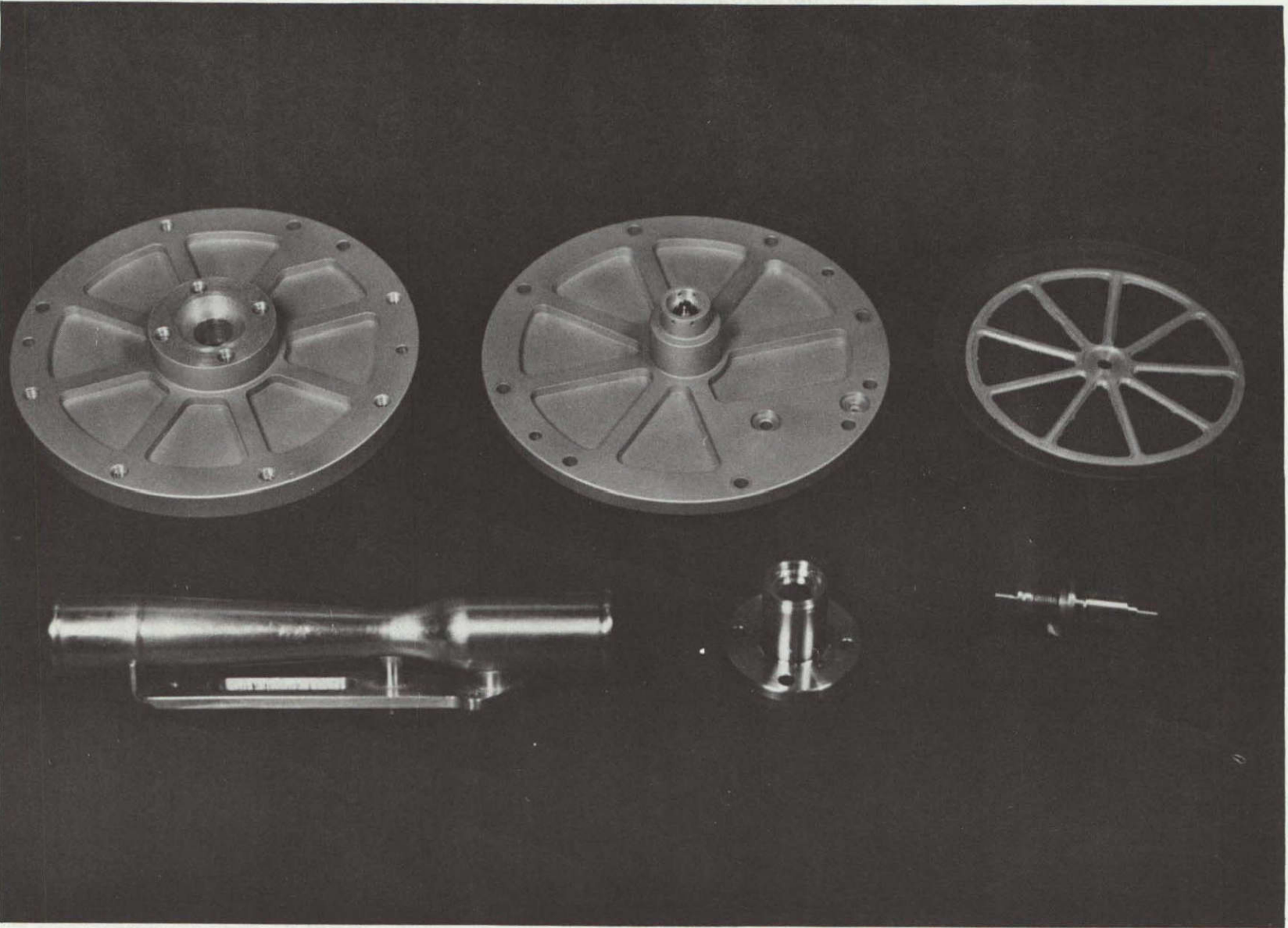
Figure 20. Primary Prototype GFI Components

TABLE VII

PROTOTYPE GFI TEST PLAN AND PROCEDURES

Operational:

(1) Shakedown and Checkout Test

    (a) Establish triggering characteristics.

    (b) Determine general operational characteristics.

(2) Determine required preload at 3.8 psia (0.27 kgf/cm^2), 5 acfm (142 alm), O_2.

(3) Determine flow rate required to trigger switch at pressures between 3.5 and 15 psia (0.25 and 1.05 kgf/cm^2) for both air and O_2. Record flow temperature at all test conditions.

(4) Determine the switch repeatability and hysteresis at 3.8 psia (0.27 kgf/cm^2).

(5) Determine GFI position sensitivity at 1-g by recording alarm flow rate at 3.8 psia (0.27 kgf/cm^2) with diaphragm

    (a) Vertical

    (b) Horizontal

    (c) At 45° to vertical

(6) Establish alarm flow rate at 3.8 psia (0.27 kgf/cm^2) with 100% humidity gas. Evaluate meter performance with moisture accumulated in compensator housing.

(7) Determine switch response at 3.8 and 15 psia (0.27 and 1.05 kgf/cm^2).

(8) Evaluate life cyclic tests based on prototype performance test and breadboard results. At end of all prototype testing, switch is tested at low current ($\sim$5 ma) and voltage ($\sim$5 volts) to establish low current triggering capability.

Environmental:

(1) Determine shock and vibration effects on meter performance.

    (a) Subject meter to harmonic excitation, 1/2-g peak-peak from 3 to 35 Hz, with the diaphragm horizontal. Recheck alarm triggering point at 3.8 psia (0.27 kgf/cm^2).

    (b) With flow rate set at 6 acfm (170 alm), subject meter to shock loading by impacting diaphragm housing to produce short duration (<100 ms), high-g (>50 g's) impulsive load. Determine if impulsive load causes meter to trigger.

    (c) Repeat (b) at flow rates between 6 acfm (170 alm) and alarm.

Structural:

(1) Subject meter to proof pressure test and recheck operation.

61

on the breadboard unit since the breadboard testing was extensive and allowed an evaluation of all performance requirements. The potentially destructive tests, such as life cyclic testing, were eliminated from the prototype test plan since (1) previous breadboard test results established performance in these areas, and (2) to reduce the likelihood of damage to the working prototype unit. All tests were conducted with the facility and procedures described in Appendix F.

IV. 3.2   Check-Out Tests

Initial check-out flow testing was performed to establish triggering characteristics and to determine the general operational characteristics of the prototype GFI. The switch was subjected to the GFI specification voltage and current of 16.8 volts and 25 milliamps, respectively. Initial flow tests were conducted by increasing and decreasing the GFI flow rate to observe switch operation. No problems were experienced with switch stickage or arcing at the specified voltage and current. In addition, repeatability of the switch triggering point was excellent. Also, no hysteresis was present in the triggering point as was the case in the initial breadboard testing. This indicates that the vendor-produced diaphragms are acceptable with respect to stiffness.

As part of the check-out tests, the preload spring was set so that the alarm would trigger at 5 acfm (142 alm) at 3.8 psia (0.27 kgf/cm^2) O_2. No readjustment of the preload spring from the original setting was required throughout the prototype testing. Since the prototype testing is probably more severe than actual usage, this indicates that the GFI should require no in-flight recalibration.

IV. 3.3   Flow Tests

Flow tests were conducted to determine the flow rate required to trigger the swtich at static pressures between 3.5 and 15 psia (0.25 and 1.05 kgf/cm^2) for both air and O_2. These test results, shown on Figure 21, reveal that the prototype GFI has the required pressure compensating characteristics. With the preload adjustment set to trigger at 5 acfm (142 alm) at 3.8 psia (0.27 kgf/cm^2) O_2, the triggering point at other static pressures remained within $\pm 1\%$ of the required alarm rate. It should be noted that some of this apparent variation occurs from difficulty in establishing flow rates accurately within 1%.

The results on Figure 21 also show that with the GFI preload adjusted to give 5 acfm (142 alm) flow rate with O_2, the alarm triggering point in air of 5.25 acfm (149 alm) is within the acceptable $\pm 6\%$ error band. The air data also exhibit the required pressure compensating characteristics.
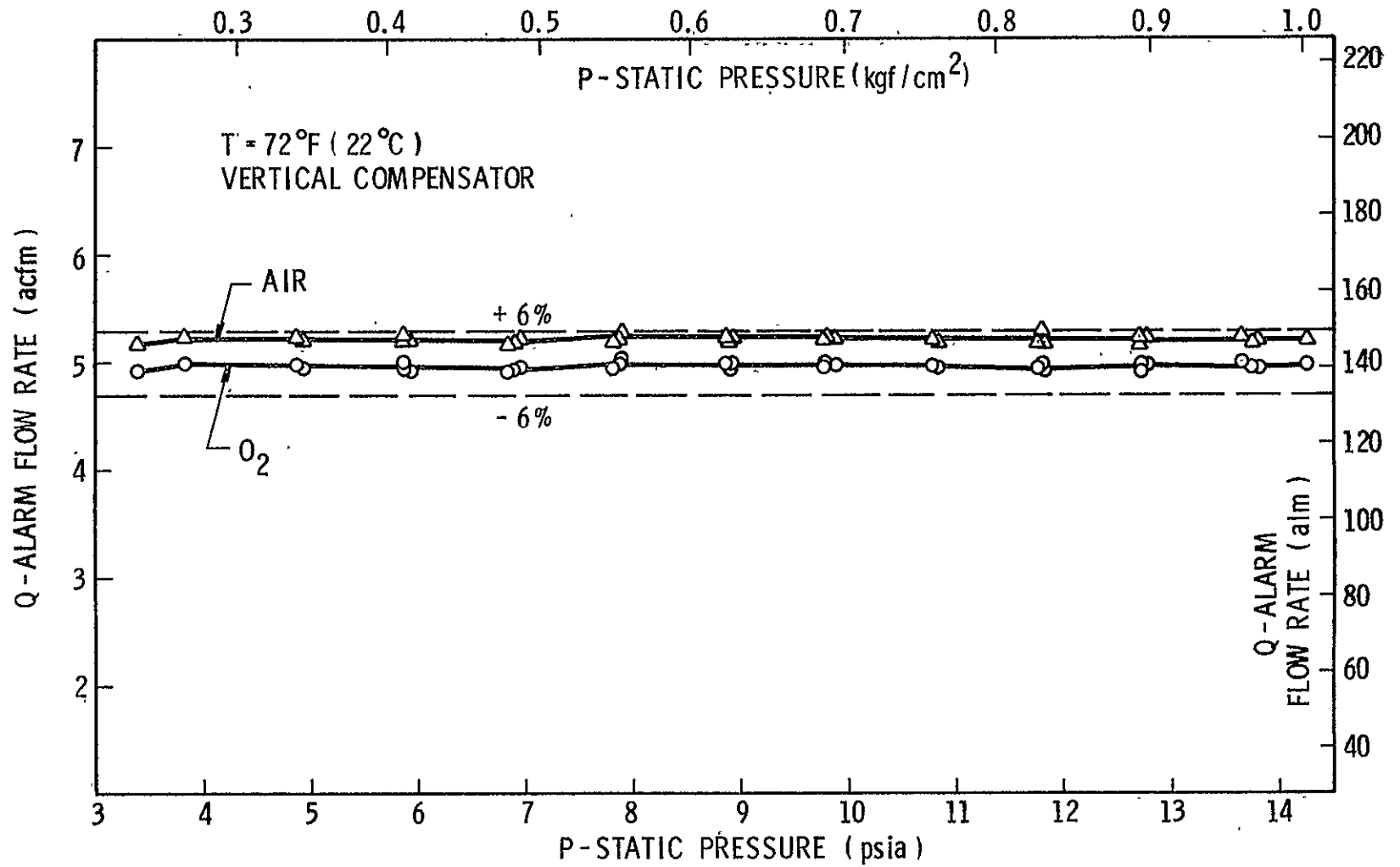
Figure 21. Prototype Alarm Q vs P for Air and O_2

The repeatability of the switch triggering point is also shown by the data on Figure 21. Excellent repeatability throughout the required static pressure range is observed. In fact, no problems with switch triggering repeatability were noted throughout the prototype test program.

IV.3.4 Position Sensitivity Tests

The results presented in Figure 21 were obtained with the compensator diaphragm in a vertical position so diaphragm weight would not introduce an undesired load on the diaphragm/aneroid assembly. To determine the sensitivity of the GFI to orientation in a 1-g environment, tests were conducted with the compensator placed at various positions with respect to the vertical. The test results are shown in Figure 22 for the GFI compensator oriented in 3 extreme positions; vertical, horizontal preload adjustment down, horizontal preload adjustment up. The results indicate a small shift in the GFI triggering point when the compensator is placed in a horizontal position. Data were also obtained with the compensator oriented at $45°$ to the vertical with both the adjustment screw up and down. The $45°$ data fell within the extremes represented by the two sets of horizontal data on Figure 22. The data obtained at all compensator orientations fell within the acceptable $\pm 6\%$ error band.

The results on Figure 22 show that the sensitivity to position is more pronounced at lower static pressures. As previously stated, this is because of the lower differential pressure forces acting on the diaphragm at reduced static pressures. The position sensitivity tests indicate that the GFI should be calibrated with the compensator in the vertical position to eliminate compensator weight effects.

IV.3.5 Switch Response Tests

The response of the prototype GFI switch was determined in the same manner as for the breadboard GFI. The flow rate was set at the normal operating condition and the pressure suddenly equalized on both sides of the compensator diaphragm by utilizing a solenoid valve between the two venturi pressure ports. The measured response was therefore the sum of the electrical response of the switch contacts plus the mechanical and fluid response of the air volume/diaphragm/bellows combination. Traces of oscillographs of the switch response are shown on Figure 23 for two flow static pressures. At the lowest and highest static pressure, the switch response is 40 and 80 milliseconds, respectively. The response measurement represents a conservative number since the time required for the solenoid valve to completely open is included. The prototype switch response is well within the required 250 milliseconds.
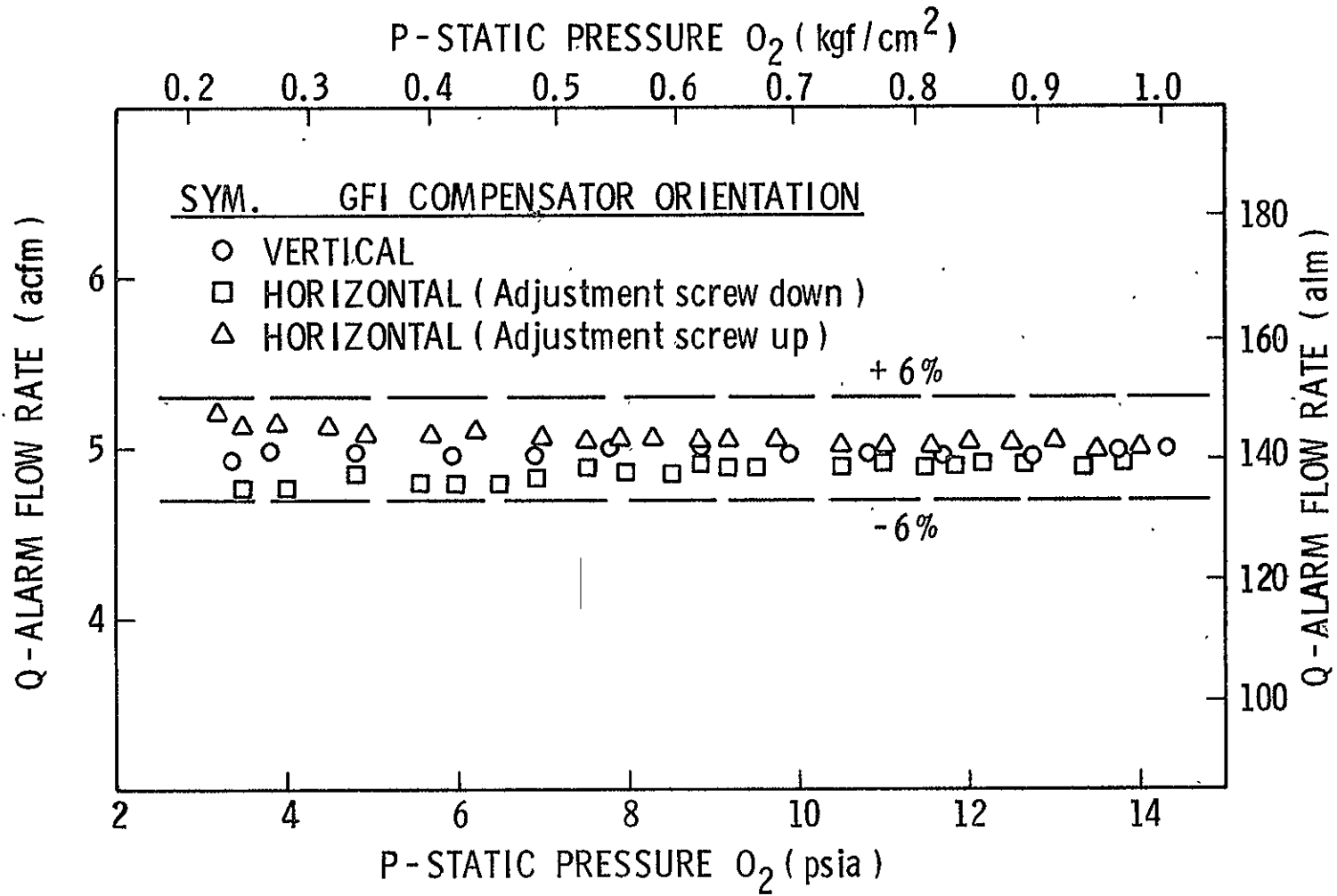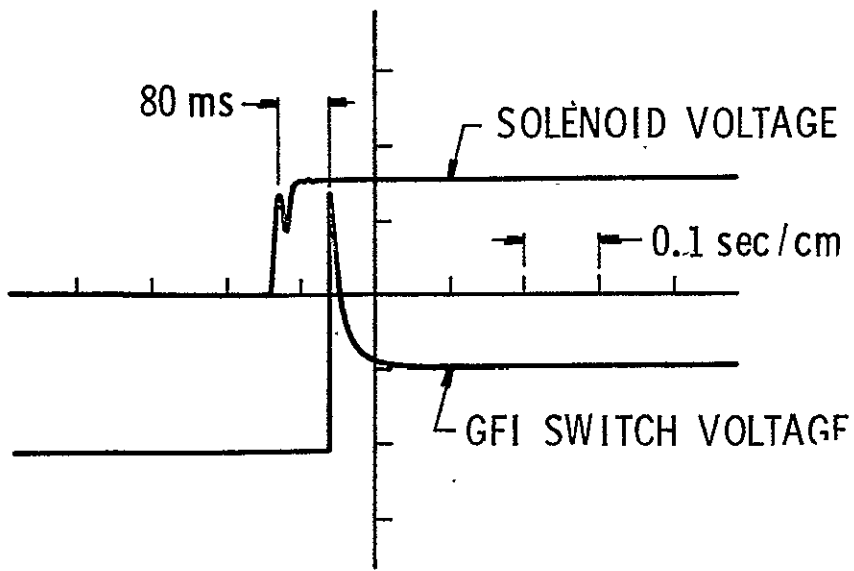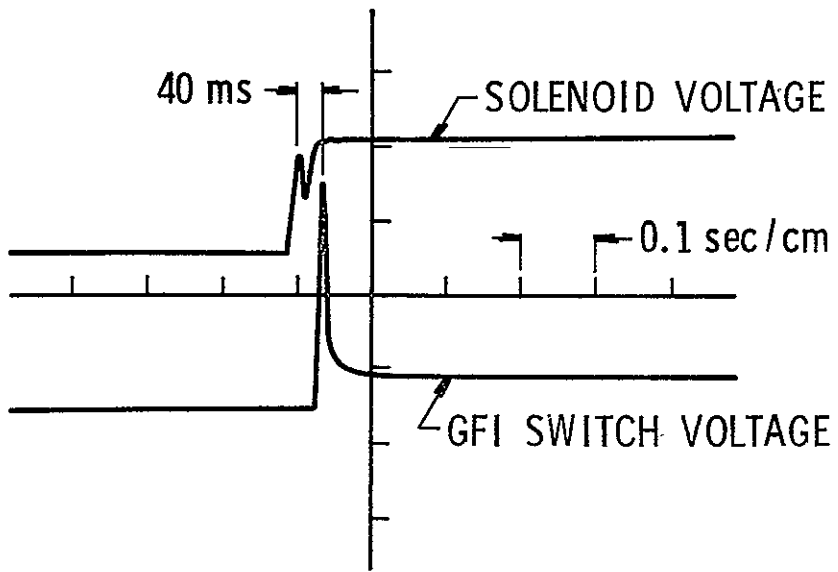
64

Figure 22. Position Sensitivity of Prototype GFI in 1g

65

(a)   P = 14.2 psia (1.0 kgf/cm^2)

(b)   P = 3.8 psia (0.27 kgf/cm^2)

Figure 23.   Prototype GFI Switch Response

IV.3.6 Vibration Tests

The integrity of the switch design was proven in the vibration testing conducted on the breadboard GFI. Additional tests were conducted on the prototype, based on NASA-furnished vibration levels pertaining to the Airlock. Prototype switch sensitivity to shock was evaluated by impacting the mechanical compensator housing with a short duration (<100 ms) 90-g impulsive load at normal operating flow and at flow rates near the alarm triggering point. Impulsive loads were applied in the direction of the aneroid axis (worst case) and were monitored by an accelerometer located on the GFI housing. No triggering of the switch was observed with the meter operating at a normal flow rate. In addition, the alarm could not be triggered at any flow rate above the pre-set alarm value. The shock loads applied in these tests are considered much more severe than the NASA Airlock shock levels which vary from 0.23 to 1.5 g, at 170 to 360 ms.

The prototype meter was harmonically vibrated with excitation in the direction of the aneroid axis, at 1/2-g peak-to-peak with a sweep rate of ~1 octave/min from 3 to 35 Hz. A subsequent recheck of meter performance revealed no change in the alarm triggering point.

No random or launch vibration level tests were conducted on the prototype GFI. Since the actual in-flight GFI vibration levels remain to be established, a final evaluation of GFI sensitivity to vibration cannot be given. However, based on anticipated levels, and vibration and shock tests conducted in this development, no problems are anticipated.

IV.3.7 High Humidity Tests

The alarm activation point was recorded with 100% humidity airflow. In order to determine the amount of moisture in the airstream, a 0.75 inch (1.91 cm) I.D. plexiglass tube was located just upstream of the GFI so the moist airflow could be observed. During testing, approximately 1/4 of the tube bottom was filled with condensate. Tests conducted with this large amount of water in the system revealed no effect on the GFI alarm triggering point. Subsequent disassembly of the compensator also indicated that water had collected inside the housing. Since it is unlikely that this much condensate would exist in a portable life support system, these tests show that the prototype GFI design should not be affected by typical moisture levels.

IV. 3. 8   Proof Pressure Tests

Proof pressure testing was conducted at the required 1.5 times the maximum operating static pressure (22.5 psia, 1.59 kgf/cm^2). The alarm triggering point at 3.8 psia (0.27 kgf/cm^2), 5 acfm (142 alm) was checked prior to and after subjecting the meter to the proof pressure. No change in the alarm triggering point was observed. The test indicated that proof pressure will not affect GFI performance.

IV. 3. 9   Life Cyclic Tests

Life cycling tests were not conducted on the prototype GFI since extensive life cycling testing was conducted on the breadboard unit. Tests on the breadboard unit revealed that the bellows/switch combination could be cycled for over 10,000 cycles without failure. The prototype GFI switch contacts are an improved design over the breadboard unit. The switch contacts in the prototype GFI are of larger diameter than the breadboard unit. In addition, the diaphragm of the prototype is smaller than the breadboard and the forces acting on the switch contacts are lower. The combination of lower force and larger contact area means that the prototype GFI switch contacts will experience less stress on each switching cycle. Therefore, the extensive life cycling testing on the breadboard unit with no failures, indicates that the prototype unit should withstand an equal number of switching cycles.

During the prototype testing, it is estimated that approximately 250 to 500 cycles of the switch contacts occurred. During all testing, no problems were experienced with switch operation and the switch triggering point remained at the pre-set value at the start of the tests. This indicates that no loss of bellows vacuum occurred. Also at the completion of all prototype tests, the switch triggered correctly at a low current and voltage of 10 ms and 4 volts. In view of this and the previous breadboard testing, we conclude that the mechanical compensator and the switch assembly should have an expected life well beyond the required 5000 life cycles. The potential for vacuum leaks from the sealed aneroid after long periods in storage was not determined experimentally, however.

IV. 3. 10   Burst Pressure and Environmental Temperature Tests

The GFI specifications require that the unit withstand a burst pressure of 30 psia (2.1 kgf/cm^2). After being subjected to this pressure, the unit is not required to be operational. The materials and dimensions of the compensator housing and venturi tube can withstand pressures well in excess of 30 psia (2.1 kgf/cm^2). Therefore, no burst pressure tests were conducted in order to prevent any possible damage to the prototype aneroid.

68

Original GFI specifications indicated that the unit could be subjected to non-use environmental temperatures between -45°F and 160°F (-43°C and 71°C). Subsequent discussions with NASA personnel indicated that a more realistic environmental temperature range is between +10°F and 130°F (-12°C and 54°C). The GFI aneroid assembly was subjected to temperatures in excess of 160°F (71°C) in the welding process, and the entire prototype unit to cold temperatures near the +10°F (-12°C) point. In addition, the design of all components accounted for the anticipated thermal expansions that would occur between -45°F and 160°F (-43°C and 71°C). Therefore, both design and actual in-use test conditions indicate that the GFI should withstand the anticipated environmental temperatures. No extensive thermal cycling tests were conducted, however.

IV.4 Failure Modes Analysis

A failure modes analysis was conducted to determine what effect different types of failure modes would have on GFI operation. In addition, the means of detecting these types of failure modes was also established. The results are tabulated in Table VIII for five different types of possible failure modes. The failure modes shown on Table VIII are listed in their order of most-likely occurrence. For a partial loss of bellows vacuum, the alarm triggering point will be reduced from its pre-set value. A complete loss of vacuum would result in the alarm triggering point occurring at approximately zero flow if the preload force is removed. Since the switch contacts may be slightly touching with no preload, a small flow rate may be required to disconnect the alarm. The means of detection for the other failure modes are indicated on Table VIII.

IV.5 Prototype GFI Conclusions

The results of the prototype GFI development indicate that completely pressure-compensating prototype GFI meeting all NASA requirements has been developed. The prototype unit has been constructed to eliminate problems experienced with the previous Apollo GFI's and should provide a trouble-free method of PLSS gas flow indication.

T.

FAILU

EFFECTS AND

Failure Mode	Effect	Means of Detection

1) Loss of Bellows Vacuum
  • Complete Loss
 	
  . Partial Loss
	Alarm triggers below 5 acfm (142 alm)
	" " " " " "
		Remove preload; no alarm at $Q \cong 0$.
		Calibration Check

2) Ruptured Diaphragm	Alarm at all Q	Alarm at $Q > 5$ acfm (142 alm)

3) Plugged Pressure Port
  • High Pressure
  • Low Pressure
	Alarm at all Q
	Alarm triggers below 5 acfm (142 alm)
		Alarm at $Q > 5$ acfm (142 alm)
		Calibration Check

4) Inoperative Switch Contacts
  • Broken-open
  • Welded shut
	No alarm at any Q
	Alarm at all Q
		No alarm at $Q = 0$
		Alarm at $Q > 5$ acfm (142 alm)

5) Broken Preload Spring	Alarm below $Q =$ 5 acfm (142 alm)	Calibration Check

V. CONCLUSIONS AND RECOMMENDATIONS

V. 1 Summary and Conclusions

A three-part program has been conducted to develop a Gas Flow Indicator (GFI) to monitor ventilation flow in a portable life support system. The first program phase identified concepts which could potentially meet the GFI requirements. In the second phase, a working breadboard GFI, based on the concept of a pressure sensing diaphragm-aneroid assembly connected to a venturi, was constructed and tested. Extensive testing of the breadboard GFI indicated that the design would meet all NASA requirements including eliminating problems experienced with the ventilation flow sensor used in the Apollo program. In the third program phase, an optimized GFI was designed by utilizing test data obtained on the breadboard unit. A prototype unit was constructed using prototype materials and fabrication techniques with several major components manufactured by outside vendors. Performance tests indicated that the prototype GFI met or exceeded all requirements.

V. 2 Recommendations

It is recommended that the mechanically compensated venturi GFI be developed into flight qualified hardware. The prototype GFI design should be updated to provide several minor improvements that were established during prototype evaluations (see Section IV. 2. 3). Multiple units should be constructed and extensive performance tests conducted to more completely establish flight hardware long term performance. Tests should include subjecting the units to realistic vibration spectra, thermal cycling tests and extended life cyclic tests. Based on the composite test results of all units, the GFI design should be finalized and flight qualified hardware produced.

APPENDIX A

HEATED TRACER GFI

HEATED TRACER GFI

Tracer methods are ideal when gas monitoring has to be accomplished under a wide range of operating conditions. Tracer methods present a direct measure of gas velocity by measuring the time required for a tracer to travel a known distance. Knowledge of the gas flow velocity, the velocity profile and the duct cross-sectional area at the flow monitoring location allows the flow rate to be directly inferred from the tracer travel time.

Operational Principles

Consider the heated tracer system shown in Figure A-1. The tracer path is located along the axis of the duct and the centerline velocity, $V_{\mathcal{L}}$, is measured. The gas flow through the duct is given by

$$Q = A V_{av} \tag{1}$$

where A and V_{av} are the duct cross-sectional area and average flow velocity respectively. The centerline velocity, $V_{\mathcal{L}}$, in terms of V_{av} is given by

$$V_{\mathcal{L}} = K V_{av} \tag{2}$$

where K is determined by the velocity profile shape. If K does not change with flow conditions, the flow rate can be determined directly by measuring $V_{\mathcal{L}}$. Since the travel time of the gas tracer is given by

$$\tau = \ell / V_{\mathcal{L}} \tag{3}$$

then

$$Q = \frac{A\ell}{K\tau} = C/\tau \tag{4}$$

which is independent of gas properties and dependent only on tracer travel time so long as changes in K are negligible.

Tracer Methods

Two tracer techniques which have been successfully demonstrated for monitoring gas flows are the ion tracer method[1,2]* and the heated tracer method[3,4]. In the former case, a small volume (tracer) of the gas stream is ionized by one of several possible methods. The heated tracer device operates in the same fashion, except that the tracer is a minute volume of gas heated as it passes a small wire. The heated tracer source consists of a pulsed heated wire. When the wire is subjected to a short duration current pulse, a circular zone of heated air results. This heated air is then propagated with the air stream at a velocity $V_{\tilde{C}}$ as shown in Figure A-1. Passage of the heated air past a temperature sensor gives a signal output after the time delay, τ , from heating pulse to sensor output. A discussion of both tracer methods is given in Reference 5.
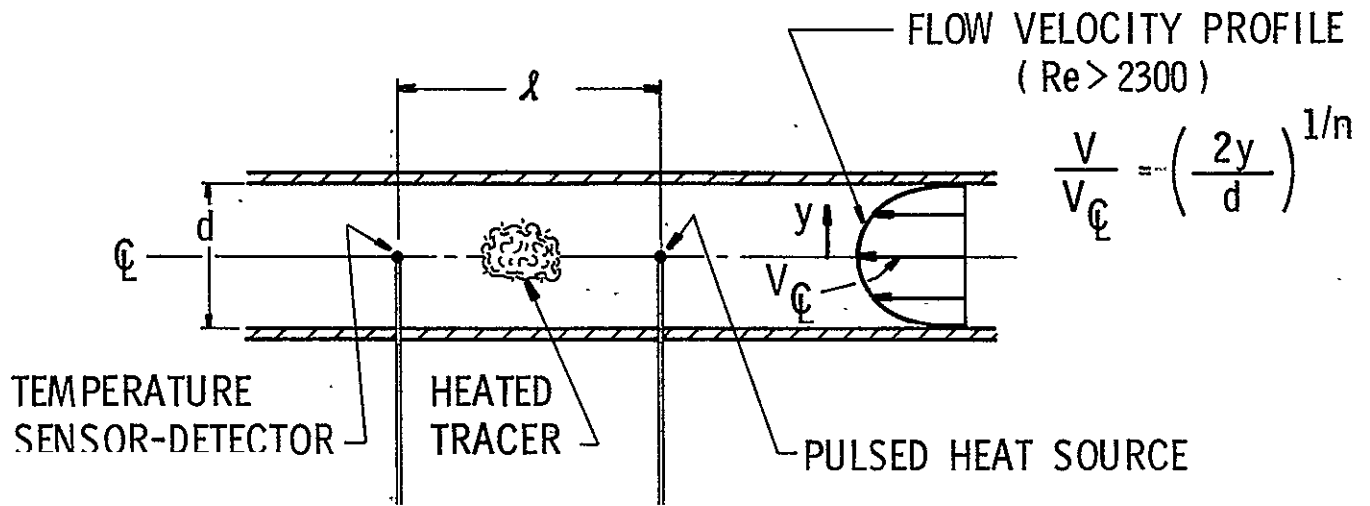
Error Sources.

For the present application the heated gas tracer has the most promise in meeting the GFI specifications since it requires less power and is safer than the ion tracer method. As indicated by Equation 4, the measurement of the tracer transient time, τ , between two sensors gives a direct indication of gas flow. Ideally this method gives an absolute flow indication meaning no calibration should be required. In actual practice, the method is subject to various sources of error which cause difficulties when flow measurements are attempted. These error sources are:

a) response of the source and detector wires,

b) dispersion of the heated gas,

c) buoyancy of the heated gas, and

d) change in flow profile with Reynolds number change.

Buoyancy problems can be eliminated when measurement velocities are large, and the distance between the tracer source and detector probe is small so travel times are minimized.

Problems with dispersion can be reduced by seeking the correct travel time from the sensor output as indicated in Figure A-2. The peak of the sensor output represents the true travel time, and therefore, any electronics must be designed to seek the peak of the detected hot gas signal. Also, travel times must be maintained at a minimum to ensure that diffusion does not reduce the cloud temperature to a point where detection is difficult.

*Superscript numbers in text denote references which are listed at the end of Appendix A.

FLOW VELOCITY PROFILE (Re > 2300)

$$\frac{V}{V_{\mathbb{C}}} = \left(\frac{2y}{d}\right)^{1/n}$$

TEMPERATURE SENSOR-DETECTOR

HEATED TRACER

PULSED HEAT SOURCE

$$Q = \frac{\pi d^2}{4} V_{av}$$

$$V_{av} = V_{\mathbb{C}} / K = \frac{\ell}{\tau K}$$

$$K = \frac{(n+1)(2n+1)}{2n^2}$$

$$Q = Cf$$

Re	n	K
≤ 2300	–	2
4 000	6	1.22
23 000	6.6	1.24
110 000	7.0	1.26

Figure A-1. Heated Gas Tracer Schematic and Important Parameters
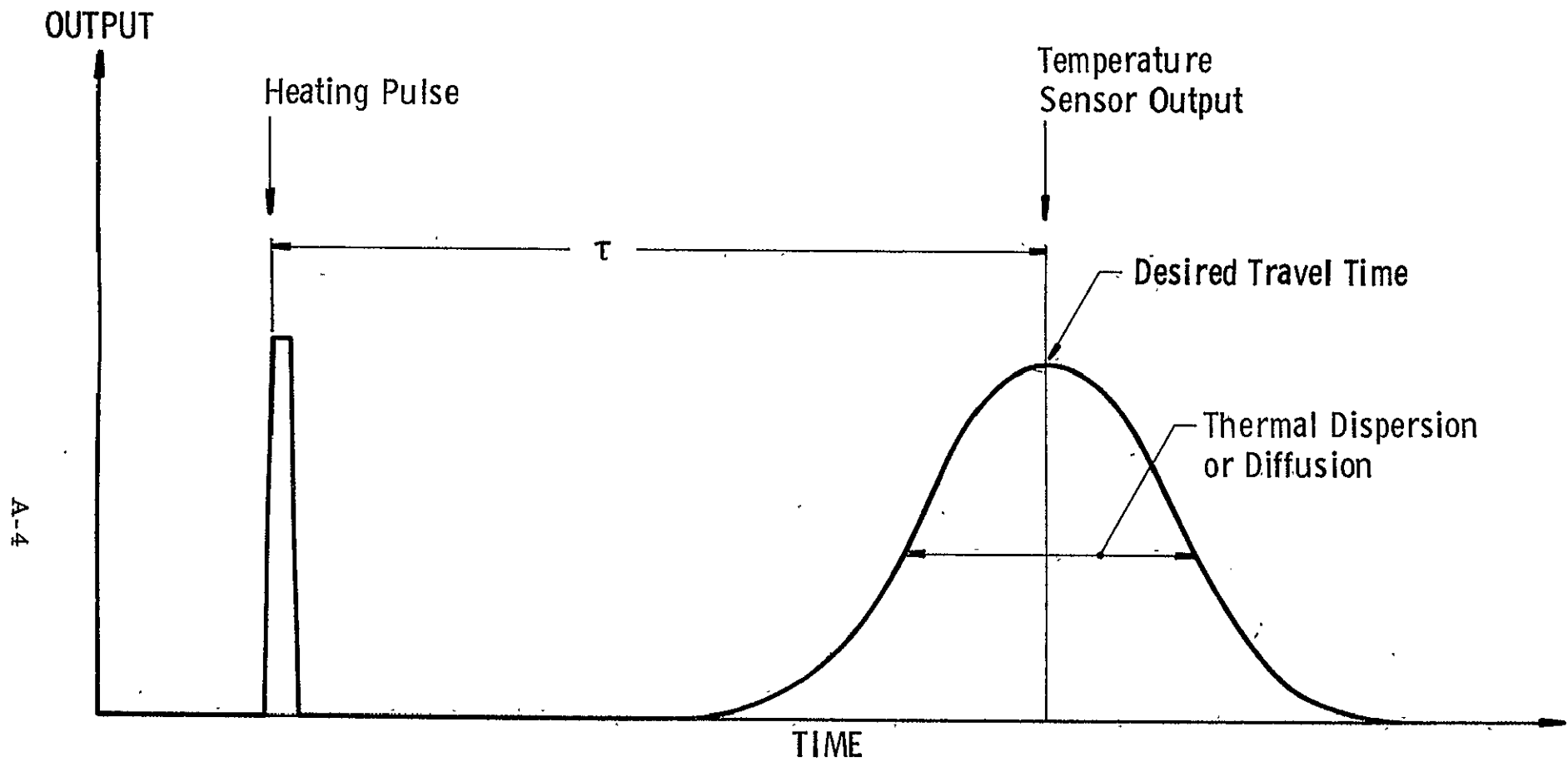
τ = True transient time of Heated Gas

Figure A-2. Desired Travel Time with Heated Tracers

Problems with velocity profile change with Reynolds number are negligible if Re is maintained in the appropriate range and the duct geometry at the measurement location is shaped properly.

One of the most difficult sources of error to overcome results from the time delay created by the thermal lag of the source and detector wires. The ideal travel time (τ) of the gas tracer was given by Equation 3; however, in an actual system, the travel time is

$$\tau^1 = \tau + \tau_s + \tau_d \tag{5}$$

where

τ_s = time to generate heat source (rise time of voltage pulse plus thermal lag of source wire)

τ_d = time delay of detected cloud due to thermal inertial of detector wire

The error in travel time created by τ_s and τ_d is given by

$$E = \frac{\tau_d + \tau_s}{\tau + \tau_d + \tau_s} \tag{6}$$

For a 6% error (0.3 acfm/5.0 acfm) the minimum tracer travel time (in ms) is given by

$$\tau_{min} = 15.7 \left(\tau_s + \tau_d \right) \tag{7}$$

Therefore, to reduce tracer travel time to eliminate the effects of dispersion and buoyancy and keep the instrument small, the delays due to thermal inertia must be small.

To estimate the effects of wire size on probe response, the following analysis was performed for both the source and detector probes. An energy balance on the source probe yields

$$\overset{(1)}{\overline{Q} \sin\frac{\pi\tau}{\tau_1}} - \overset{(2)}{\rho \, \Psi \, C_p \frac{dT}{d\tau}} = \overset{(3)}{hA \left(T - T_g \right)} \tag{8}$$

A-5

where

(1) -   Energy input to source wire (assumed a half-sine wave)

(2) -   Change in internal energy of source wire during $d\tau$

(3) -   Net heat flow from source wire to gas stream during $d\tau$.

and

C_p = specific heat of the wire

ρ = density of the wire

V =· wire volume

A = wire surface

T = wire temperature

T_g = gas temperature

dT = temperature change during $d\tau$

h = forced convection heat transfer coefficient

$\overline{Q}$ = amplitude of input energy pulse

τ_1 = period of input pulse

The solution of this equation with the boundary condition ($T = T_g$ @ $\tau = 0$) is

$$\frac{T - T_g}{\overline{Q}/hA} = \frac{\sqrt{1 + (C^1/m)^2}}{1 + (C^1/m)^2} \left[\sin \delta \; e^{-m\tau} + \sin (C^1 \tau - \delta) \right] \tag{9}$$

where

C^1 = π/τ_1

δ = $\tan^{-1} (C^1/m)$

m = $hA/\rho V C_p$

A-6

This equation can be used to determine the temperature-time history of the source wire as a function of input energy wave form, wire properties and wire geometry.

When the heated cloud leaves the source probe, it diffuses in space as it travels between the source and detector wire. If the travel time between the source and detector wire is too great, the cloud will diffuse to the point where its temperature is so low that it cannot be detected with any degree of accuracy. To determine the effects of diffusion with a hot gas cloud, the temperature time-history at the center of a heated point source was calculated using the following equation[6]

$$\frac{T - T_g}{T_w - T_g} = \frac{4/3 \pi S^3}{(4 \alpha \pi \tau)^{3/2}} \tag{10}$$

where

S = radius of the heated cloud.

α = thermal diffusivity of the gas cloud

T_w = initial temperature of the cloud = max source wire temperature

τ = time difference between $T = T_w$ and $T = T$

This equation can be used to determine the decay in tracer temperature as a function of travel time τ. Figure A-3 shows the decay of the cloud center temperature as a function of time for various volumes of heated gas tracer. The results indicate that for small volumes of heated gas, the temperature at the center of the cloud decays rapidly from the maximum wire value at pulse generation.

The response of the detector wire to the passing gas cloud was also analyzed to determine the detection delay time, τ_d. Performing an energy balance on the detector wire yields

$$\rho \, C_p \, \forall \frac{dT}{d\tau} = hA \, (T_c - T) \tag{11}$$

where

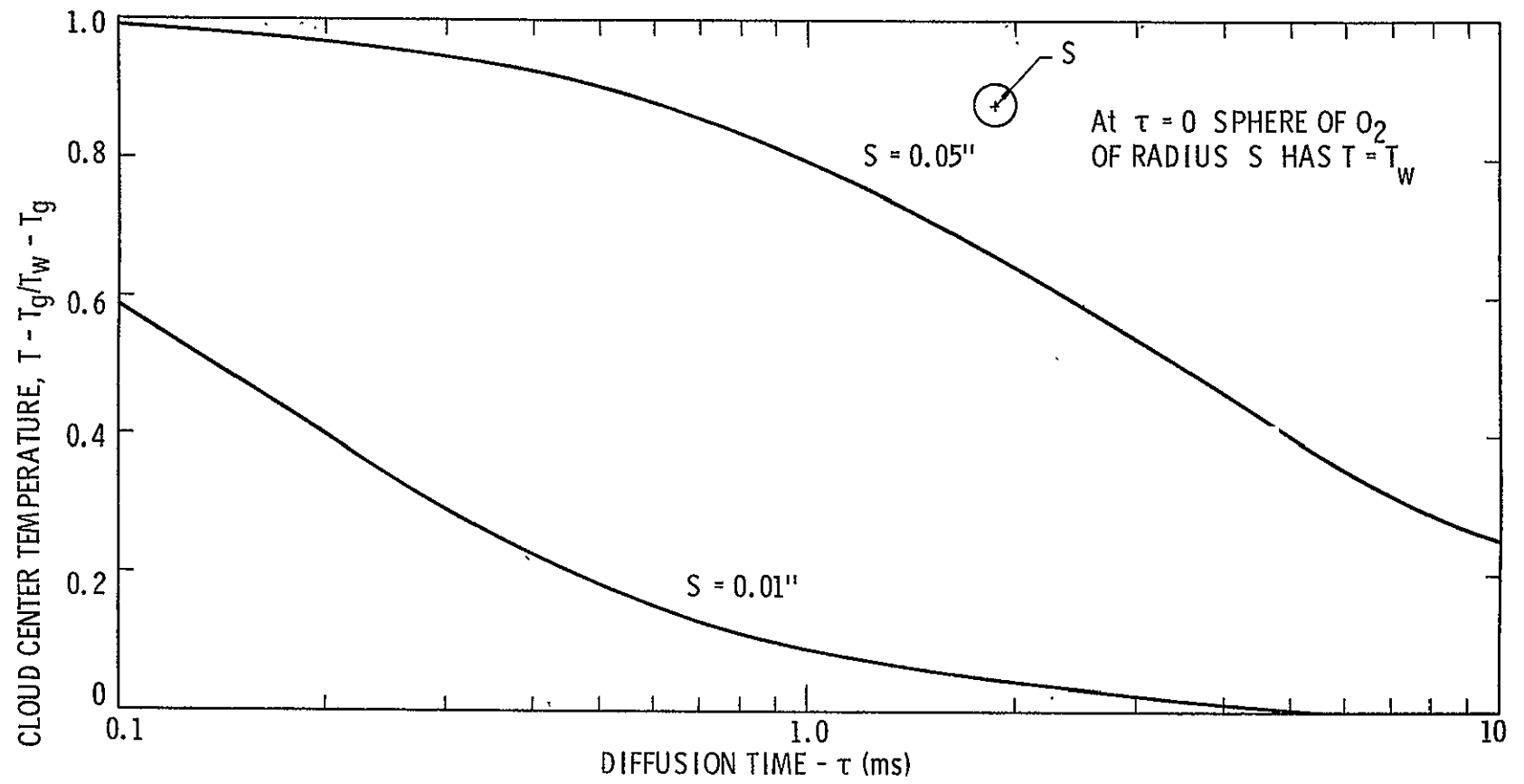T_c = gas cloud temperature distribution

T = detector wire temperature

Figure A-3. Diffusion of Heated Gas Cloud

Assuming at $\tau = 0$, $T = T_g$ and that the gas cloud temperature distribution is given by

$$T_c = C (T_w - T_g) \sin \frac{\pi \tau}{\tau_2} + T_g$$

where

C = a fraction reflecting a reduction in the gas cloud peak temperature resulting from diffusion

τ_2 = period of the gas cloud

The solution of equation (11) is

$$\frac{T - T_g}{C (T_w - T_g)} = \frac{\sqrt{1 + \left(\frac{\pi}{\tau_2 m}\right)^2}}{1 + \left(\frac{\pi}{\tau_2 m}\right)^2} \left[\sin \delta \, e^{-m\tau} + \sin \left(\frac{\pi \tau}{\tau_2 m}\right) - \delta \right] \tag{12}$$

where

$$\delta = \tan^{-1} \left(\frac{\pi}{\tau_2 m}\right) \tag{13}$$

Equation (12) can be used to determine the response of the detector probe to the heated tracer.

Implementation of Heated Tracer Method

Various methods are available to implement the heated tracer technique. One method is a pulse-regenerative or "sing-around" method where the detected tracer retriggers the tracer source and the frequency, f, of the retrigger pulses gives a direct measure of the flow rate. Therefore, the GFI flow rate is given by

$$Q = Cf \tag{14}$$

A possible pulse regenerative circuit for electronically implementing this scheme is shown in Figure A-4. A Pulse Circuit, upon receiving a trigger signal from the Starting or Shaping circuits emits a pulse signal
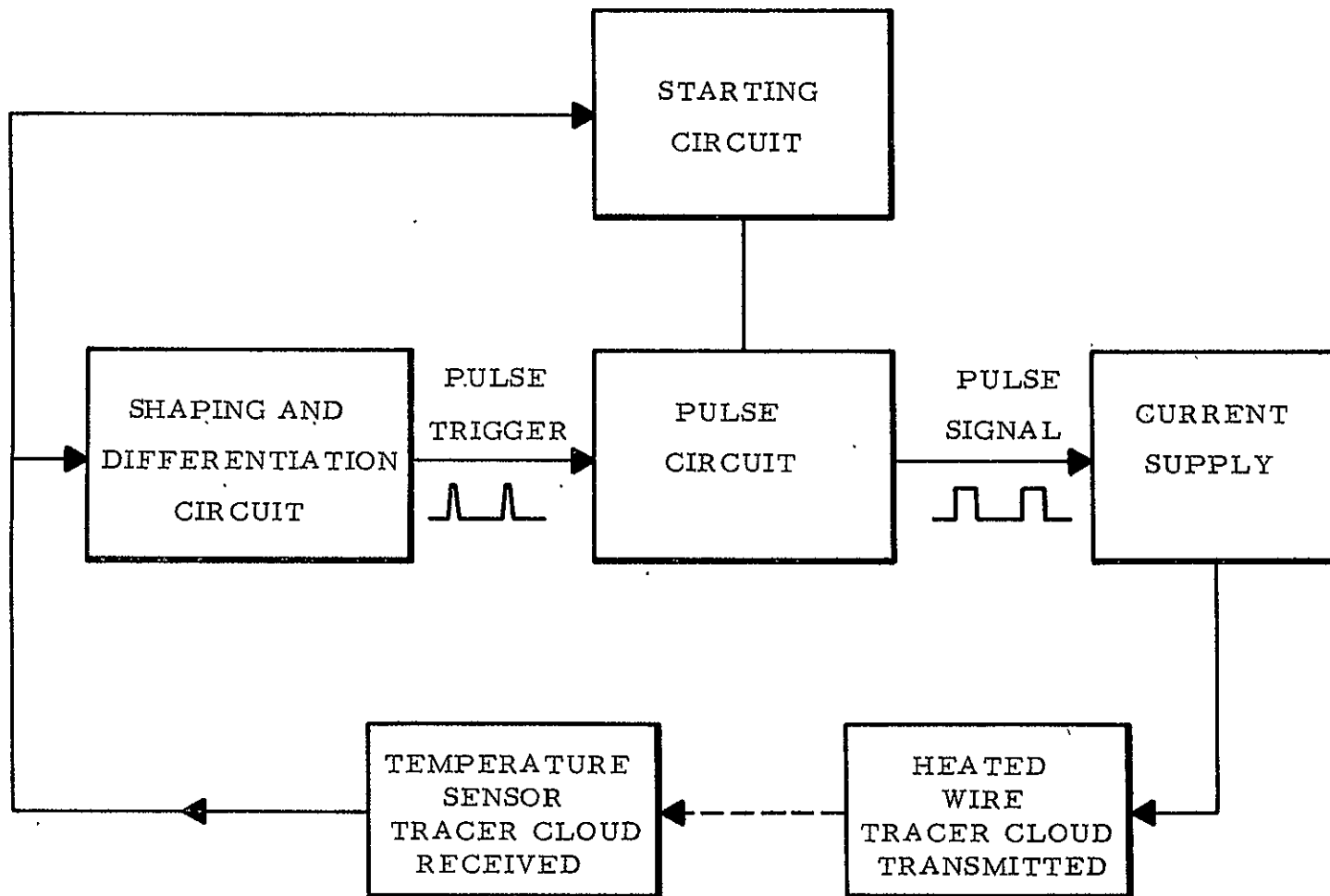
A-9

Figure A-4. Block Diagram of Electronics for Pulse Heated Wire GFI Measurement Device

of certain controlled duration which causes heating of the source wire.
After the transport delay, τ^1, the Temperature Sensor feeds a regenerative signal back through the Shaping Circuit which, in turn, retriggers the Pulse Circuit. The electronics required in each block shown in Figure A-4 are implemented with existing, low cost, solid state analog devices. Circuitry of this type was successfully used in the ion tracer anemometer described in Reference 7.

An alternate method for implementing the heated tracer technique is used in an instrument developed by K-West Co.[8] for the Airlock portion of the Skylab program. This system uses a constant pulse rate at the source wire and measures the time-of-flight of a slug of air heated to slightly above ambient temperature. The arrival of the thermal pulse is detected by a quasi-correlation technique, which permits measurements at signal to thermal-background-noise ratios of less than one to one. The electronics for this method appear more complex than the pulse-regenerative method with the primary advantage being the ability to process a poorer detector signal.

Several types of temperature sensors are available. However, the chosen sensor must have the required sensitivity and frequency response. Possible candidates are small wires, thermistors or commercially available probes such as DISA manufactures. Whichever implementation is used, both the source and detector wires must have rapid response to eliminate errors in the measured travel time of the tracer. Therefore, small, delicate, fast response probes are inherent to this device.

Preliminary Design Considerations

The results in the previous section have been utilized to provide preliminary design information for use in evaluating the heated tracer GFI. As part of this effort the various sources of error were evaluated; power requirements were estimated and final instrument size and weight were estimated.

Flow Profile Effects

Figure A-5 shows Reynolds number vs kinematic viscosity for reasonable GFI duct diameters at Q = 5 acfm. The kinematic viscosity range shown on Figure A-5 covers the spectrum of specified operating conditions. This figure indicates that laminar flow may be difficult to maintain over all conditions of temperature, pressure and gas composition. However, the factor, K, for Re's above the laminar region
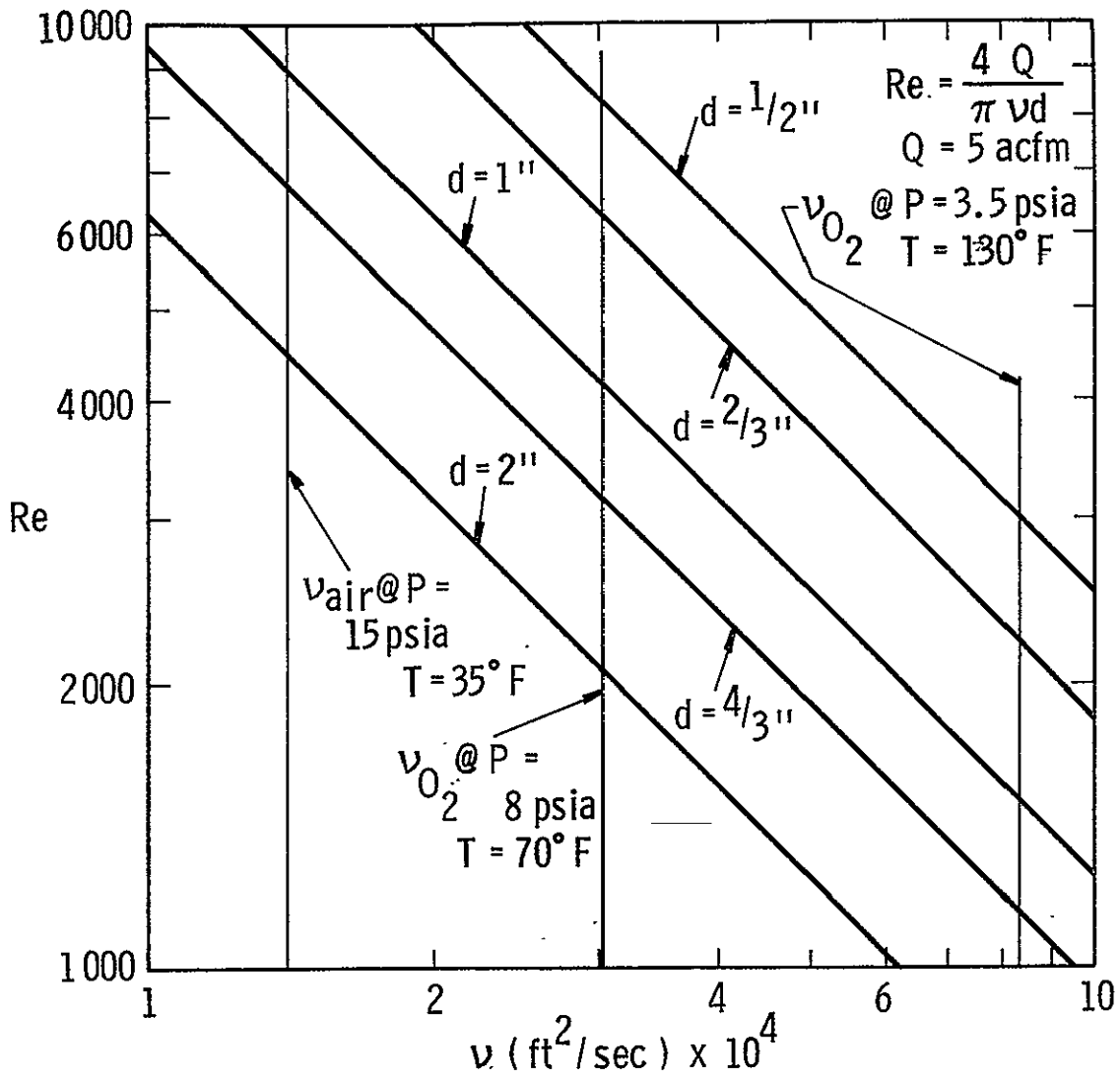
Figure A-5. Reynolds No. versus Kinematic Viscosity @ Q = 5 acfm

is given by

$$\frac{1}{K} = \frac{V_{av}}{V_{\mathcal{L}}} = \frac{2n^2}{(n+1)(2n+1)}$$

where n and K as a function of Re are given in the following table

Re	n	K
$\leq 2.3 \times 10^3$	---	2.0
4.0×10^3	6.0	1.26
2.3×10^4	6.6	1.24
1.1×10^5	7.0	1.22

This table indicates that if the GFI Reynolds number is maintained above 2300, and fully developed turbulent flow is present, only a 2% change in K will occur for $4 \times 10^3 < Re < 3 \times 10^4$.

Figure A-6 is a plot of Reynolds number versus flow rate for various diameter GFI ducts at the highest value of ν. This figure shows that a reasonable duct diameter of 1/2 inch will result in a Re > 2300 at flow rates above 3.8 acfm. If the transition Re = 2300, the GFI will operate in the turbulent flow regime from 7 acfm down to a flow rate well below the alarm value. Any change in profile because of transition to laminar flow will cause the meter to indicate a higher than actual flow rate; however, if this transition occurs at a low rate relative to the alarm value, the GFI will still indicate an alarm flow rate, and the alarm will not deactuate.

Transition from laminar to turbulent flow is sometimes delayed to Re's greater than 2300 with the actual transition Re depending on upstream flow disturbances. This possible source of measurement error created by profile change will have to be established experimentally; however, if the tracer transport path is located off the duct $\mathcal{L}$ the variation in K with Re will be reduced. Also, the values of K in the previous table are for fully developed velocity profiles and the tracer path can be located just downstream of a contraction where profiles are relatively flat regardless of Re. Therefore a variety of methods exist to reduce inaccuracies from flow profile changes.

$$R_e = \frac{4}{\pi} \frac{Q}{d\nu}$$

$\nu = 8.35 \times 10^{-4} \text{ ft}^2/\text{sec}$

O_2 @ 3.5 psia, 130° F

$R_e = 2300$

$d = 1/4''$

$d = 1/8''$

$d = 1/2''$

$d = 5/8''$

$d = 3/4''$

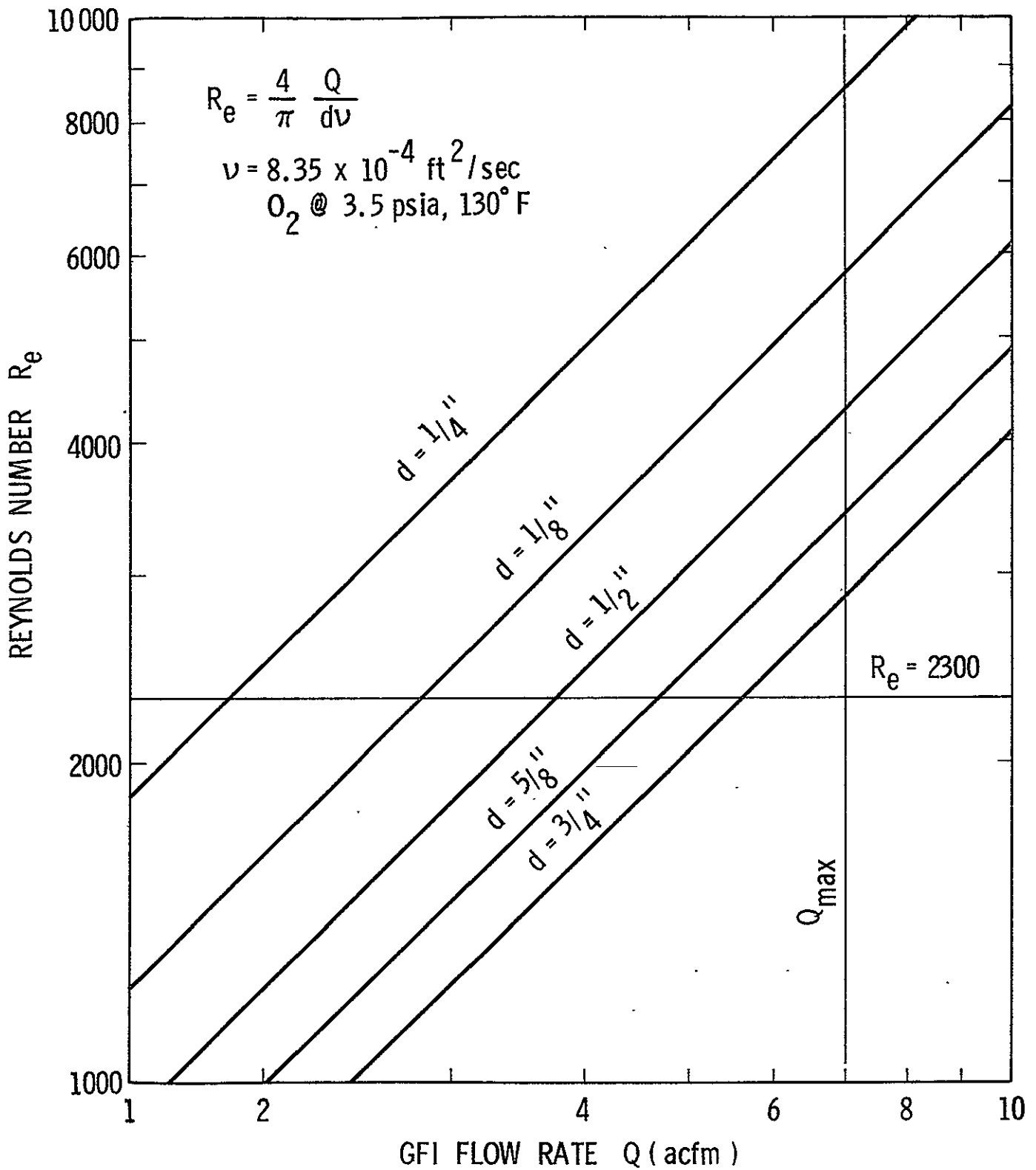Q_{max}

REYNOLDS NUMBER R_e

GFI FLOW RATE Q (acfm)

Figure A-6. Reynolds Number versus GFI Flow Rate @ $\nu = 8.35 \times 10^5 \text{ ft}^2/\text{sec}$

Figure A-7 shows the GFI average duct velocity versus flow rate for realistic duct diameters. For the 1/2 inch diameter duct the average flow velocity will range between 0 and 86 ft/sec.

Probe Response Characteristics

The smallest wires that are available for detector or source probes are on the order of $d_w = .0002$ inches. Delay times, τ_d and τ_s were calculated for a 1/8"-0.2 mil platinum wire, since a wire of this size would result in the smallest possible error due to time delays.

In determining probe response characteristics, the following conditions were assumed for purposes of calculating the heat transfer coefficient, h. These conditions are

$$T_g \quad\quad = \quad 35°F$$

$$T_w - T_g \quad = \quad 250°F$$

$$T_a \quad\quad = \quad (T_w + T_g)/2$$

$$V_g \quad\quad = \quad 60 \text{ fps}$$

$$P_{O_2} \quad\quad = \quad 8 \text{ psia}$$

and h is given by

$$\frac{h \, d_w}{K_{O_2}} = C_1 \, (\text{Re})^{C_2}$$

where C_1 and C_2 are functions of Re based on d_w and all gas properties are evaluated at T_a.

Figure A-8 shows the source response for various input pulse widths. The curves indicate that wider pulse widths result in a larger value of peak wire temperature, T_w. The greatest possible value of $\left[T - T_g /(Q/hA) \right]$ is 1.0 which would determine the final wire temperature if a steady state energy of Q was applied to the source wire.
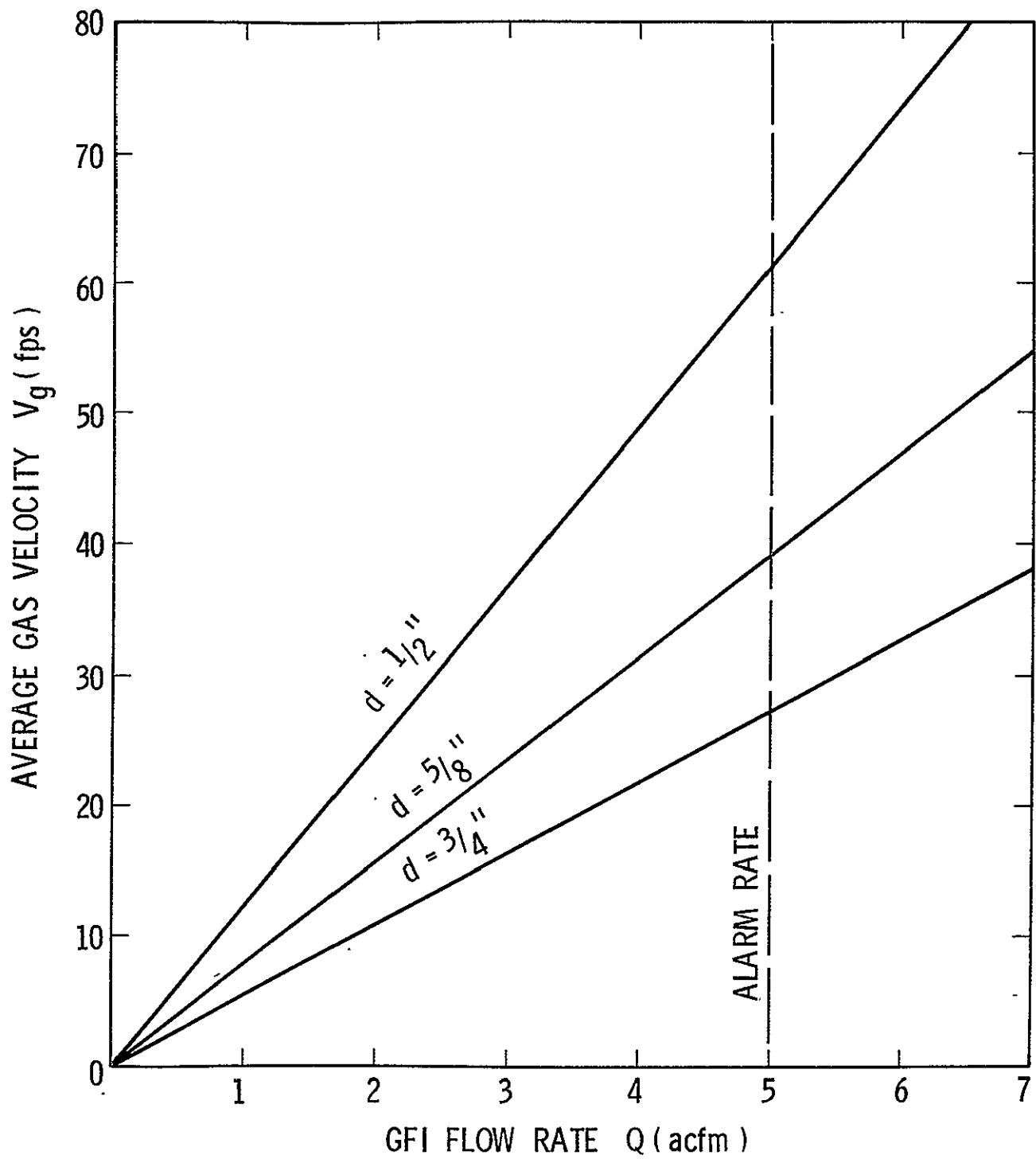
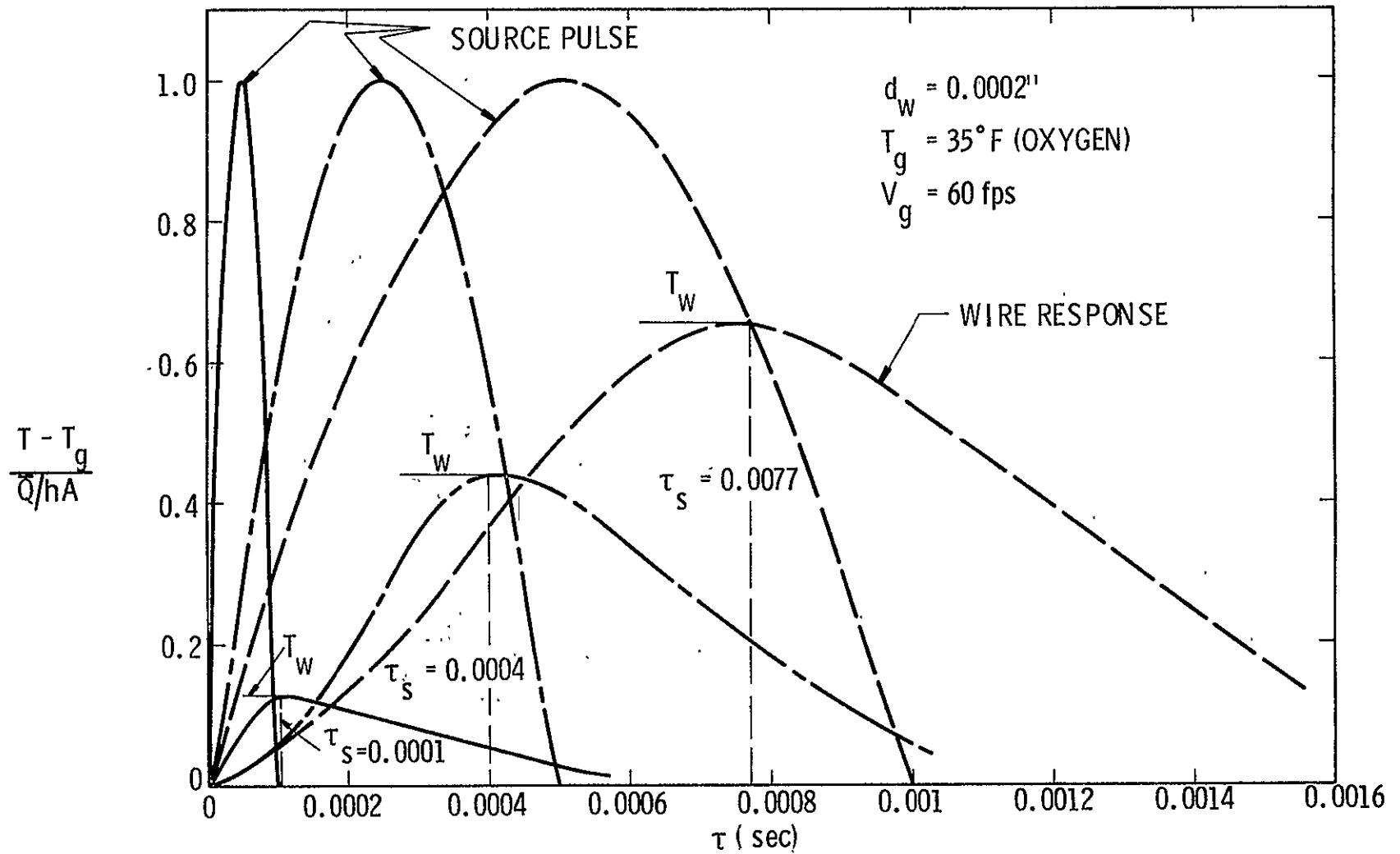Figure A-7. Average Duct Velocity versus Flow Rate

A-16

Figure A-8. Source Wire Response vs Input Waveform

Figure A-8 also shows the trade-off between obtaining maximum wire temperature and minimum delay time between the peak wire temperature and the initiation of the source pulse. Typical values of τ_s range from 0.1 to 0.8 ms. For larger diameter wires, the peak temperature values and delay times become correspondingly worse.

Response of the detector wire is shown in Figure A-9a and b for a passing hot gas cloud with two different base time periods. Since the true travel time of the gas cloud occurs at its peak, the delay at the detector wire, τ_d, is represented by the time difference between the passage of the peak of the hot gas cloud and the peak temperature response of the detector wire. Results in Figure is typically on the order of .25 - .5 milliseconds. In addition, the results show that there is a reduction between the temperature in the passing cloud and the peak response temperature of the detector wire. The results also indicate that the more diffused gas clouds create a larger time delay, but the peak detector wire temperature is closer to the gas cloud value. Larger wires increase delay time and reduce maximum recorded temperature as evidenced by the 1 mil wire results in Figure A-9a.

The results in Figures A-3, A-8, and A-9 were used to determine the heated tracer GFI geometry required to give the needed measurement accuracy. Previous discussions on profile characteristics have indicated that a diameter of 1/2 inch is optimum. Utilizing this diameter and the typical delay times for the source and detector probe of 0.1 and 0.4 ms respectively, a minimum travel time given by Equation (6) is 7.75 milliseconds. The separation distance, ℓ, between detector and source probe to produce a travel time of 7.75 milliseconds in an 1/2 inch diameter duct at 5 acfm is 5.8 inches.

Therefore to maintain instrument accuracy at 6%, at the alarm flow rate, requires $\ell \cong 6$ inches when utilizing 0.2 mil probes. Larger probes will cause a greater probe separation distance to maintain the 6% error at 5 acfm.

Knowledge of the duct diameter, flow rate and separation distance allows an estimate of the probability of buoyancy induced error. At the alarm flow rate of 5 acfm, a 0.5 inch diameter GFI would have an average flow velocity $\cong 60$ fps. At 60 fps and $\ell = 6$ inches, $\tau = 8.3$ milliseconds. Since typical cloud deflections due to buoyancy in 8 ms are on the order of .05 inches no buoyancy problems are anticipated.

L-2

A-18

$$T_c = T_g + C(T_W - T_g) \sin \left(\frac{\pi \tau}{.001} \right)$$

$\Delta \tau$ $\tau_d = 0.25 \, ms$

$\frac{T - T_g}{C(T_W - T_g)}$

T

$d_W = 0.2 \, mils$

T

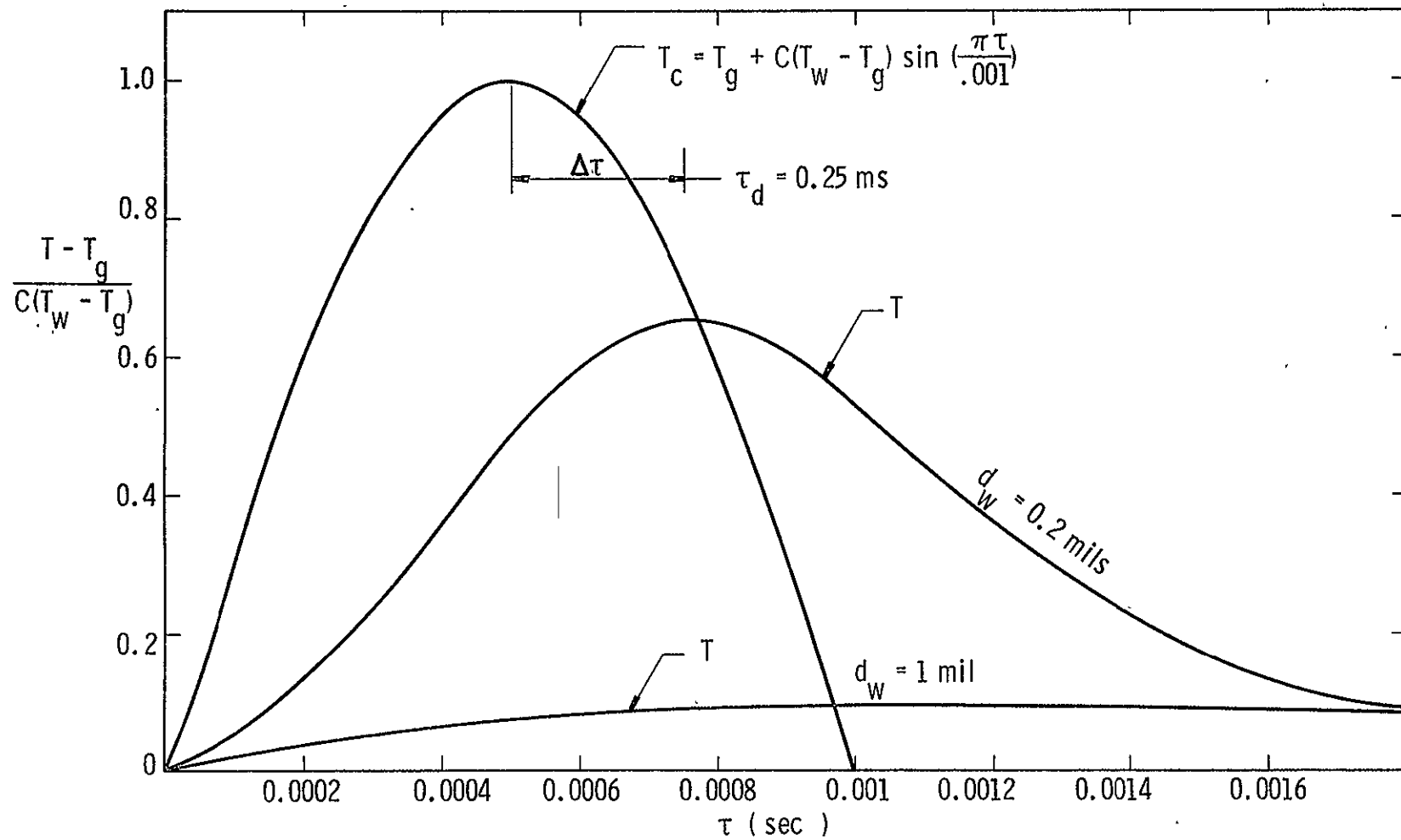$d_W = 1 \, mil$

$\tau \; (sec)$

Figure A-9a.   Detector Wire Response to Heated Tracer Cloud of 1 ms Duration
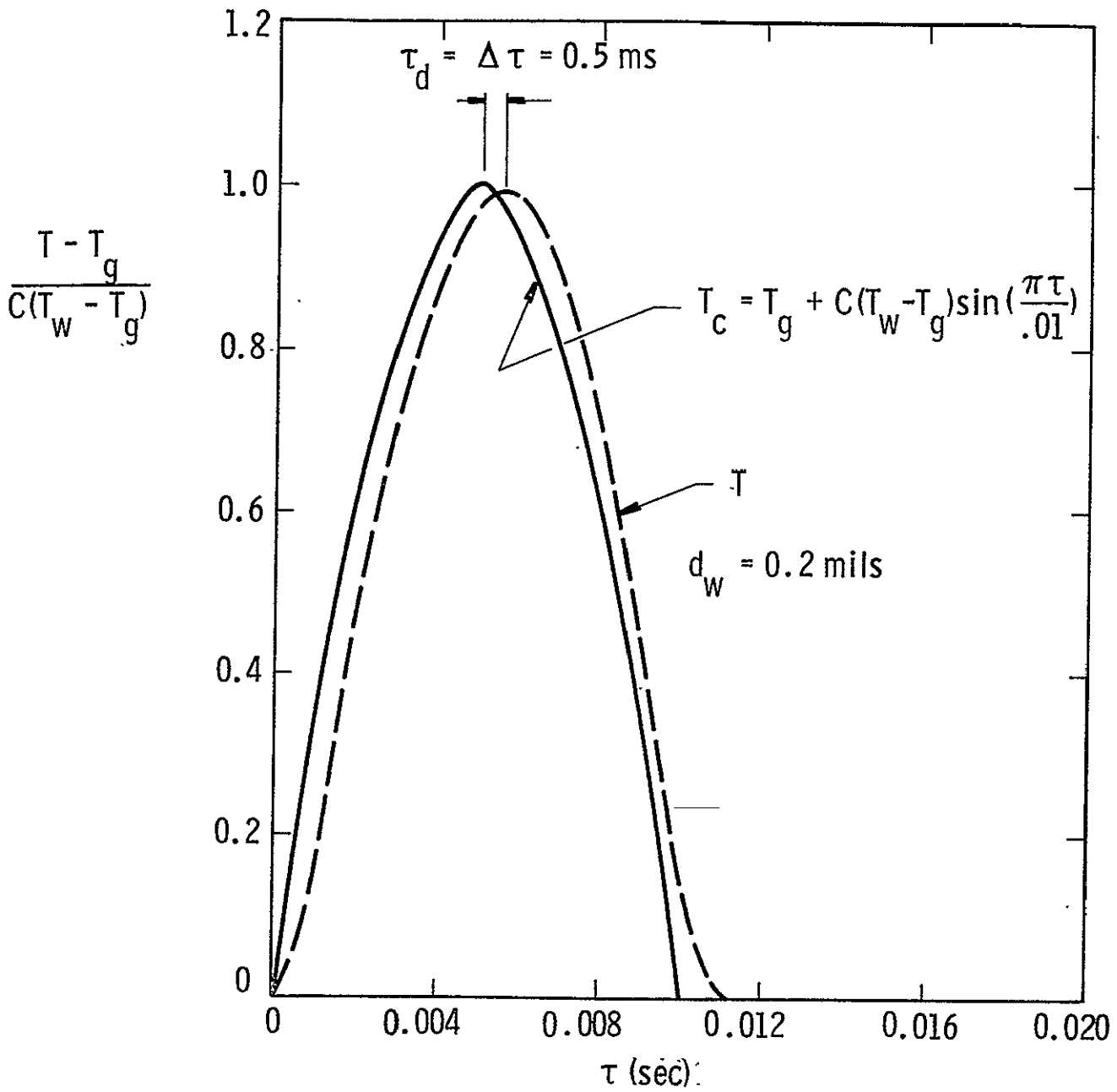
Figure A-9b. Detector Wire Response to Heated Tracer Cloud of 10ms Duration

$$\tau_d = \Delta\tau = 0.5\,\text{ms}$$

$$T_c = T_g + C(T_w - T_g)\sin\left(\frac{\pi\tau}{.01}\right)$$

$$\dot{T}$$

$$d_w = 0.2\,\text{mils}$$

$$\frac{T - T_g}{C(T_w - T_g)}$$

$$\tau\ (\text{sec})$$

A-20

Power Requirements

The results of the previous analysis can be used to determine the power input required to provide an operational GFI. Enough power must be supplied to the source probe to allow sufficient temperature at the detector in order that the passing gas cloud can be easily observed. Power input to the source must consider that

1) the maximum source wire temperature is reduced in a pulsed situation, for a given energy input amplitude, due to thermal inertia of the source wire,

2) the heated tracer temperature is reduced due to diffusion as the tracer travels between the source and detector, and

3) the maximum detector temperature is lower than the passing heated tracer temperature due to thermal response of the detector wire.

For example, if $T_w - T_g = 250°F$ and a 0.1 millisecond pulse period is utilized to trigger the detector wire, then the peak power amplitude, Q, required to produce the maximum wire temperature of $250°F$ above the gas stream temperature is .446 watts.

Next, turning to the effects of diffusion, Figure A-8 is used to estimate the heated cloud temperature at the detector wire. Since tracer travel times are on the order of 10 milliseconds, the results in Figure A-8 indicate that the temperature of the gas cloud at the detector will be about 25% of the source wire temperature, or for $T_w - T_g = 250°F$, $T - T_g \cong 60°F$. Referring to Figure A-9, the peak detector wire temperature will be between 65 and 90% of the cloud temperature at the detector wire, therefore the maximum detector temperature will be approximately $40°F$ above the free-stream gas temperature. This is sufficient for detection in most systems and indicates that a .446 watt input power amplitude should provide an ample tracer.

Other power requirements result from the necessary signal processing circuitry. An estimate of this power based on using circuitry similar to that given in Reference 7 is 0.5 watts maximum. An additional power requirement of 0.5 watts for the alarm triggering circuit is required for a final estimate of 1.5 watts of total power consumption.

Weight, Volume and Pressure Drop Characteristics

Figure A-10 shows an overall view of the heated tracer GFI indicating the important dimensions. Essentially the design consists of a long tube which carries the gas flow past the source and detector probes which are placed at the required separation distance. The electronic circuitry is located in a case which is attached to the flow tube. The flow tube dimensions reflect the values calculated in the GFI analysis, and the size of the electronic component case is based on the anticipated volume required to house the electronics.

A rectangular box, 3 1/8 x 2 1/8 x 9 inches, would encompass the GFI in a 60 in^3 volume. The actual instrument volume requires about half of this space or 30 cu in.

The weight of the GFI was estimated by assuming that all metal components were made of stainless steel and by measuring the weights of typical circuit boards of the size indicated on Figure A-10. This resulted in a total weight estimate of 1 pound of which 3/8 lb was for metal components and the remainder for electronic circuitry.

Pressure drop for this instrument was estimated at the pressure drop flow specifications presented in the statement of work. In a 1/2 in. pipe at the specified operating conditions Re = 5200. This results in a smooth pipe friction factor = .035 and a pressure drop in the 9 in. length of .267" H_2O. Therefore, the heated tracer GFI will have a pressure drop slightly less than that specified in the statement of work.
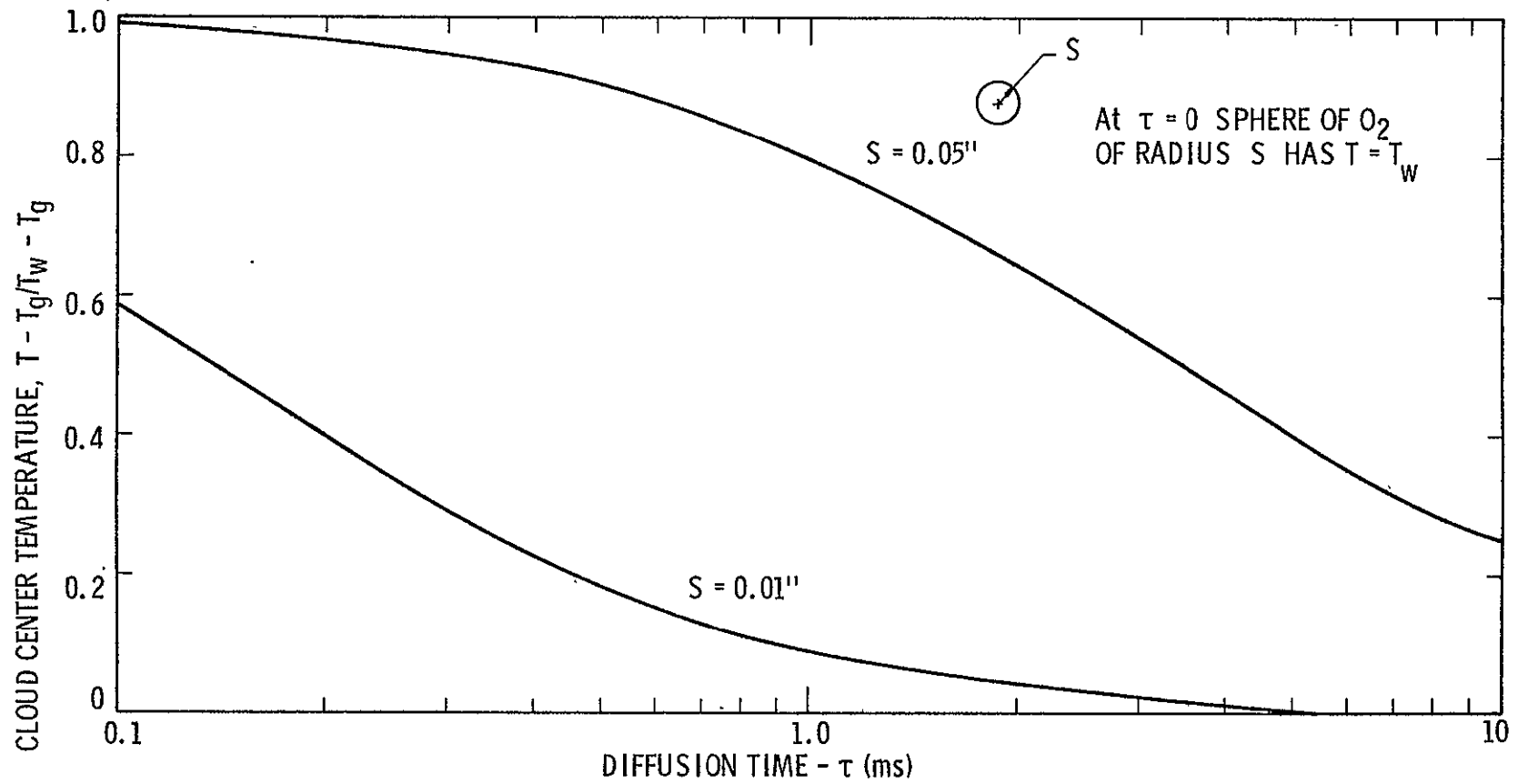
Figure A-3. Diffusion of Heated Gas Cloud

Heated Tracer References

1. Lilienfeld, P., Solon, L. R., and DiGiovanni, H. J., "Ion Tracer Anemometer for the Measurement of Low Density Air Flow," _Review of Scientific Instruments,_ 38, 3, pp. 405-409, March 1967.

2. Cady, W. M., "Velocity Measurements Using Ions as Tracers," _Physical Measurements in Gas Dynamics and Combustion, High Speed Aerodynamics and Jet Propulsion Series,_ Princeton University Press, 1954.

3. Walker, R. E. and Westenberg, A. A., "Absolute Low Speed Anemometer," _Review of Scientific Instruments,_ 27, 10, pp. 844-848, October 1956.

4. Kung, Robin J. and Binder, G. J., "Ultra Low-Speed Anemometry," Colorado State University, Fort Collins, Colorado, Grant DA-AMC-28-043-65-G20, June 1967. (AD 658172)

5. Bass, R. L. III., Owen, T. E., Gerlach, C. R., and Suhler, S. A., "Low Velocity Gas Flow Measurement," Final SwRI Technical Report, Contract No. NAS8-26117, prepared for NASA-Marshall Space Flight Center, Alabama, February 1971. (Also NASA-CR 103096)

6. Jakob, Max, _Heat Transfer,_ John Wiley & Sons, Inc., p. 336, 1949.

7. Bass, R. L. III., Suhler, S. A., and Owen, T. E., "An Ion Tracer Anemometer for Low Velocity Gas Flow Measurement," Final Technical Report, Contract No. NAS8-27619, prepared for NASA-Marshall Space Flight Center, Alabama, October 1972.

8. Hill, R. D. and McGunigle, R. D., "Quasi-Correlation Circuit for Thermal Pulse, Time-of-Flight Flowmeter," K West Corp.

APPENDIX B

TURBINE METER GFI

TURBINE METER GFI

Turbine meters have been developed to a high degree of accuracy and reliability for use in liquid flow measurements, and to a lesser extent, in gas flow measurement.[1]* The most notable features of turbine meters are:

(a)   low pressure loss

(b)   wide flow measurement range (20:1 and greater), and

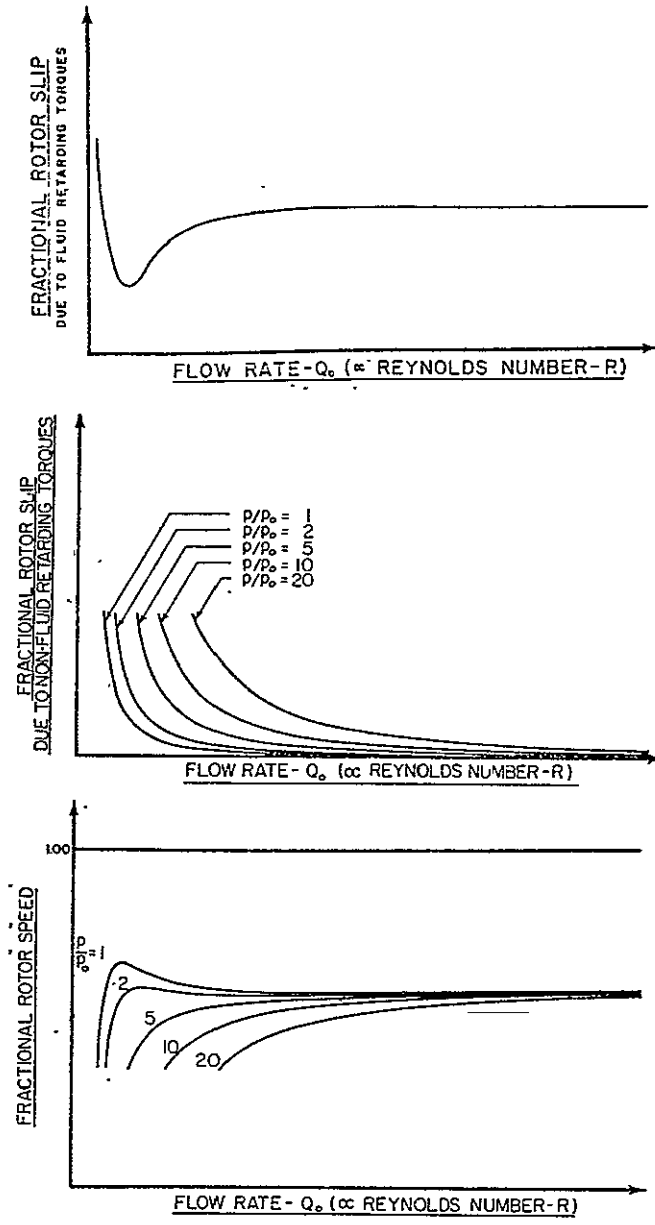(c)   output signal linear with flow rate under many conditions.

Briefly, a turbine meter is a propeller or turbine wheel mounted normal to the flow direction inside a duct. Readout is usually in the form of electrical pulses generated by the blade tips as they pass a magnetic sensor. However, some meters are equipped with direct gear drives which are connected to totalizing recording equipment.

Within the last decade, considerable effort has been made to develop turbine meters for gas flow measurement under various conditions. Analytical methods have been devised to predict meter performance for gases at any condition based on a meter tested in air at standard conditions.[2]

The major consideration in the use of turbine meters for low pressure gas measurement is the retarding torque on the turbine wheel. This retarding torque is produced by bearing drag, fluid drag, and readout device drag. The analytical study in Reference 2 predicts the behavior shown in Figure B-1 due to retarding torques under various flow conditions. The mechanical or nonfluid retarding torque is the major source of linearity and repeatability problems in low pressure gas flow at low Reynolds numbers. These problems are in addition to the predicted variations and are due to the non-repeatability of mechanical friction.

The difficulties mentioned above have largely been overcome according to reference material[3] furnished by Quantum Dynamics, Inc. Available test data from Quantum Dynamics are shown in Figures B-2, B-3, and B-4 and indicate insignificant calibration changes between 1 atmosphere and 1/3 atmosphere pressure for the meter shown in Figure B-5 operating in air. Further testing to pressures as low as 1 psia has been performed by the

---

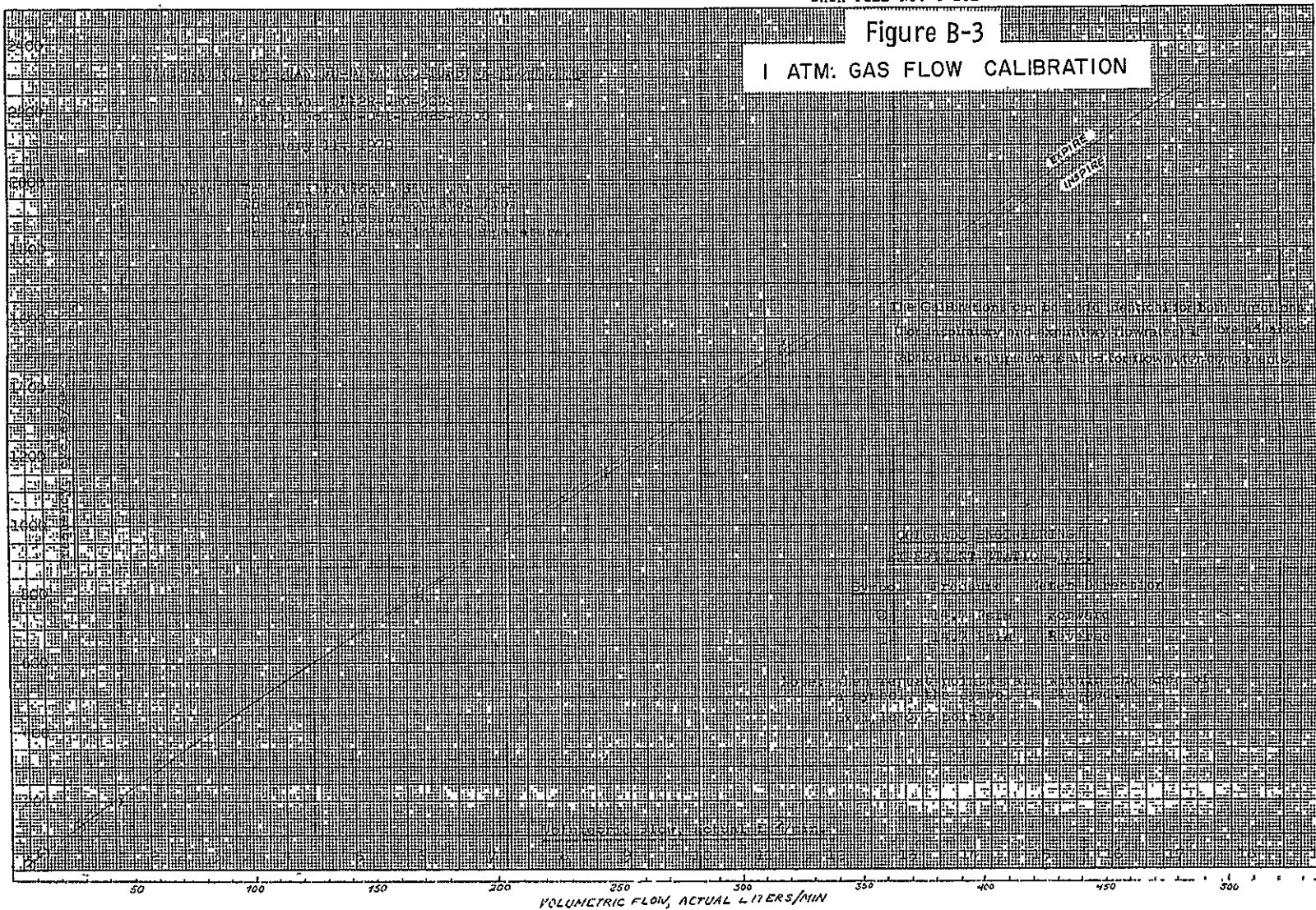*Superscript numbers in text denote references which are listed at the end of Appendix B.

FRACTIONAL ROTOR SLIP DUE TO FLUID RETARDING TORQUES

FLOW RATE-Q_0 ($\propto$ REYNOLDS NUMBER-R)

FRACTIONAL ROTOR SLIP DUE TO NON-FLUID RETARDING TORQUES

$P/P_0 = 1$
$P/P_0 = 2$
$P/P_0 = 5$
$P/P_0 = 10$
$P/P_0 = 20$

FLOW RATE- Q_0 ($\propto$ REYNOLDS NUMBER-R)

FRACTIONAL ROTOR SPEED

1.00

$\frac{P}{P_0} = 1$
2
5
10 20

FLOW RATE- Q_0 ($\propto$ REYNOLDS NUMBER-R)

Q_0 = Volume flow rate at std. conditions

P = Operating pressure

P_0 = Reference pressure

Figure B-1. Effect of Various Flow Conditions on Turbine Meter Performance

Figure B-2
1/3 ATM. GAS FLOW CALIBRATION

Figure B-3

I ATM: GAS FLOW CALIBRATION

VOLUMETRIC FLOW, ACTUAL LITERS/MIN

VERY LOW FLOWRATE CALIBRATION AT ⅝ PSIA SUB-ATMOSPHERIC PRESSURE

FLOWMETER CALIBRATION
PART NUMBER   XNFM875A-1
SERIAL NUMBER 002X-A
TEST FLUID   AIR
PRESSURE   5 PSIA
TEMPERATURE   534°R

△ TEST 004 - CALIBRATION
● TEST 005 - VERIFICATION FOLLOWING GAS
             PURGE TESTS

FLOWRATE (CFM)

FIGURE 1   REW 10/70

FLOWMETER CALIBRATION
PN   XNFM875A-1
SN   002X-A
TEST FLUID   AIR
PRESSURE   5 PSIA
TEMPERATURE   533°R

⊙ TEST 006 - CALIBRATION
▲ TEST 007 - VERIFICATION FOLLOWING GAS
             PURGE TESTS

FLOWRATE (CFM)

FIGURE 2   REW 10/10

Figure B-4. Turbine Meter Calibrations at Low Flow Rates (P = 5 psia)

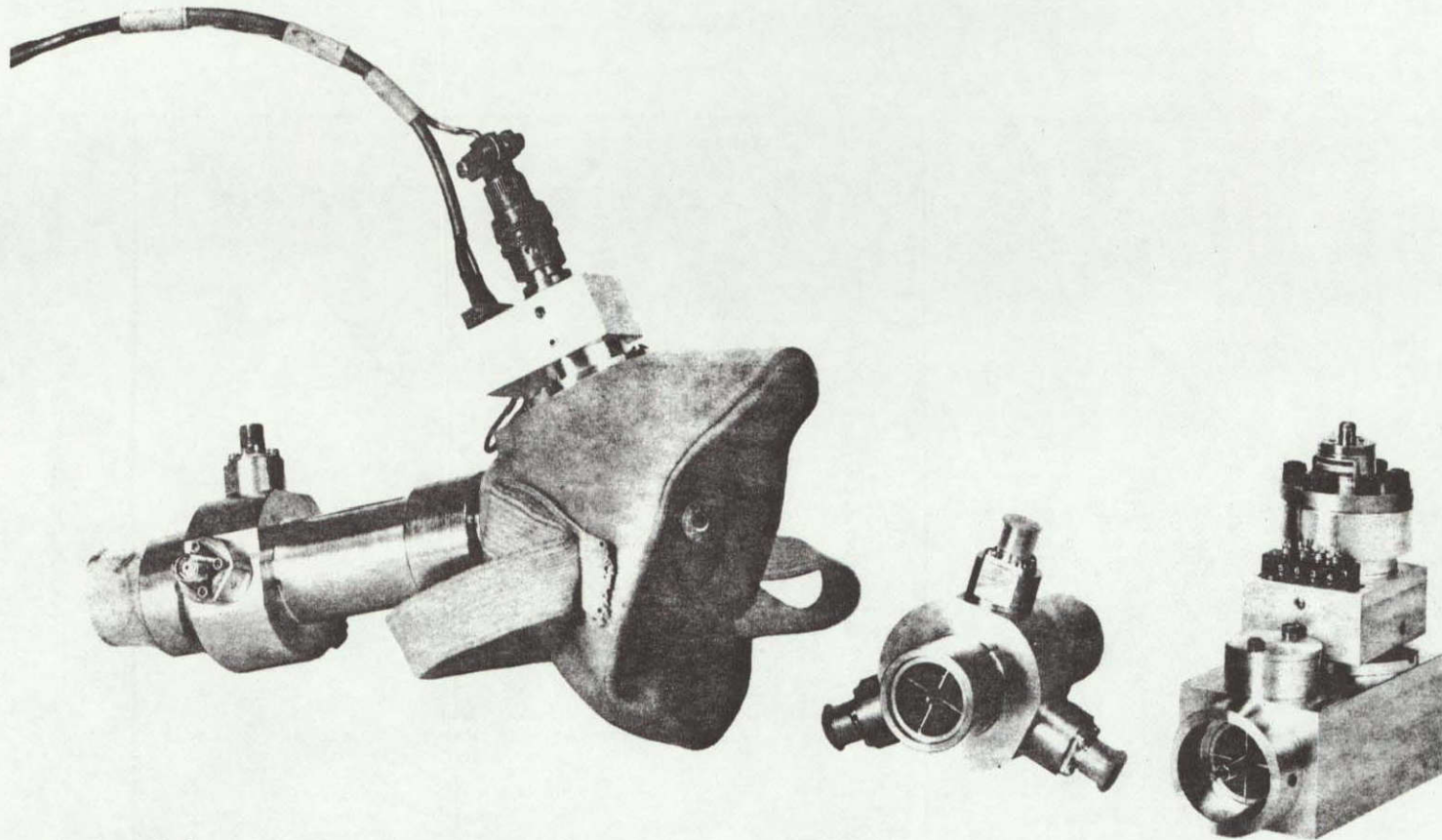Figure B-5.
3/4" BI-DIRECTION RESPIRATORY FLOWMETER

DYNAMIC ABS. PRESSURE
ABS. TEMP. PLUG-IN

manufacturer with only slight calibration shifts below 3.5 psia. Claims of relative immunity from temperature and humidity effects are also made. Turbine bearing life, according to the manufacturer, is about 4 weeks without lubrication and over 30 weeks with lubrication.

Based on the Quantum Dynamics reference material, the turbine meter would fit inside a 4 x 4 x 4 inch box for a total volume of 64 in^3. The actual instrument volume would require about 15 in^3 and weigh about 0.5 lbs.

Quantum Dynamics has built turbine meters for respiratory flow measurement, and are familiar with space oriented programs such as Skylab. A turbine meter with characteristics such as those indicated by the Quantum Dynamics reference material would be an attractive instrument for GFI, since the GFI application is much less demanding than respiratory flow measurement. The flow meter package would be small and the electronics would be relatively simple since no correction would be required for pressure and temperature effects. Interchangeability of turbine units without need of recalibration is also a desirable characteristic claimed by Quantum Dynamics. The meter should be capable of meeting GFI response requirements, judging from respiratory measurement data. Severe vibration requirements have also been met by the Quantum Dynamics meter according to independent tests.

The most obvious potential problem with a turbine meter of this type is the possibility of having foreign matter interfere with the free rotation of the turbine wheel. This problem could possibly be overcome by an inline filter whose pressure drop, when added to the pressure drop of a turbine meter, would be within GFI limits.

The development of a precision turbine meter is obviously unnecessary if the Quantum Dynamics meter will suffice. Therefore, an attempt will be made to obtain a Quantum Dynamics meter on loan for test purposes, even though currently available meters may not be optimum for the GFI application. As part of the test activity, the turbine meter will be modified as required to meet the GFI specifications and its final operating characteristics established.

Turbine Meter References

1. Shafer, M. R., "Performance Characteristics of Turbine Flow-meters," _Trans ASME_, Vol. 84, 1962, pp. 471-485.

2. Lee, W. F. Z. and Evans, H. J., "Density Effect and Reynolds Number Effect on Gas Turbine Flowmeters," _Journal of Basic Engineering_, December 1965.

3. Liu, F. F., Compilation of test data and descriptive material on Quantum Dynamics Turbine Meters.

APPENDIX C

VORTEX SHEDDING METER GFI

VORTEX SHEDDING METER GFI

The Vortex Shedding Meter (VSM) has been analyzed for a PLSS application. It can be shown, theoretically, that the VSM is independent of fluid density, viscosity, temperature, and pressure. This statement is quantitatively qualified in the following text. The discussion will be in essentially two parts. In the first part, operating principles of the VSM are given and an error analysis is performed. The second part is devoted to sensors and electronics required to implement the VSM technique.

Operating Principles

Geometrically, the VSM is simply a tube of diameter D with a small rod of diameter w placed on the diameter of the tube. The rod used to generate the vortices need not be a circular cylinder, but the forthcoming discussion assumes the rod to be of circular cross section. Figure C-1 shows a sketch of the VSM.

If the longitudinal axis of a cylinder is placed perpendicular to the velocity vector, V, several events take place. For Reynolds numbers less than 1, the flow around the cylinder is completely viscous. As the Reynolds number is increased from 2 to about 30, the boundary layer separates symmetrically from the two sides of the cylinder and two weak, symmetrical standing eddies are formed. The equilibrium of the standing eddies is maintained by the flow from the separated boundary layer, and the eddies increase in length with increased velocity in order to dissipate their rotational energy to the free-stream fluid. At some Reynolds number, depending on the shape of the cylinder, the width of the confining channel, and the free stream turbulence, the eddies break off and wash downstream. This gives rise to the celebrated Karman Vortex trail. Above this critical Reynolds number to about 120, the vortices are shed in an alternating fashion from one side to the other. The result is a staggered double row of vortices in the wake of the object. Von Kármán determined the spacing as

$$\sinh \frac{\pi a}{b} = 1 \quad \text{or} \quad \frac{a}{b} = .281$$

where a and b are given in Figure C-2. The entire vortex system moves with respect to the fluid at velocity V_v which varies as the strength of the vortices and inversely as the spacing b between them. The velocity

DETAIL OF FLOW OBSTRUCTION

FLOW

ROD

IMBEDDED
THERMISTOR

FLOW

TRIANGULAR
OBSTRUCTION

SHEDDING VORTEX

HOSE FITTING REQUIRED
AT EACH END

D

FLOW

8D

1D

THIS LENGTH REQUIRED TO MINIMISE UPSTREAM TURBULENCE

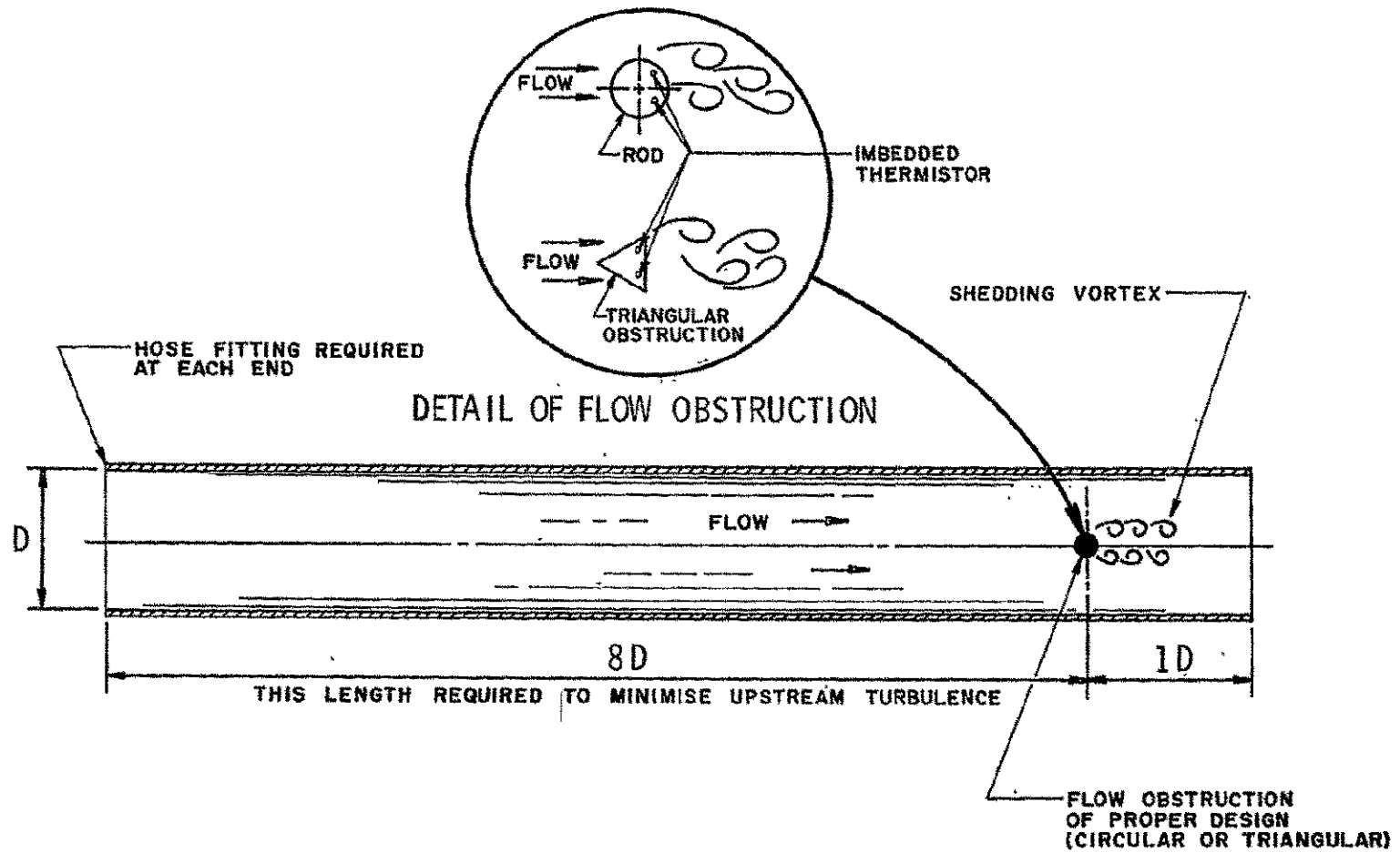FLOW OBSTRUCTION
OF PROPER DESIGN
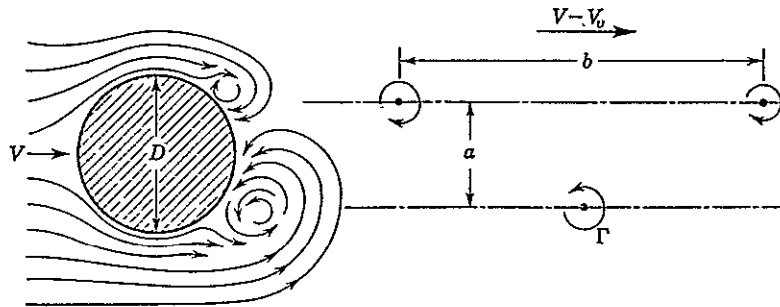(CIRCULAR OR TRIANGULAR)

Figure C-1. Vortex Shedding Meter (VSM) Concept for GFI Application

Figure C-2. The Kármán Vortex Trail Following a Cylinder

of the vortex trail downstream with respect to the cylinder will be $V - V_v$. Therefore, the frequency of shedding from one side of the cylinder is

$$f = \frac{V - V_v}{b} \tag{1}$$

The frequency has been given by G. I. Taylor to be about

$$f = .198 \frac{V}{w} \left(1 - \frac{19.7}{Re} \right) \tag{2}$$

For Reynolds numbers above 120 it is difficult to preceive the vortex trail, but the eddies continue to shed alternately from each side up to about a Reynolds number of 20,000. Equation (2) has been plotted as Figure C-3. As the Reynolds number is increased, the shedding frequency becomes more and more dependent on V alone. The basic operating principle is then to obtain an output frequency proportional to the flow rate, Q, or

$$f = KQ \qquad Re > 500 \tag{3}$$

Error Sources

In this section, a quantitative analysis is performed to show the magnitude of the error generated from changes in temperature, pressure, viscosity, gas constant, and geometry. The approach used in this error analysis is to write a general equation for the vortex shedding frequency, f, in terms of all variables.

$$f = \zeta (w, D, T, P, V) \tag{4}$$

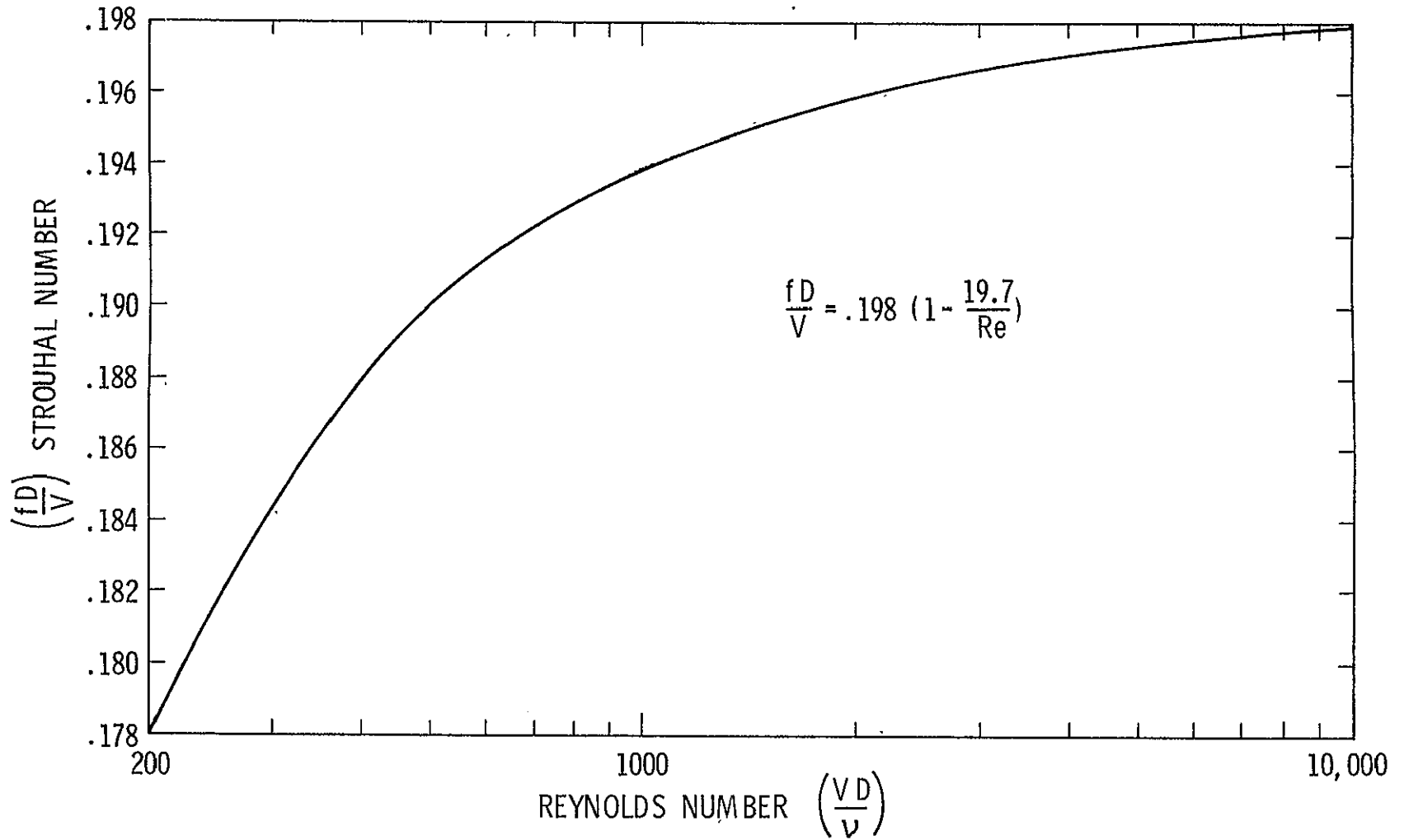$$\frac{fD}{V} = .198 \left(1 - \frac{19.7}{Re}\right)$$

Figure C-3. Strouhal Number vs. Reynolds Number

The total differential is then obtained by partial differentiation in order to quantitatively evaluate each sensitivity factor. For simplicity, assume w and D are given and are fixed values. To account for flow blockage, a blockage factor has been defined as β . It is obtained as follows

$$\beta = \frac{\text{frontal area of cylinder}}{\text{duct cross section area}}$$
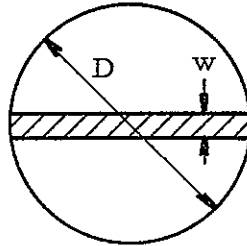
$$\% \text{ Blockage} = \beta = \frac{Dw}{\frac{\pi}{4}D^2} = \frac{4}{\pi}\frac{w}{D} = 1.273 \frac{w}{D} \quad (w << D)$$

Figure C-4 shows a plot of D vs β .

Equation (2) is rewritten as follows

$$Re = \frac{wV}{\nu} = \frac{(\frac{4w}{\pi D})(\frac{D\pi}{4}) V}{\nu} = \frac{\beta D\pi}{4} V \tag{5}$$

substituting (5) into (2) we have

$$f = \frac{.198}{w} (V - 25.1 \frac{\nu}{\beta D}) \tag{6}$$

The simplified Sutherland equation and the perfect gas law is used to obtain a functional form of ν .

$$\nu = \frac{\mu}{\rho} = \frac{gRuT}{P}$$

from

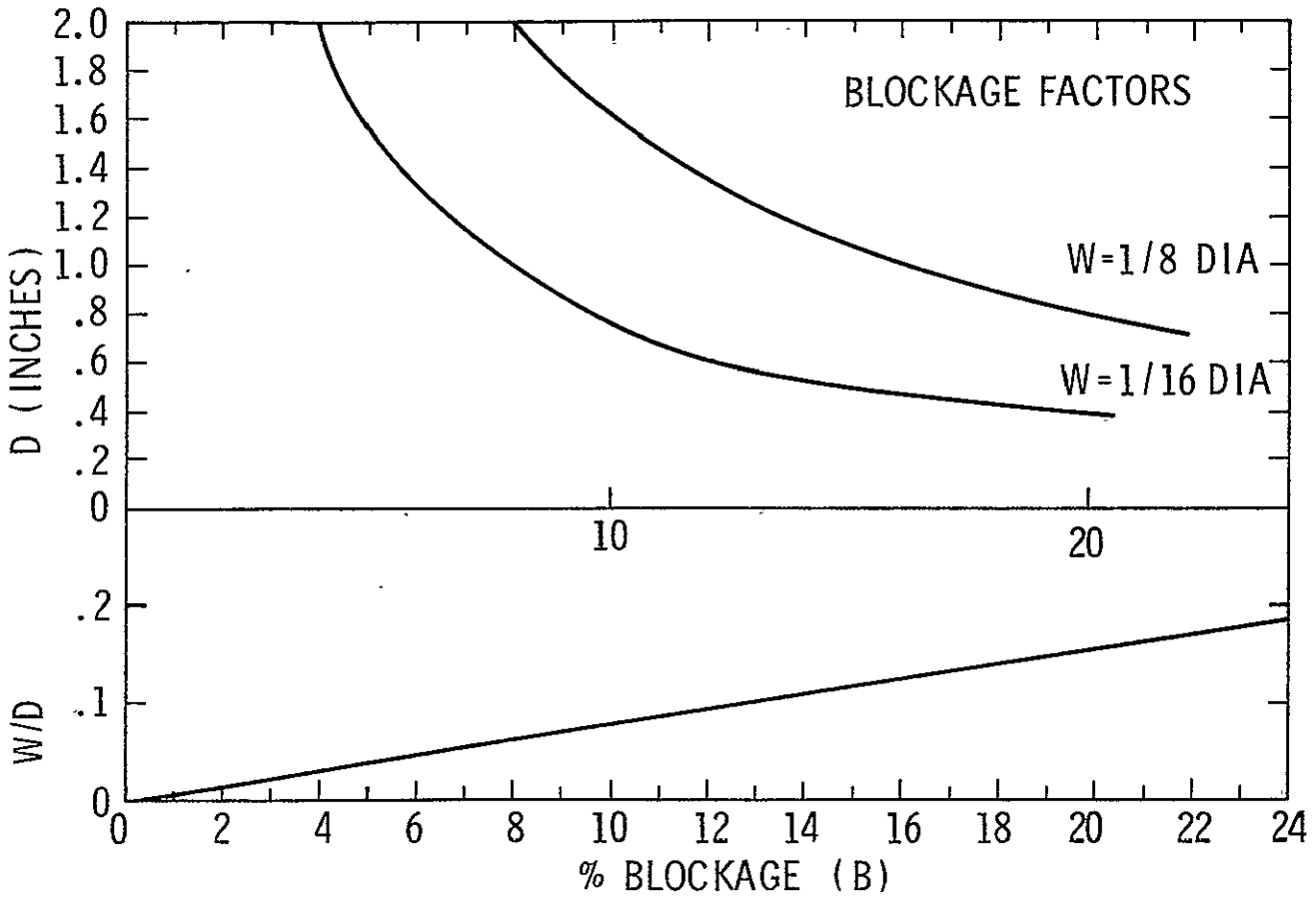$$\frac{\mu}{\mu_r} = \left(\frac{T}{T_r}\right)^n \quad 0.5 < n < 1.0$$

Figure C-4. Percent Blockage vs. $\frac{W}{D}$ And D

we obtain

$$\nu = \frac{u_r \, g \, R \, T^{n+1}}{P \, T_r^{\,n}} = \frac{C \, T^{n+1}}{P}$$

Equation (6) is now written in the form

$$f = \frac{.198}{w} \left(V - 25.1 \, \frac{C \, T^{n+1}}{P \cdot \beta \, D} \right)$$

where

D = Duct diameter (ft)

β = Blockage factor = $\dfrac{\text{frontal area of cylinder}}{\text{duct cross section area}}$

P = System static pressure (psfa)

T = Temperature (°R)

$C = \dfrac{g \, R \, \mu_r}{T_r^{\,n}}$ ($g = 32.2 \text{ ft/sec}^2$)

R = Gas constant

μ_r = Reference absolute viscosity at reference temperature, T_r

n = $.5 < n < 1$, exponent used in Sutherland equation describing temperature-viscosity relation for a gas ($n = .76$)

f = frequency of shedding (Hz)

V = free stream velocity (ft/sec)

w = diameter of cylinder (ft)

Re = Reynolds number based on cylinder diameter

In order to perform an error analysis the total differential is written

$$df = \frac{\partial f}{\partial V} \cdot dV + \frac{\partial f}{\partial T} \, dT + \frac{\partial f}{\partial P} \, dP + \frac{\partial f}{\partial w} \, dw + \frac{\partial f}{\partial D} \, \partial d$$

Since the geometry is fixed, dw and dD equal zero. The final equation is written as

$$f + \Delta f = \frac{.198}{w} \left(V - 25.1 \frac{CT}{P \beta D}^{n+1} \right) + \frac{.198}{w} \Delta V + \ldots$$

$$\frac{4.97C}{w \beta D} \left[\frac{T^{n+1}}{P^2} \Delta P - \frac{(n+1) T^n}{P} \Delta T \right] \tag{8}$$

Using the above expression, the sensitivity factors may be obtained as

$$\frac{\Delta f}{\Delta V} = \frac{.198}{w} \qquad\qquad (dT = 0, \ dP = 0) \tag{9}$$

$$\frac{\Delta f}{\Delta T} = \frac{4.97 \, CT^n}{w \, P \, \beta \, D} \, (n+1) \qquad\qquad (dV = 0, \ dP = 0) \tag{10}$$

$$\frac{\Delta f}{\Delta P} = \frac{4.97 \, CT^{n+1}}{w \, \beta \, D \, P^2} \qquad\qquad (dV = 0, \ dT = 0) \tag{11}$$

For purposes of illustration, assume β = .1 (10% blockage), w = .0625 in., n = .76, D = .795 in., T = 70°F, P = 3.7 psia, and the gas is air.

Therefore,

$$\frac{\Delta f}{\Delta V} = 38.02 \ Hz/ft/sec$$

$$\frac{\Delta f}{\Delta T} = -.31 \ Hz/°R$$

$$\frac{\Delta f}{\Delta P} = .18 \ Hz/psf$$

For the assumed operating point of 70°F and 3.7 psia,

$$f + \Delta f = (38.02 \ V - 92.32) + 38.02 \ \Delta V - .31 \ \Delta T + .18 \ \Delta P$$

For a constant velocity of 24.2 ft/sec which is the velocity thru a duct of a diameter of .795 inches at 5 acfm,

$$f + \Delta f = 827.76 - .31 \ \Delta T + .18 \ \Delta P$$

The errors introduced because of a temperature and/or pressure change would be

$$\%\varepsilon_T = \frac{\Delta f_T}{f} = \frac{.31 \, \Delta T}{827.76} \, (100) = -.0375 \, \Delta T$$

$$\%\varepsilon_P = \frac{\Delta f_P}{f} = \frac{.18 \, \Delta P}{827.76} \, (100) = .0217 \, \Delta P$$

In other words, the fundamental frequency is lowered by .0375% per degree R and it is shifted up by .0217% per psf assuming ΔT and ΔP were positive. Figure C-5 shows a plot of $\Delta f/\Delta T$ for various conditions and Figure C-6 shows a similar plot for $\Delta f/\Delta P$. It should be noted that the constant, C, accounts for gas composition. If the gas had been oxygen, the value of C would have increased by a factor of only 1.024.

In summary, the vortex shedding phenomena is very strongly velocity dependent and is rather insensitive to absolute viscosity, temperature and pressure for Reynolds numbers above about 1000. (To dramatize this insensitivity of environmental conditions, the preceeding analysis was performed at a low Reynolds number of 780 where sensitivities are higher). The analysis is also based upon fixed geometry conditions, however, slight changes in w will alter the sensitivities. It is seen that a 5% increase in w will decrease $\Delta f/\Delta P$ and $\Delta f/\Delta T$ by about 10%. This could be beneficial in the event that a coating were to build up on the rod during use, thus actually decreasing $\Delta f/\Delta T$ and $\Delta f/\Delta P$, but the 5% increase in w would decrease the primary sensitivity term, $.198/w \, \Delta V$, by about 5%.

Implementation of the VSM

It is not uncommon to see shedding frequencies as high as 1000 Hz or higher. The most difficult problem to overcome in the implementation of the VSM will be the sensing technique. Many methods have been proposed such as thermal techniques, ultrasonics, force measurement, and optical sensors. The most realisitc implementation for GFI is the thermal technique discussed below.

Heated Thermistor (Constant Temperature Mode)

A thermistor can be mounted in such a fashion that it will sense the vortex shedding velocity currents. Several locations have been considered and they are diagramed in Figure C-7. The sensor
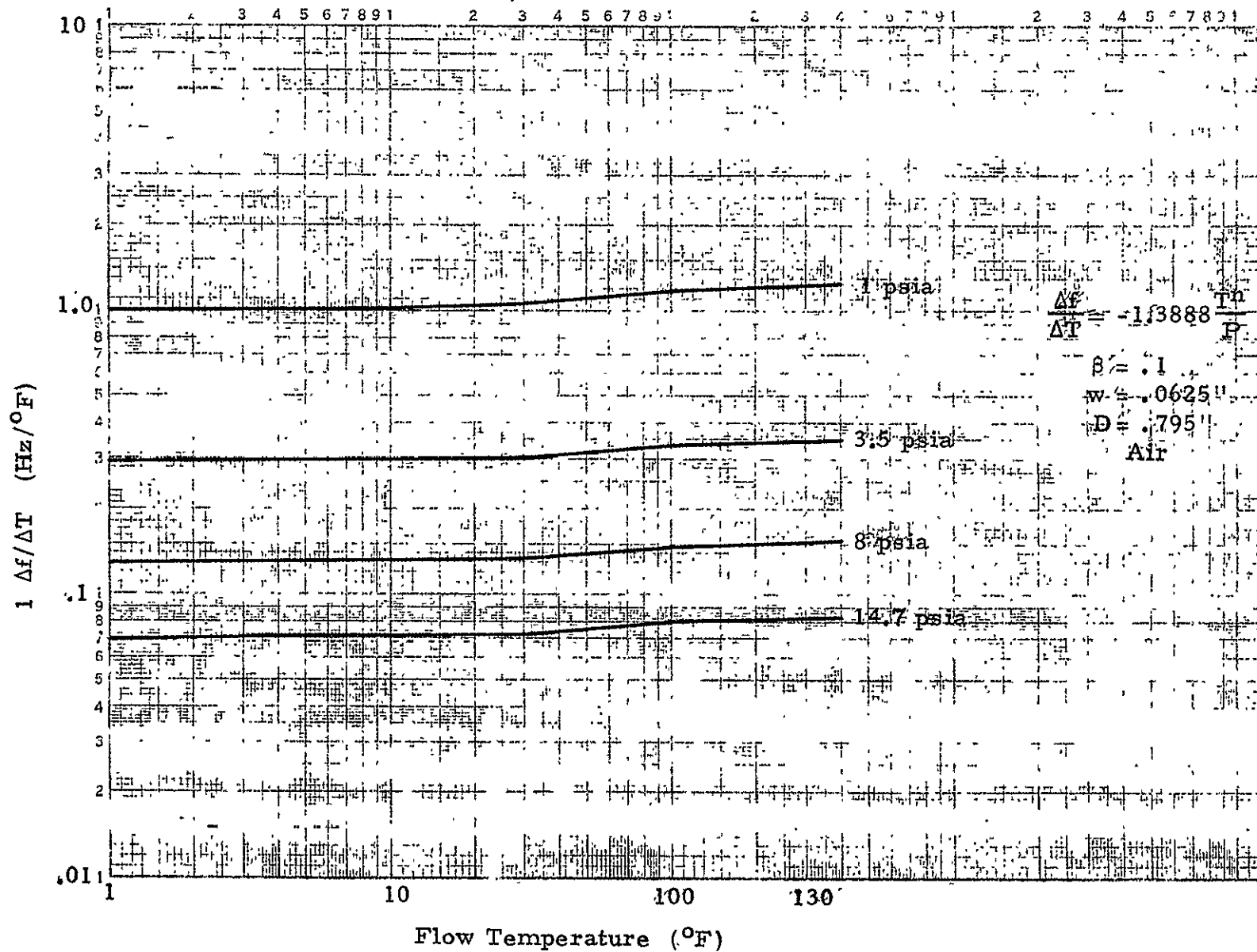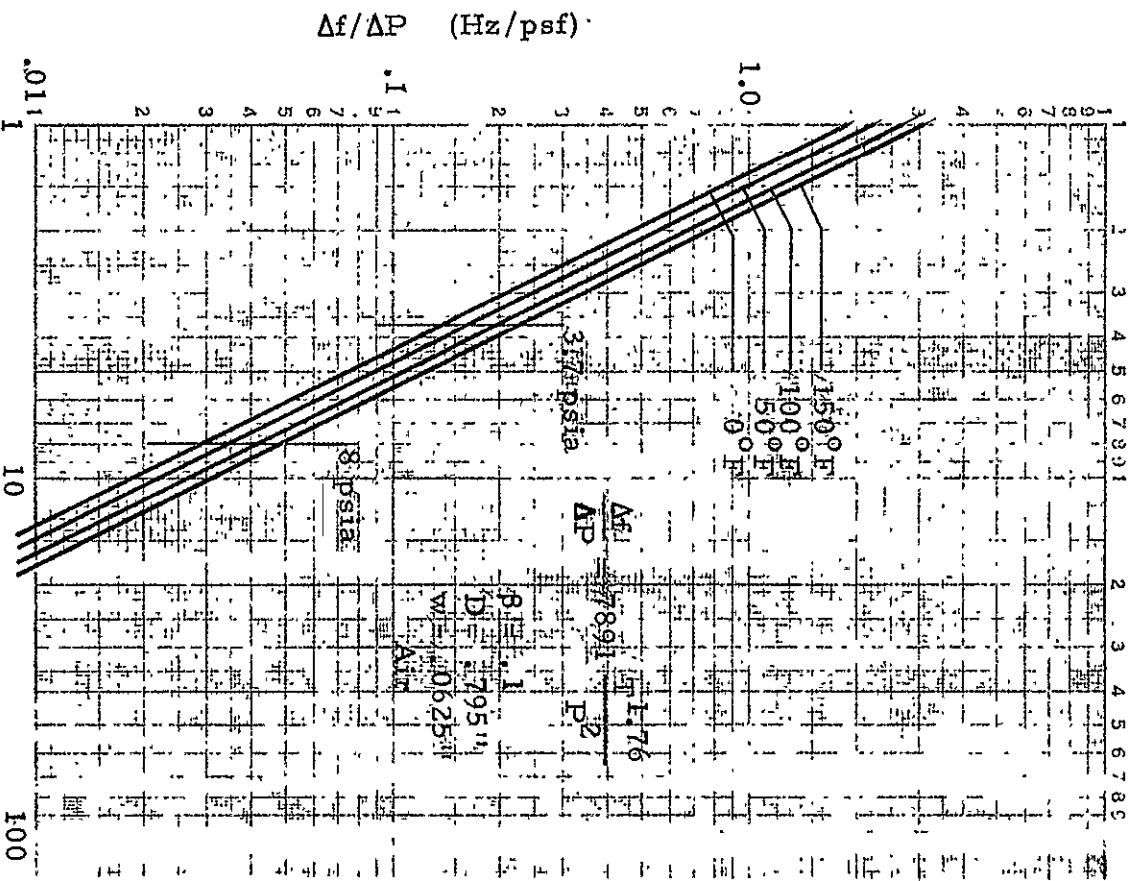
Figure C-5. $\Delta f/\Delta T$ vs T at Constant P

Figure C-6. $\Delta f/\Delta P$ vs P at Constant T
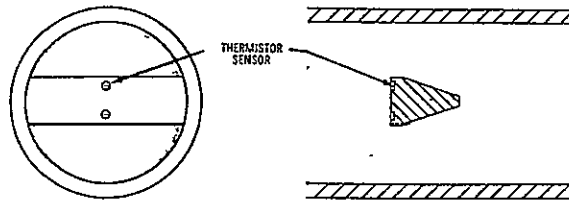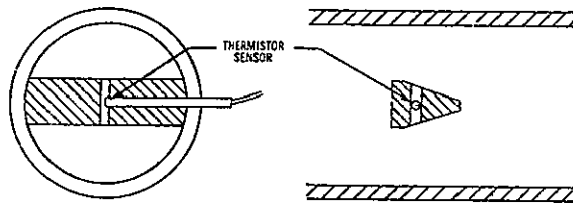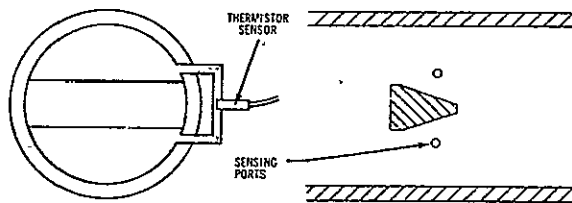
$\Delta f/\Delta P \quad (Hz/psf)$

(a) FRONT FACE THERMISTOR TECHNIQUE

(b) CENTRAL THERMISTOR TECHNIQUE

(c) EXTERNAL THERMISTOR TECHNIQUE

Figure C-7. Placement Of Sensor

placement as shown in Figures C-7b and 7c would be much less sensitive to moisture and contamination. It would be more economical to try several sensor locations on an experimental basis rather than attempt a theoretical solution at this time. The following paragraphs will develop a functional form for the output voltage across a thermistor as a function of velocity.

A thermistor is a negative temperature coefficient resistor that exhibits large resistance changes with small variations in temperature. The fundamental equation describing this variation of resistance vs temperature is

$$R(T) = R(T_o) \, e^{\left(\frac{\overline{C}}{T} - \frac{\overline{C}}{T_o}\right)} \left(\frac{\overline{C}}{T}\right)$$

where

$R(T)$ = thermistor resistance at temperature T

$R(T_o)$ = thermistor resistance at reference temperature T_o

$\overline{C}$ = thermistor constant $\cong \alpha \, (T_o)^2$

α = resistance coefficient $(\Delta R/R_o)/°K$

The power consumed is given by

$$P = \gamma \, \Delta T = \gamma \, (T - T_a)$$

where

T_a = fluid temperature

γ = thermal dissipation constant $(mW/°K)$

The thermal dissipation constant is a rather complex function of the heat transfer coefficient which is given as

$$\gamma = A_E \left[\frac{1}{\dfrac{A_E}{K_t A_t/D_1} + \dfrac{1}{h_c + h_r}} \right] + \frac{K_L A_L}{L}$$

‘where

A_E = effective thermistor heat transfer area (in^2)

A_L = lead cross section (in^2)

A_t = thermistor cross section

D_1 = conduction distance

L = lead length (in)

K_t = thermistor thermal conductance

K_L = lead thermal conductance

h_c = convection heat transfer coefficient

h_r = radiation heat transfer coefficient

For the moment, if we assume

$$h_r << h_c$$

and

$$\frac{A_L K_L}{L} << 1 \qquad \text{(or the lead losses are small)}$$

$$\gamma = \frac{A_E}{\dfrac{A_E}{K_t A_E/D} + \dfrac{1}{h_c}} = \frac{A_E}{C + \dfrac{1}{h_c}} = \frac{A_E h_c}{h_c C + 1}$$

if $h_c C << 1$, then $\gamma = A_E h_c$ or the power required is $P = A_E h_c$ which is a more familiar form of the heat transfer equation.

There are several forms of the heat transfer coefficient depending upon its mode of operation, but the form that most likely applies here is

$$h_c = A' + B' (Re)^{.5}$$

C-14

or

$$h_c = A + B \sqrt{u}$$

Therefore, the functional form of the power required is

$$P = \left[A + B \sqrt{u} \right] A_E \Delta_T = \frac{E(T)^2}{R(T)}$$

or

$$R(T_o) e^{(B/T - B/T_o)} A_E \left[A + B \sqrt{u} \right] \Delta T = E(T)^2$$

If T remains a constant, then

$$E(T)^2 = F + G \sqrt{u}$$

when E(T) is the voltage across the thermistor at temperature T .

Differentiating both sides

$$2E\, dE = \frac{G}{2 \sqrt{u}}\, du$$

from which the sensitivity is derived as

$$\frac{dE}{du} = \frac{G}{4 \sqrt{u} \, (F + G \sqrt{u})^{1/2}}$$

It would be much more expedient to obtain F and G experimentally, but it should be kept in mind what variables affect F and G . For the intended application these variations in F and G are not of major concern because we need only to measure a shedding frequency. An amplitude variation of the output signal may be tolerated because the velocity in the duct V is related to the vortex shedding frequency, while the sensor output is related to the local velocity, u , in the neighborhood of the shedding vortices.

Thermistor Electronic Circuit

It is anticipated that a simple feedback circuit would be employed to maintain the thermistor at a constant temperature. Since the frequency response of the thermistor may not be high enough for this application, a lead compensator would most likely be inserted into the control loop to improve the high frequency response by utilizing the following circuit.
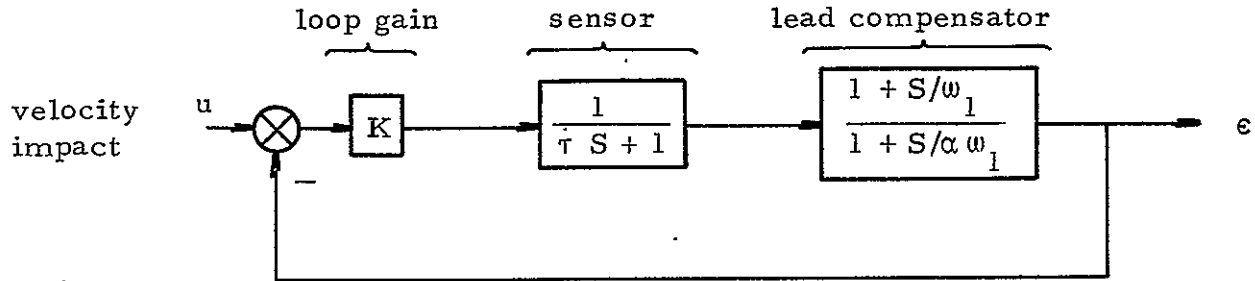
To date, the details of the circuit configuration have not been fully investigated.

Preliminary Design Considerations

Thus far, most of the error sources and an acceptable means of implementation have been identified. In this section we will provide preliminary design information for producing an optimum VSM GFI.

Duct Sizing

Since $V_{av} = 4Q/\pi D^2$, variations in D can greatly affect V_{av} and as seen in equation (8) the output frequency is more sensitive to V than any other variable. If we follow thru with our original example where D = .795" and w = .0625", it is noted that the output frequency is 825 Hz at 4.7 acfm and 930 Hz at 5.3 acfm. The period range (1/f) is from 1.21 ms to 1.075 ms at Q of 4.7 and 5.3 acfm respectively and the output frequency at 5 acfm is 877 Hz or a period of 1.14 ms. Therefore the period determining alarm circuit would be set at 1.14 $\pm$ .065 ms. For periods greater than 1.21 ms the alarm would continue to ring. Greater sensitivities can be obtained by reducing duct diameter since $\Delta V/\Delta Q$ becomes larger.

w/D Ratio

The diameter of the shedding rod, w, greatly effects the output frequency but has a minor effect on the ΔT and ΔP sensitivity terms.

One of the unknowns is the effect of varying w/D which is related to the blockage factor. Equation (8) was developed assuming w small compared to D . The final effects of w/D will have to be determined experimentally since β will effect the local velocity which could alter the shedding characteristics.

Inlet Turbulence

One of the requirements for the VSM is that the inlet turbulence intensity $\sqrt{u^2/V}$ be small. The limiting value should be determined by test.

Vanes

Straightening vanes should be installed on an as needed basis. They should be installed only if the turbulence intensity is unacceptable or the flow is skewed.

Weight, Volume and Pressure Drop Characteristics

Figure C-8 shows an overall view of the VSM-GFI indicating important dimensions. A rectangular box, 6 x 2 x 2 1/2 inches, would encompass the VSM-GFI in a 30 in^3 volume. The actual instrument requires about 20 in^3. The estimated weight is .75 pounds.

The electronic package is attached to the side wall of the VSM in such a fashion to conduct heat away from or into the electronic sub-strate material. This is done in order to somewhat thermally stabilize the substrate.

Pressure drop for this instrument was estimated at the pressure flow specifications presented in the statement of work. In a .795 in. pipe at the specified operating conditions Re = 2790. For this particular design, the Reynolds number is in the critical zone. The final design would be modified to avoid this condition. Nevertheless, a conservative friction factor of .07 is used in the pressure drop calculation. For a duct of 6 inches in length the pressure drop is approximately .03 inches of water which is well below the .25" H_2O maximum requirement.

Power Requirements

The VSM requires power for the sensor and the signal conditioning electronics.

ELECTRICAL
CABLE

ELECTRONIC CIRCUIT
BOARD

VORTEX SHEDDING ROD
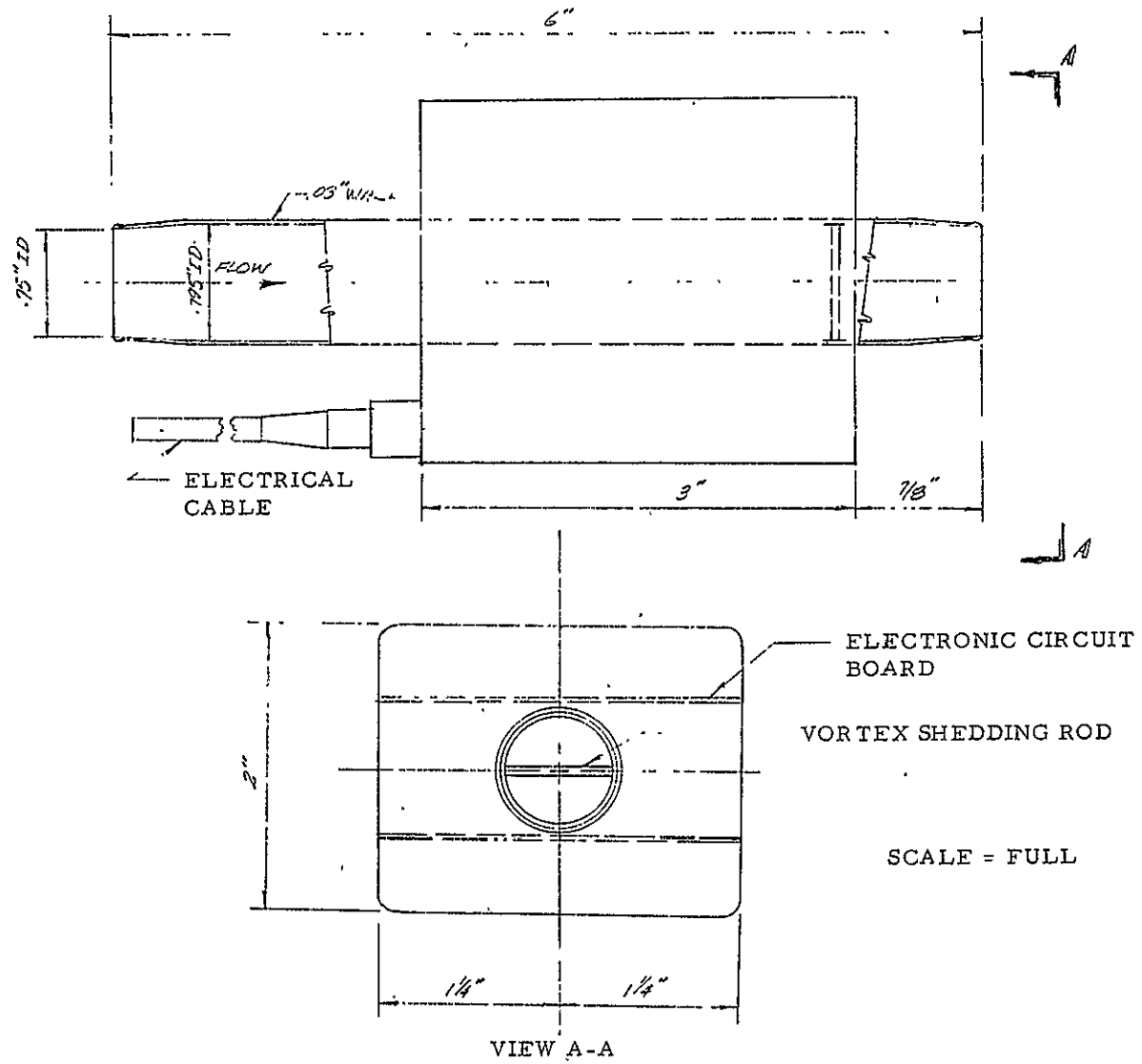
SCALE = FULL

VIEW A-A

Figure C-8. Dimensional Envelope of VSM-GFI

Sensor

A typical average thermal dissipation constant for a thermistor is .15 mW/°F. For an acceptable sensitivity of the thermistor to sense vortex currents, by convective cooling, the thermistor should be operated about 30°F above the ambient temperature. If the thermistor is operated at a constant temperature of 160°F, then the worst case power would be at a gas temperature of 35°F or $\Delta T = 125°F$. The power required would be 18.75 mW.

Electronic Package

The electronic porcessing is composed of several sections. They are (1) a servo loop to control the thermistor, (2) a detector circuit, (3) a decision logic section, and (4) an alarm circuit. While the exact details of a plausable circuit have not been considered in detail, a reasonable estimate of the power required is possible by estimating the number of active elements of each section. Several decision circuits have been considered and they are designated as D-1, D-2, and D-3. The following table presents the estimated power consumptions.

TABLE C-I

Section	No. of Elements	Power/Element	Total Power
Servo Loop	2 op-amps 1 power amp	6 mW	36 mW
Detector	1 op-amp	6 mW	6 mW
D-1	*See note ---	---	900 mW
D-2	---	---	359 mW
D-3	---	---	751 mW
Alarm Switch	---	---	6 mW

*Final powers were derived from preliminary circuit diagram.

At present the least power configuration would be the system using the D-2 decision circuit and its total power consumption is estimated as 40.7 mW. The more sophisticated circuit would consume 948 mW.

APPENDIX D

DIFFERENTIAL PRESSURE GFI

DIFFERENTIAL PRESSURE GFI

Three differential pressure concepts have been evaluated and ranked in order of their preference as a GFI sensor; the three concepts are (1) pitot-static sensor, (2) venturi meter, and (3) an orifice meter. All three of these meters basically operate by measuring a differential pressure created within the meter. The analysis has shown that the optimum concept is the venturi meter, and that the venturi meter can be implemented in several ways to produce a satisfactory GFI sensor.

Pitot-Static Probe GFI

The pitot-static probe yields a differential pressure which is the difference between the total pressure and the local static pressure. This resulting ΔP is equivalent to the dynamic pressure $(1/2 \rho V^2)$ and can be easily used to determine the velocity or flow rate if the density, ρ, is known. For application as a GFI sensor, the ΔP produced at the minimum flow rate and density must be in a range that can be accurately measured with state of the art pressure transducing instrumentation. The minimum ΔP will occur for the limiting case where the gas density is a minimum or

$$R = R \text{ for air} = 53.3 \text{ ft-lb/lb}°R$$

$$P = 3.5 \text{ psia}$$

$$T = 130°F$$

$$Q = 4.7 \text{ acfm}$$

Figure D-1 presents the minimum alarm dynamic pressure produced versus line diameter for the above conditions. In general, the differential pressures developed are in a range which can be readily sensed by commercially available pressure transducers.

Sensitivity to Flow Profile

To minimize flow interference effects, the total pressure probe should be mounted in a line with as large a cross sectional area as possible. However, the pitot probe will measure the local or centerline velocity which is related to the actual flow rate by
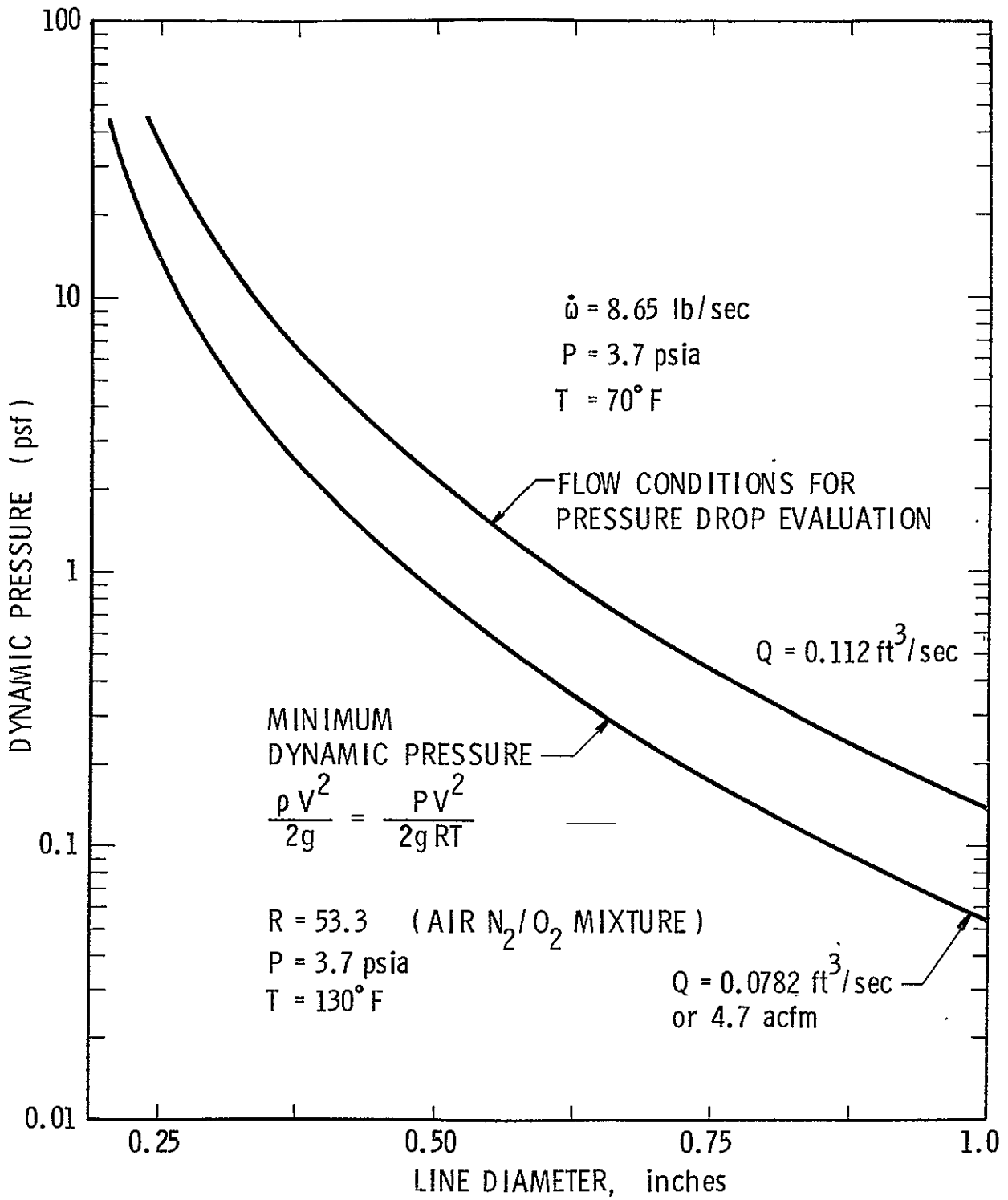
D-1

Figure D-1. Dynamic Pressure versus Line Diameter

$$Q = \frac{V_{\mathfrak{E}} A}{1 + 1.43 \sqrt{f}} \tag{1}$$

where f is a function of the Reynolds number. Since the GFI might operate over a considerable variation in Reynolds number, it would be desirable to have a nearly constant value for f over the entire operating Reynolds number range. Figure D-2 presents the GFI operating Reynolds number for various values of the line diameter, d. From Figure D-3, which reveals the variation in f with Re and relative roughness, f is constant for $e/d = .016$ over the range $3000 < Re < 13,000$. Referring again to Figure D-2, it becomes obvious that $d \cong 1/2''$ is the optimum line diameter for producing a constant f over the sensor Re range. Not only does f vary considerably in the range $Re < 3000$, but equation (1) becomes invalid.

The maximum diameter which produces $Re > 3000$ for all operating conditions (gases, temperatures, and pressures) is $d = 1/2$ inch. The highest alarm Re produced is 1.92×10^4, based on a maximum GFI sensing or actuation flow rate of 5.3 cfm and in a $1/2''$ diameter line. The friction factor, f, will vary from $f = .038$ @ Re = 3000 to $f = .04$ @ Re = 19,200. For a constant centerline velocity, the maximum change in the average velocity can be computed from equation (1). If $f = .039$ is assumed the correct value for f over the entire Re range, then the actual flow rate, Q_a, will be related to the sensed flow rate by

$$\frac{Q_a}{Q_s} = \frac{1.43 \sqrt{f_a + 1}}{1.43 \sqrt{.039 + 1}} = .997$$

or (2)

$$Q_a = 99.7\% \ Q_{sensed}$$

Thus the maximum error in flow rate sensed due to changes in the velocity profile shape with Re is less than $1/2\%$ if a carefully selected value for f is used over the entire Re range. Other techniques to lower the sensitivity of velocity profile to Re can reduce this error even futher.

Differential Pressure and Pressure Drop Characteristics

From Figure D-1 the minimum alarm differential (dynamic) pressure to be sensed by the pitot-probe in the $1/2''$ diameter line is $\Delta P = .153'' H_2O$,
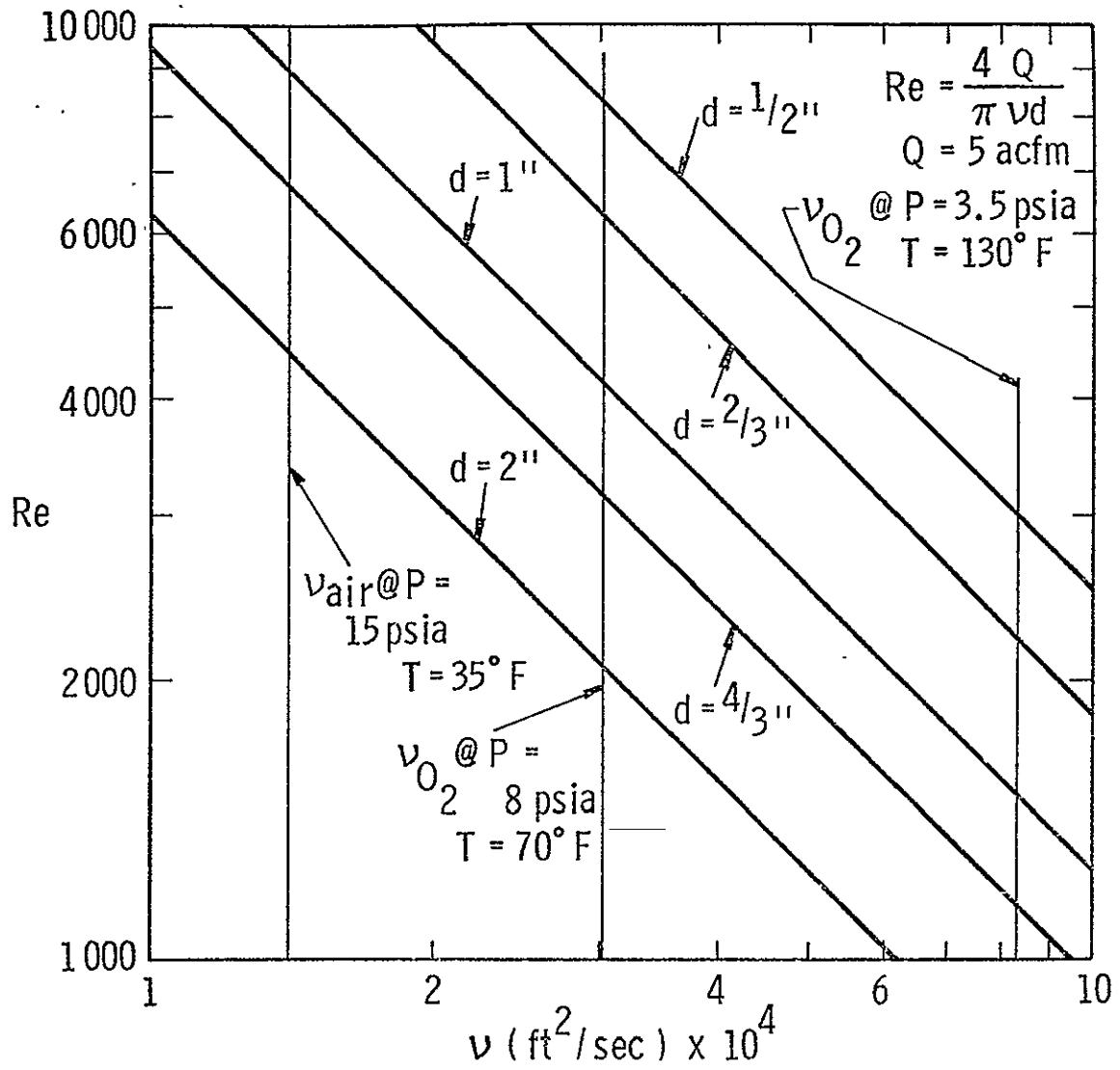
Figure D-2. Reynolds No. versus Kinematic Viscosity @ Q = 5 acfm

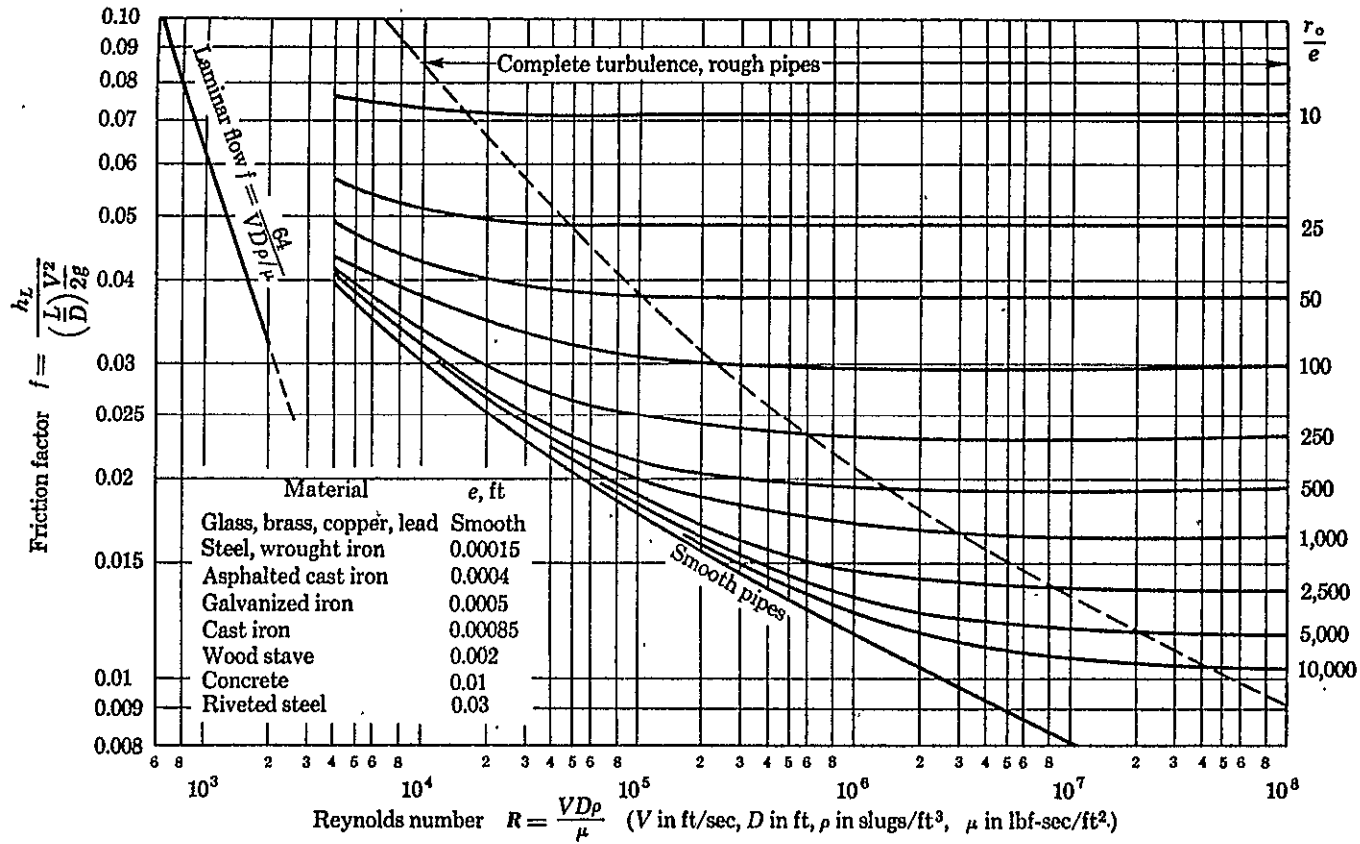Figure D-3. Friction Factor as a Function of Reynolds Number and Relative Roughness

while the maximum ΔP (required for sensor deactuation) is $1.13'' H_2O$ at $P = 15$ psia, $T = 35°F$ and $R = 48.3$ ft-lb/lb°R. The largest ΔP occurs at 15.0 psia and $Q = 7$ acfm or $\Delta P_{max} = 1.979'' H_2O$. A good pressure transducer to cover the operating range would be a $0 - 2'' H_2O$ differential transducer.

The GFI must also meet the requirement

$$\Delta P_{GFI} \leq .25'' H_2O \quad @ \quad \dot{w} = 8.65 \text{ lb/hr } O_2$$
$$P = 3.7 \text{ psia}$$
$$T = 70°F$$

The pressure drop that would exist from friction losses in a GFI of this design have been estimated at the above condition by

$$\Delta P = f\left(\frac{L}{d}\right)\frac{\rho V^2}{2}$$

The dynamic pressure at the above condition is 2.1 psf. A $L/d = 10$ will be required to produce the required velocity profile and therefore

$$\Delta P = .150'' H_2O$$

Losses due to diffusion from the $1/2''$ diameter line to the $3/4''$ line can be minimized in a well designed diffuser. From diffuser data, at AR = 2.25, $K_d = .06$, and

$$\Delta P_{diffuser} = .06 (2.1) = .126 \text{ psf} = .024'' H_2O$$

for a total pressure drop of $.174'' H_2O$.

Sensitivity to Temperature, Pressure and Gas Variations

Since the GFI must operate with various gases, (air to O_2) pressure levels, and temperature ranges, it is important that the instrument be self compensating or that reliable calibration be obtained for each expected operating condition. The volume flow rate is related to the temperature, pressure, differential pressure and gas constant by

$$Q = \frac{A \sqrt{\frac{2g \, RT \, \Delta P}{P}}}{1 + 1.43 \sqrt{f}}$$

Since f can be made nearly constant for all conditions, then

$$Q = K \sqrt{RT \frac{\Delta P}{P}} \qquad \text{where} \quad K = \frac{A \sqrt{2g}}{1 + 1.43 \sqrt{f}}$$

For the required gas temperature range of $35° < T < 135°F$ then the variation in measured flow rates due to T is

$$Q_1 = K \sqrt{\frac{R \Delta P}{P}} \sqrt{T_1}$$

$$Q_2 = K \sqrt{\frac{R \Delta P}{P}} \sqrt{T_2}$$

and

$$\frac{Q_1 - Q_2}{Q_1} = \frac{\sqrt{T_1} - \sqrt{T_2}}{\sqrt{T_1}} = \frac{\Delta Q}{Q_1} = .0472$$

or the max % error in Q due to temperature is equal to 4.72%. Likewise, the percent error due to a deviation in R is determined to be

$$\frac{\Delta Q}{Q_1} = \frac{\sqrt{R_1} - \sqrt{R_2}}{\sqrt{R_1}} \times 100$$

$$\frac{\Delta Q}{Q_1} = \pm 2.5\%$$

The ratio of the actual to the measured volume flow rate, assuming mean values of T = 83° and R = 50.8 will always be in the range

$$.932 < \frac{Q_{actual}}{Q_{measured}} < 1.068$$

or the actual flow rate will be within 6.8% of that measured by the GFI.

The nominal value for sensor actuation is 5.0 acfm. If the sensor measures 5.0 acfm, then the actual acfm is

$$4.66 < Q_a < 5.34 \text{ acfm}$$

This is slightly outside the specified range; however, if the assumptions are made that

(1) $50° < T < 80°F$ (Normal Operating Range)

(2) $48.3 < R < 53.3$ ft-lb/lb°R

then $4.81 < Q_a < 5.20$ and no compensation is required for temperature or gas mixture.

If the normal operating temperature range is 50° to 80°F and the gas mixture varies from pure O_2 to air, then the actual flow rate will always be (under the worst condition)

$$Q_{actual} = (.961 \text{ to } 1.0405) \ Q_{measured}$$

The flow relation for a pitot probe type meter is

$$Q = AK \sqrt{\frac{\Delta P}{P}} = K' \sqrt{\frac{\Delta P}{P}}$$

where

$$K' = \frac{\sqrt{2g \ RT}}{1.43 \ \sqrt{f} + 1}$$

If the operating pressures are specified, for example,

$$P = 3.7 \pm .25 \text{ psi}$$

$$P = 8 \pm .25 \text{ psi}$$

$$P = 15 \pm .25 \text{ psi}$$

then a calibration curve can be obtained for each pressure level and the

instrument compensated by adjustment of the calibration constant K'. For example,

$$Q = \frac{K'}{\sqrt{P}} \sqrt{\Delta P} = \frac{K'}{\alpha_1} \sqrt{\Delta P} \quad \text{for 3.7 psi}$$

and

$$Q = \frac{K'}{\alpha_2} \sqrt{\Delta P} \quad \text{for 8.0 psi}$$

$$Q = \frac{K'}{\alpha_3} \sqrt{\Delta P} \quad \text{for 15.0 psi}$$

By letting Q equal the desired actuation flow rate, Q_a, the pressure drop at actuation is

$$\Delta P_{act} = \left(\frac{Q \alpha_n}{K'} \right)^2 = \left(\frac{Q P}{K'} \right)^2$$

If a pressure transducer is used with a sensitivity of C volts/psi, the output will be

$$E = C \Delta P_{act}$$

The voltage output at which activation of the alarm occurs is

$$E \leq C \left(\frac{Q P}{K'} \right)^2$$

Thus if E falls below an adjustable, preset level, a switch can be activated and the buzzer or alarm can be made to actuate until

$$E > C \left(\frac{QP}{K'} \right)^2$$

If the static pressure is uncompensated, and the GFI sensitivity is preset for each operating pressure range, then a measuring error exists, depending on the actual operating pressure level and that assumed for the preset.

For example, suppose the nominal operating pressure is $8.0 \pm .25$ psia as originally specified in the scope of work.

Then

$$7.75 < P < 8.25$$

Using 8.0 psi as the preset value, the maximum ratio between the actual Q and that sensed by the GFI will be (due to static pressure errors only)

$$\frac{Q_{actual}}{Q_{measured}} = \frac{\sqrt{P_{set}}}{\sqrt{P_{actual}}} = \sqrt{\frac{8.0}{8.25}} = .9847$$

When this error is combined with the maximum deviations that are expected in temperature and gas-mixture compensation, the max deviation between measured and actual Q is

$$\frac{Q_{actual}}{Q_{measured}} = (.9847)_{pressure} \times (.9856)_{temp} \times (.9751)_{gas}$$

$$\frac{Q_a}{Q_m} = .9463 \text{ or } 1.0567$$

The maximum percent error in Q sensed is 5.67% which is within the specified limits.

Similar calculations at other pressure set points reveal that at the lowest pressure (3.5 psia) an 8% error in the measured flow rate can occur. To maintain the error at 6% at 3.5 psia requires the actual static pressure in the GFI to be $\pm 3.2\%$ of that used for the system preset. Otherwise, some form of pressure measurement and compensation will be required to keep

$$4.7 < Q_a < 5.3 \text{ acfm}$$

Static Pressure Compensation

If it should be desirable to have an instrument which completely compensates for static pressure, then a static pressure transducer <u>and</u> a differential transducer must be used in the GFI. Since

$$Q = K' \sqrt{\frac{\Delta P}{P}}$$

or

$$\frac{\Delta P}{P} = \left(\frac{Q}{K'} \right)^2$$

The value $(Q/K')^2$ is a constant at a given actuation flow rate and $\Delta P/P$ is constant at all operating conditions. Each transducer will have a sensitivity of

$$\frac{\Delta P}{P} = \frac{C_1 E_1}{C_2 E_2} = \left(\frac{Q}{K'} \right)^2$$

And the voltage ratio required for actuation is

$$\frac{E_1}{E_2} \leq \frac{C_2}{C_1} \left(\frac{Q}{K'} \right)^2$$

An air pressure switch can also be implemented with a pitot static probe to sense the pressure differential and actuate where ΔP drops below a preset critical level.

For example, the differential pressure range over which the alarm actuates is

$$\Delta P \leq \left(\frac{QP}{K'} \right)^2$$

For each static pressure level required, the ΔP critical can be calculated, and the switch preset to make contact for all ΔP's below ΔP_c.

This can be implemented by providing a ΔP_c vs. P' static curve with each instrument. The switch could then be manually set to actuate at $\Delta P < \Delta P_c$.

These switches are commercially available items.

Summary of Pitot Static GFI Concept

A pitot-static type GFI sensor can be made to operate or actuate when the actual volume flow rate drops below $5 \pm .3$ acfm. This instrument can be designed such that the temperature and gas-mixture ratio (Q_2/N_2) require no compensation. It can also be designed to operate independently of actual pressure as long as the GFI static pressure is within 3.2% of that assumed when the GFI sensitivity is preset. If the static pressure cannot be known within 3.2% apriori then some form of pressure compensation is required. This can be accomplished with 2 pressure transducers and actuation is accomplished by a preset voltage ratio.

If the static pressure and temperature are variables over a range greater than

$$P'_a = P \text{ set } \pm 3.2\%$$

$$T_a = T \text{ set } \pm 15\%$$

then a GFI which completely compensates for these variations must be developed. Two possible schemes for this compensation are described in the section describing the venturi meter and are applicable to all the differential pressure concepts.

Orifice Meter GFI

The thin-plate, sharp edged orifice can be employed in a manner similar to that of a pitot-static probe GFI sensor. A common arrangement consists of a thin flat plate having a circular hole concentric with the pipe. Pressure connections or "taps" for measuring the differential pressure across the orifice plate are located at the interior pipe walls on each side of the orifice plate as shown in Figure D-4. By measuring the line static pressure and temperature, the GFI can be fully compensated for variations in these parameters, or it can be implemented in a manner similar to that described for the pitot-static meter.
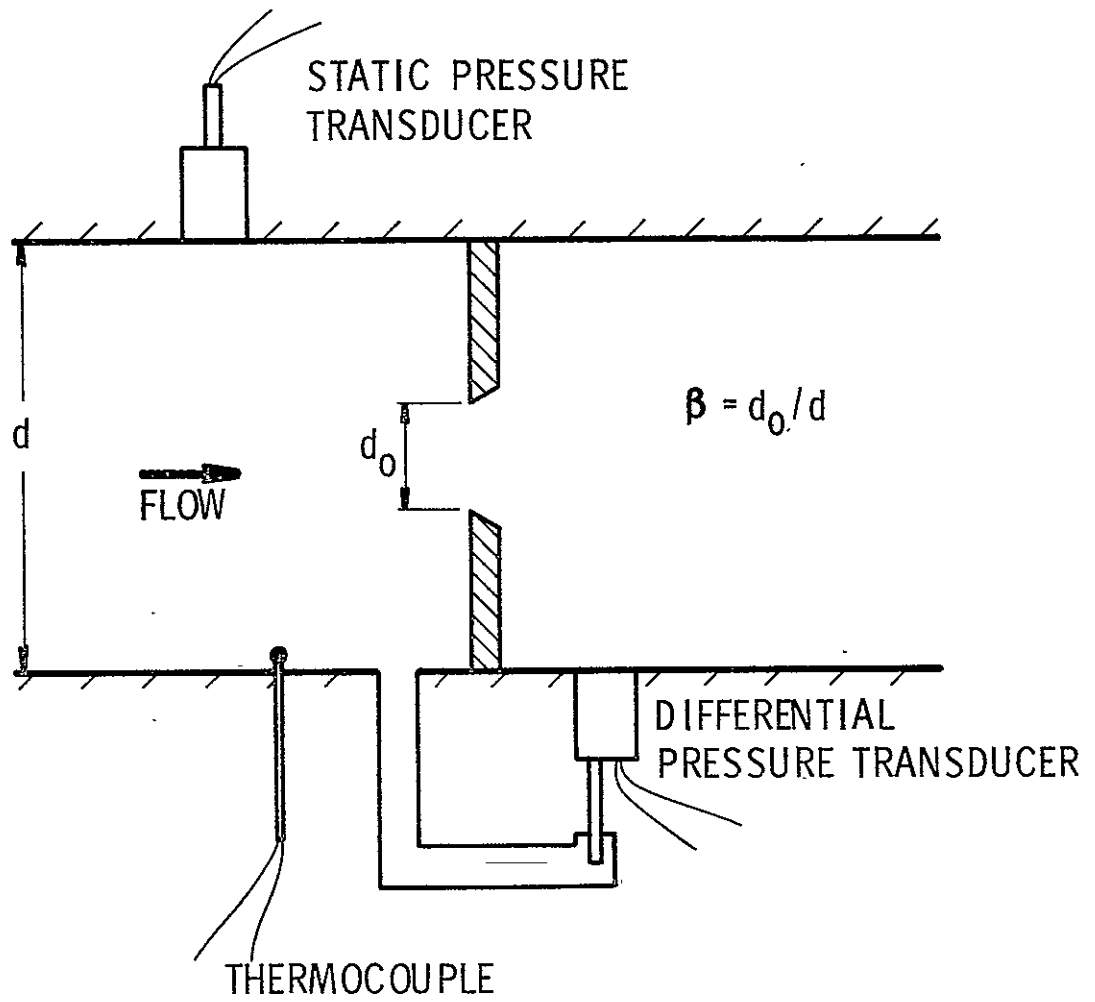
STATIC PRESSURE TRANSDUCER

$\beta = d_0/d$

d

FLOW

d_0

DIFFERENTIAL PRESSURE TRANSDUCER

THERMOCOUPLE

Figure D-4. Orifice Meter Volume Flow Sensor

The actual volume flow rate, Q_a, is related to the differential pressure by

$$Q_a = A_o C_d \sqrt{\frac{2 \Delta P}{\rho}} = A_o C_d \sqrt{\frac{2g \, RT \, (\Delta P)}{P}}$$

The magnitude of the pressure differential can be adjusted over a wide range for a given flow rate, Q_a, simply by varying the $A_o C_d$ combination of the orifice. To determine the best $A_o C_d$ combination, the pressure drop, ΔP, versus β (β = orifice to duct diameter ratio) was determined at the critical flow conditions

$$\dot{W} = 8.65 \text{ lb/hr}$$

$$P = 3.8 \text{ psia}$$

$$T = 70°F$$

and $\quad d = .75$ inches,

which matches the inlet and exit GFI line diameters.

To make these calculations, the variation of C_d with Reynolds number is shown in Figure D-5 for various values of β (d/D).

Figure D-6 shows the total GFI sensor ΔP versus β for the critical conditions. Note that minimum acceptable β which will not exceed $\Delta P = .25'' H_2O$ is equal to .71.

Assuming $\beta = .75$ is chosen for the orifice to provide some margin of safety, then the maximum and minimum GFI <u>actuation</u> pressures are

$$.093 < \Delta P_{actuation} < 1.11'' H_2O$$

A suitable pressure transducer or pressure switch can be obtained to operate in this range; however, the wide C_d variation with Re eliminates the orifice meter from further consideration. Note in Figure D-5 that for $\beta = .75$, C_d varies from .755 at Re = 13,000 to $C_d = 1.01$ @ Re = 1900. This variation in C_d would be extremely difficult to compensate; therefore, the pitot probe and venturi type GFI sensors appear more promising.
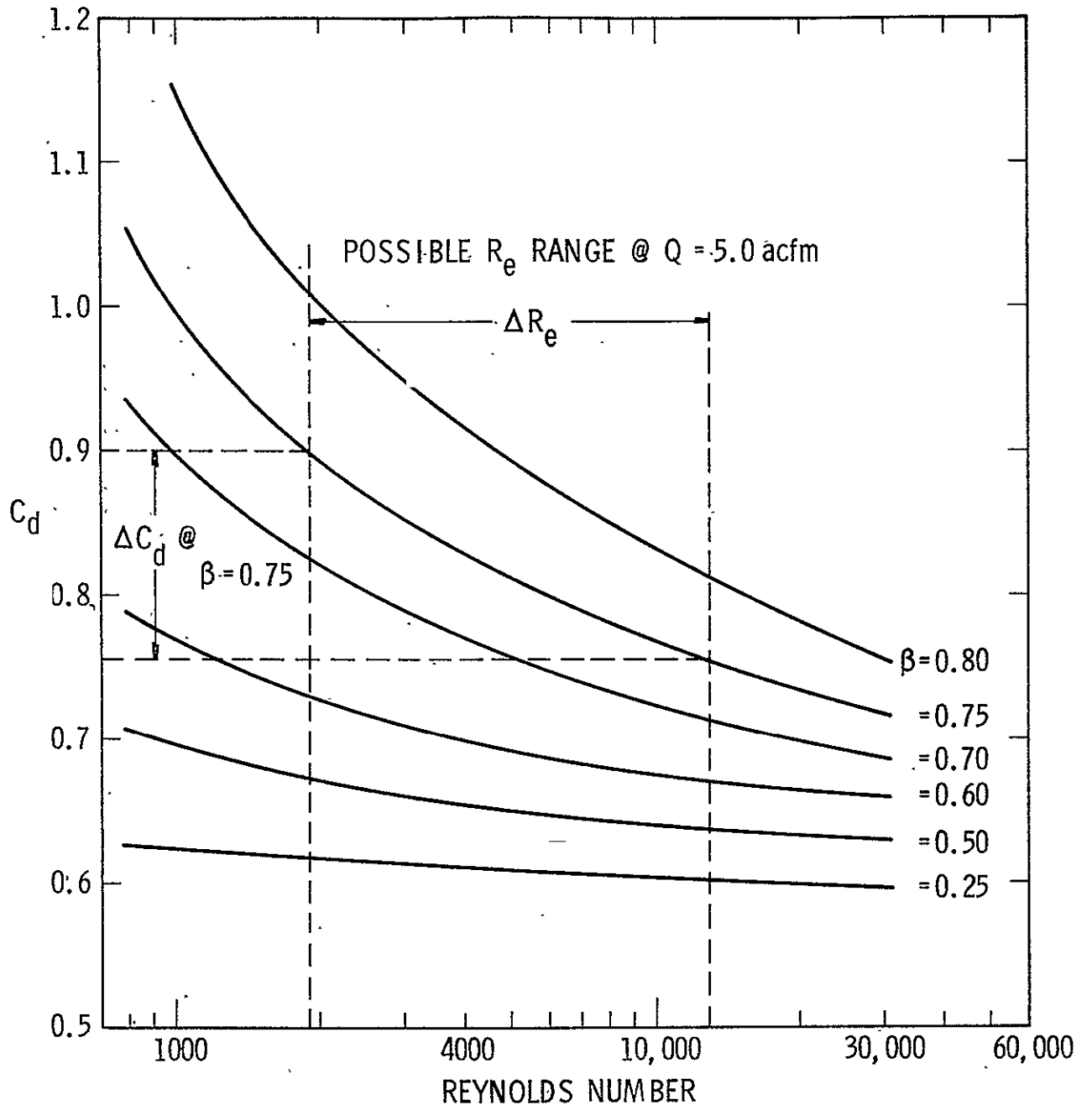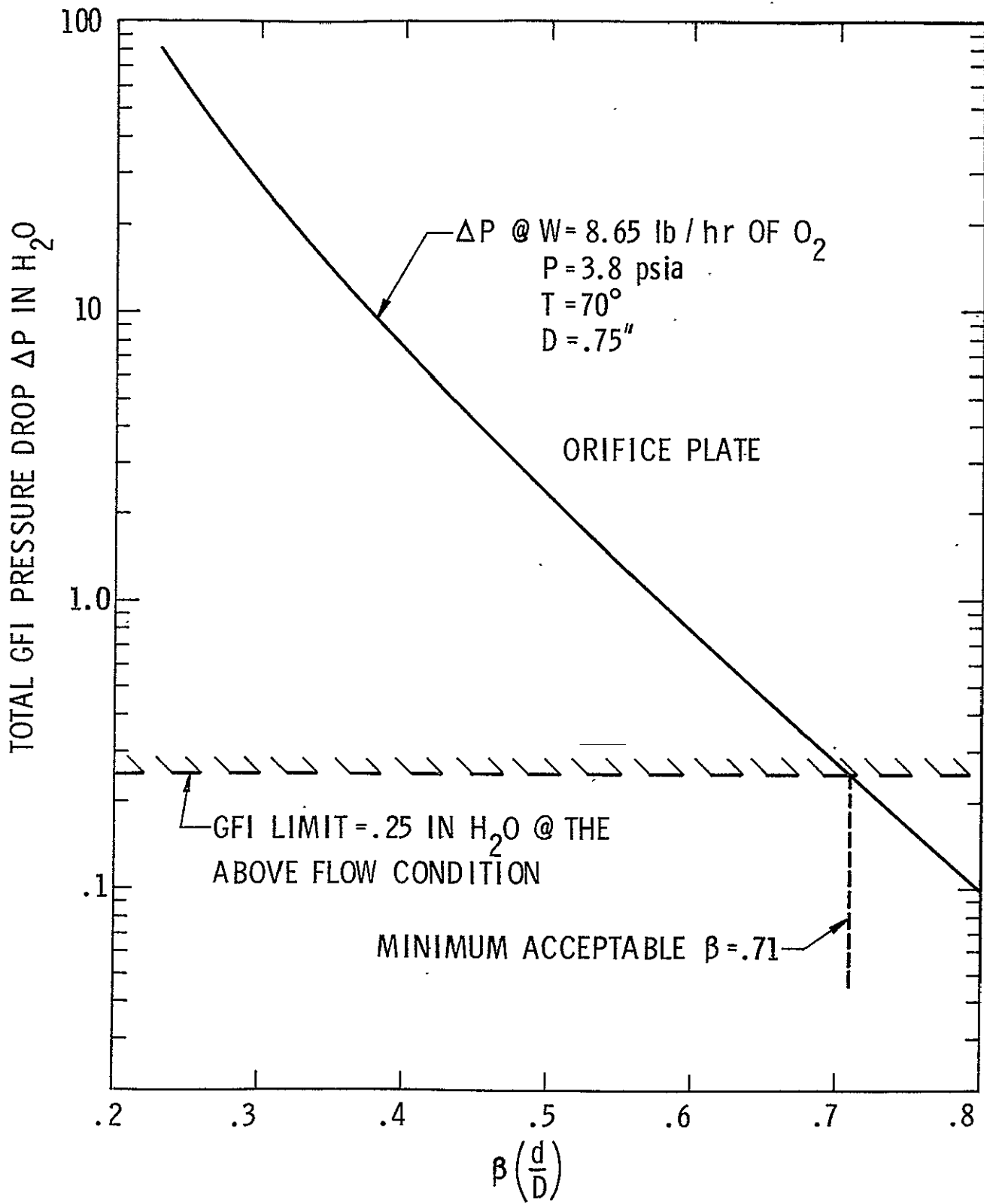
Figure D-5. Orifice C_d vs R_e

Figure D-6. Total Orifice Pressure Drop vs. β

Venturi GFI Sensor

The venturi meter concept for GFI consists of a venturi tube with a converging section, a throat, and a diverging section, (see Figure D-7). The function of the converging section is to increase the velocity of the fluid and lower its static pressure according to the Bernouilli equation. A static pressure difference between the inlet and throat is developed and this pressure differential is measured and correlated with the rate of flow. The diffuser at the end of the throat serves to convert the velocity head back to pressure head. For a properly designed venturi meter, the total pressure loss in the GFI sensor can be made equal to 10% of the measured or developed differential pressure.

Operational Characteristics

The volume flow rate in a venturi which is derived from the Bernouilli and the fluid continuity equation is

$$Q_2 = Q = A_2 \sqrt{\frac{2\,\Delta P}{\rho\,(1 - A_2/A_1)^2}}$$

where subscripts 1 and 2 refer to inlet and throat area respectively. From the equation of state, Q in terms of the gas pressure and temperature is

$$Q = \frac{A_2}{\sqrt{1 - (A_2/A_1)^2}} \sqrt{\frac{2g\,RT\,\Delta P}{P}}$$

This is an ideal relation which assumes uniform velocity distributions at the inlet and throat, and no friction. Thus, there exists a small difference between the actual and ideal flow rates which can be corrected by employing an experimentally determined coefficient, C. Dimensional analysis and experience has shown that C is a function of throat Reynolds number. Figure D-8 presents the variation of C with Re for common venturi meters. The actual volume flow rate is threfore given by

$$Q = \frac{A_2\,C}{\sqrt{1 - (A_2/A_1)^2}} \sqrt{\frac{2g\,RT\,\Delta P}{P}}$$
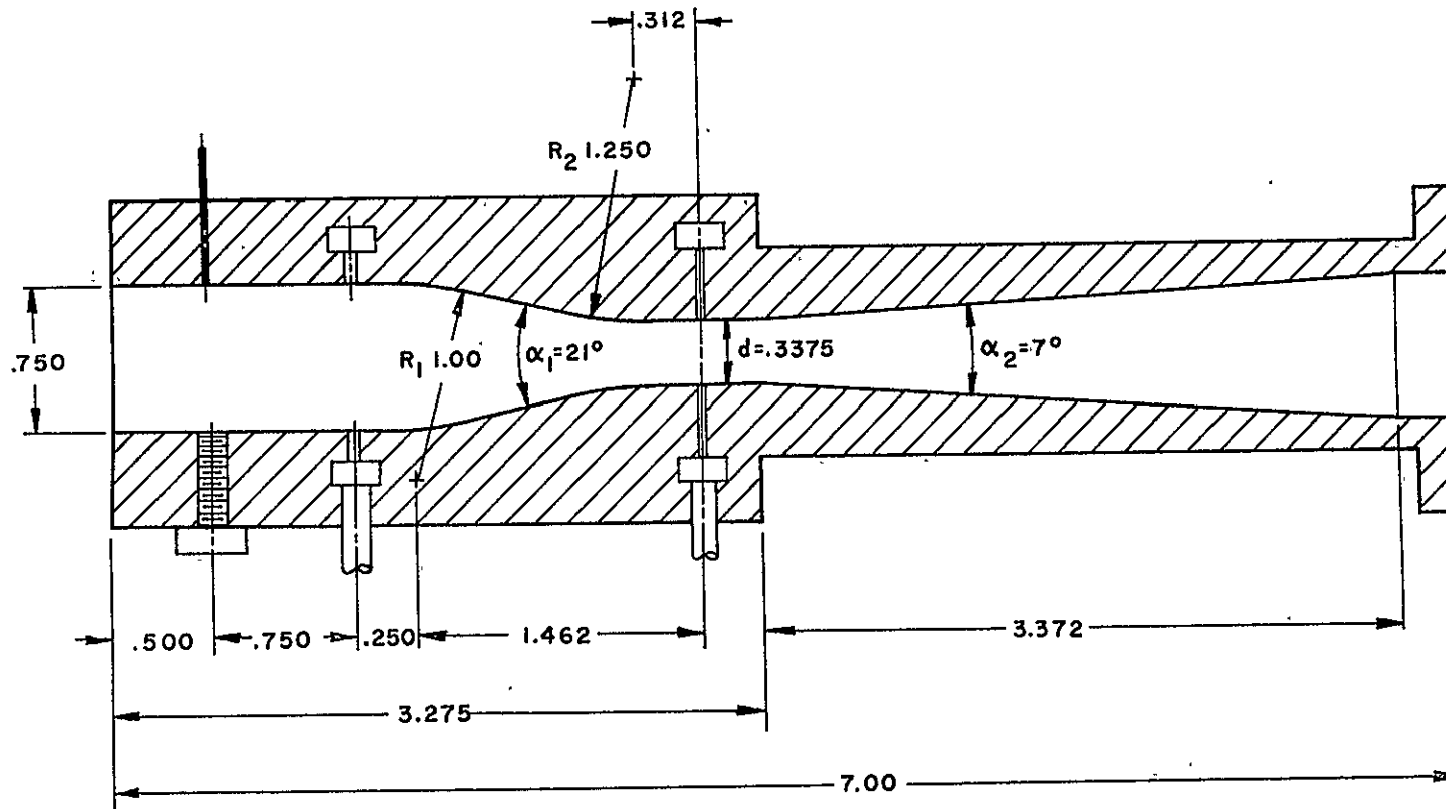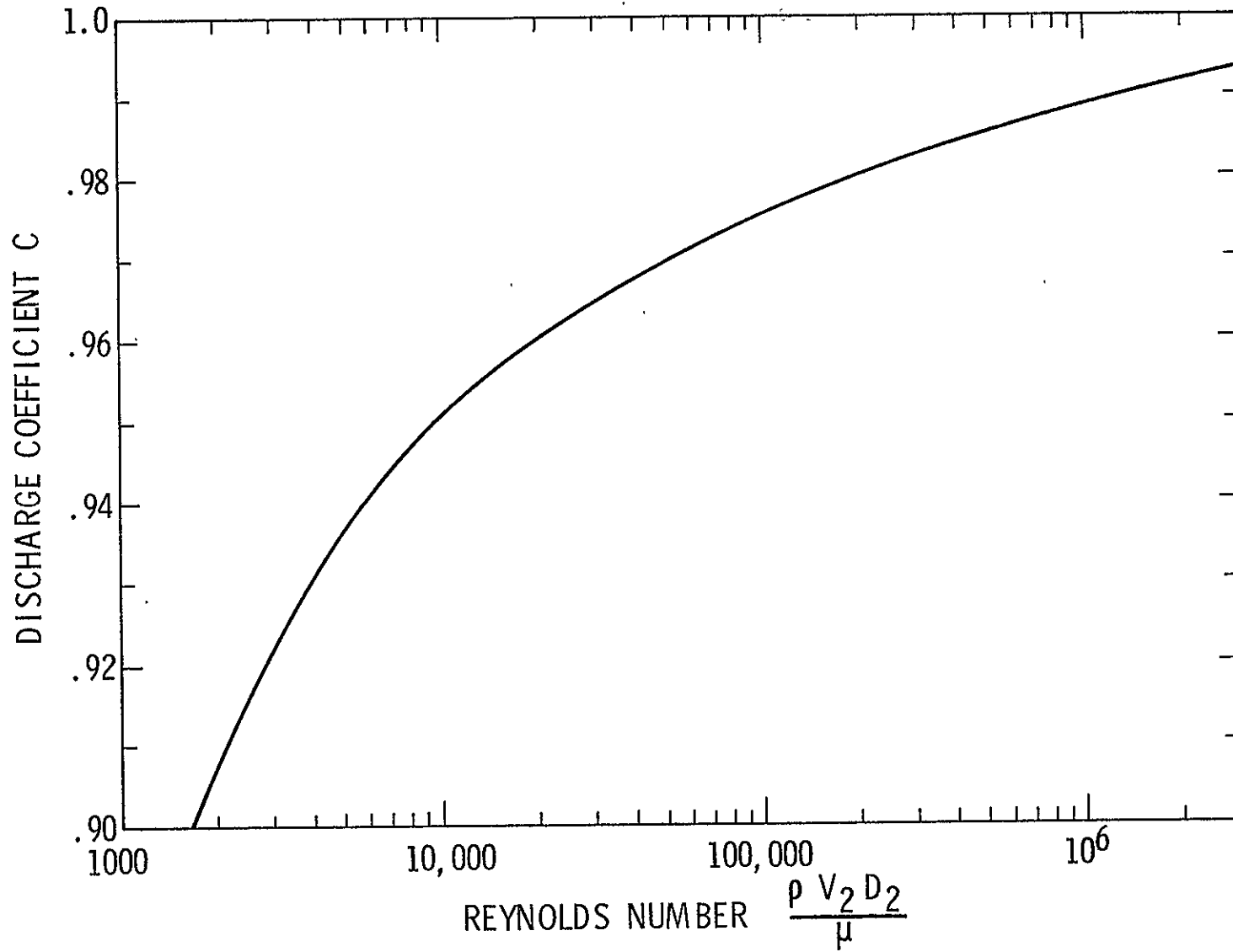
Figure D-7. Venturi Design For GFI Application

Figure D-8. Venturi Discharge Coefficient

Uncompensated Venturi

If the flow gas temperature falls in the range

$$50° < T < 80°F$$

then by setting $T = 65°$, $R = 50.8$ and $P = P \pm .030$, the actual flow rate will differ from the sensed rate by

$$\frac{Q_a}{Q_s} = \sqrt{\frac{T_a}{T_{set}} \frac{R}{R_{set}} \frac{P_a}{P_a(1 - .03)}}$$

Hence, if the temperature range is 50° to 80°F and the gas constant, R, varies from 48.3 to 53.3 (pure O_2 to air) and the pressure is known within 3% of P_{set}, then the GFI can be made to actuate when

$$\frac{Q_a}{Q_s} = 1.055$$

If, however, these parameters exceed the above limits, some form of compensation is required.

The differential pressure required for actuation can be calculated for each nominal operating pressure. A pressure switch can then be made to actuate when the ΔP falls below this critical level, corresponding to 5 acfm.

Electronic Temperature and Pressure Compensated Venturi

If $35° < T < 130°$, then compensation is definitely required to maintain $Q_a/Q_s \leq 1.06$. From the venturi flow equation

$$\Delta P = \frac{P_s Q^2}{2g\, R T A_2^2} (1 - (A_2/A_1)^2)$$

or

$$\Delta P = K_v P_s \frac{Q^2}{T}$$

where

$$K_v = \frac{1 - (A_2/A_1)^2}{2g\, R\, A_2^2}$$

For a known static pressure,

$$\Delta P = K_v' \left(\frac{Q^2}{T}\right)$$

Using a differential pressure transducer and a thermocouple to sense ΔP and T, there will exist sensitivities such that

$$\Delta P = C_1 E_1 \qquad\qquad C_1 = \frac{psi}{volt}$$

$$T = T_R + C_2 E_2 \qquad\qquad C_2 = \frac{\circ}{volt}$$

Electronically, T can be made proportional to voltage; i.e.,

$$T = C_3 E_3$$

and

$$C_1 E_1 = K_v' \left(\frac{Q^2}{C_3 E_3}\right)$$

$$E_1 E_3 = K_v' \left(\frac{Q^2}{C_1 C_3}\right)$$

Thus the product of the two outputs $E_1 E_3$ represents the voltage level at which $Q = 5$ acfm. Thus when

$$E_1 E_3 \leq K_v' \left(\frac{Q^2}{C_1 C_3}\right)$$

the alarm actuates. For both temperature and pressure compensation

$$\Delta P = \frac{P_s Q^2}{2g \, RT \, A_2^{\,2}} \left(1 - (A_2/A_1)^2 \right)$$

$$\Delta P = C_1 \text{ Volts}$$

$$T = C_2 \text{ Volts}$$

$$P_s = C_3 \text{ Volts}$$

$$K_v = \frac{1 - (A_2/A_1)^2}{2g \quad R \quad A_2^{\,2}}$$

or

$$C_1 E_1 = \frac{C_3 E_3}{C_2 E_2} K_v Q^2$$

Thus when:

$$\frac{E_1 E_2}{E_3} = \frac{C_3 K_v Q^2}{C_1 C_2} = \text{emf}_{(actuate)}$$

the alarm will actuate.

Assuming a 1% accuracy in each of the transducers and thermo-couples, the actual Q is related to the sensed Q in the compensated venturi by

$$Q_a = \frac{A_2 \, C}{\sqrt{1 - (A_2/A_1)^2}} \sqrt{\frac{2g \, RT \, (\Delta P)}{P}}$$

$$Q_s = \frac{A_2 \, C}{\sqrt{1 - (A_2/A_1)^2}} \sqrt{\frac{2g \, RT \, (1.01) \, \Delta P \, (1.01)}{P \, (.99)}}$$

$$\frac{Q_a}{Q_s} = \sqrt{\frac{1.01 \ (1.01)}{.99}} = 1.0165$$

Figure D-8 presents the variation in C, the venturi flow coefficient versus Reynolds number. The throat Re range at Q = 5.0 acfm is

$$4200 < Re < 28,000$$

and the variation in C is

$$.93 < C < .965$$

By selecting C = (.965 + .930/2) = .947, and if the variation of C with Re is included as well as the 1% sensor error, the actual flow is related to the sensed flow by

$$\frac{Q_a}{Q_s} = \frac{.965}{.947} \sqrt{\frac{1.01 \ (1.01)}{.99}} = 1.0344$$

or

$$Q_a = Q_s \pm 3.44\% \ Q_s$$

which is well within the limits required.

The electronic circuit required to multiply and divide the voltage signals and provide E = CT would be a major development area for the electronically compensated GFI.

Power Requirements of the Electronically Compensated Venturi

Since a venturi, orifice, or pitot-static type GFI sensor all require the same type instrumentation to electronically sense and compensate for changes in environmental conditions, the power requirements for each concept are approximately equal. The uncompensated venturi and the mechanically compensated venturi require no power other than that needed to sound the alarm when the switch is closed.

To electronically compensate for environmental changes, and to sense the pressure differential, the following components will be required, as a minimum:

(1)   differential pressure transducer
(2)   absolute pressure transducer
(3)   thermocouple

In addition, an electronic circuit will be required to condition the output signals; that is, the three voltage outputs must be multiplied and divided as follows

$$Q \, \alpha \, \left(\frac{E_1 \, E_1}{E_3} \right) = \text{the emf required to actuate the alarm}$$

To calculate total power requirements, the power needed will be broken into two components:

(a)   Power required to operate transducers.

(b)   Power required to condition output signals.

Ideally, the proposed pressure transducers should be both small and light, and require a small amount of power.

To sense the <u>environmental</u> pressure and thus compensate for changes in this pressure, a Kistler Model XTL-190-25 pressure transducer has been selected. This transducer is quite small and can be screwed directly into the wall of the GFI (mounted flush with the inner wall). This transducer is equipped with a reference tube which may be sealed to produce an absolute pressure transducer. This transducer requires 5 - 10 volts input and has nominal bridge resistance, R = 1000 ohms. The approximate power required to operate this transducer is ~ .025 watts. The sensitivity of this transducer is

$$\text{sensitivity} = \frac{80 \text{ mv}}{25 \text{ psi}} = 3.2 \text{ mv/psi}$$

To sense the differential pressure, the pressure transducer must operate over the range .97 to 10.3 inches H_2O for the venturi. To be conservative, the transducer should be operational over the range

$$0.5 < \Delta P < 15'' H_2O$$

Table D-I presents a summary of the commercially available differential pressure transducers applicable to the venturi-type GFI. Note that only the CCC4PL21 and the Sensotec ZDL may be used in a wet/wet application. The others require clean, dry air on the reference side of the transducer. Hence, the humidity of the internal fluid may not permit the utility of these transducers. Of the remaining two, the CCC Model 4PL21, which is a LVDT type, has the smallest volume, weight, and also the highest sensitivity.

TABLE D-I

DIFFERENTIAL PRESSURE TRANSDUCER EVALUATION

Model	Type	Power volts, d.c.	(Nom.) ma	Sens (Nom.) mv/psi	Temp Sens % FS/°F	Weight	Volume d x l	Range (P)
CCC 4PL21	LVDT	24	35	8,300	.01	14	2.0 x 4.3	$\pm$ .3 psid
*Viatran 215	S.G.	0 - 15	35	83	.02	28	4.0 x 3.25	0 - 15" H_2O
*Setra Model 236	C	16	35	10,000	.01	4	1.5 x 3.0	+ 0 - .5 psid
Sensotec ZDL	S.G.	0 - 10	29	17	.005	20	3.5 x 3.0	0 - 20" H_2O
*Statham	S.G.	10	30	80	.01	11	2.2 x 4.1	0 $\pm$ 5 psid

*Indicates reference pressure port must contain only clean, dry gas.

The total power required by the electronically compensated venturi is the sum of the power required by the two pressure transducers plus the power needed to condition the output and actuate the alarm. The power required to drive the signal conditioning circuitry is approximately .180 watt. The total power (signal conditioning plus transducer requirements) is ~ 1.0 watt.

Mechanically Compensated Venturi

A third method of implementing the venturi meter system as a GFI sensor is through complete mechanical compensation for P and T as shown in Figure D-9. This system consists basically of a pressure switch which actuates the alarm when the differential pressure corresponds to Q = 5 $\pm$ .3 acfm. To compensate for static pressure variations, an aneroid barometer diaphram is employed to off-set the switch contact points, thereby changing the differential pressure required for actuation in proportion to the static pressure level. A bi-metalic element is also employed to compensate for gas temperature changes. The counter balance can be used to decrease the acceleration sensitivity of the sensor.

Size and Pressure Drop Considerations

The basic dimensions proposed for the GFI venturi-meter are shown in Figure D-7. These dimensions were obtained by basing the sensor design on a maximum pressure drop of .25 inches H_2O at the critical flow conditions

$$W = 8.65 \text{ lb/hr } O_2$$

$$T = 70°$$

$$P = 3.7 \text{ psia}$$

The differential pressure developed at any flow condition (pressure, temperature, flow rate, gas molecular weight) is

$$\Delta P = \frac{P Q^2}{2 C^2 RT A_2^2} \left(1 - (A_2/A_1)^2 \right)$$

The constant C is a function of the throat Reynolds number and is given by
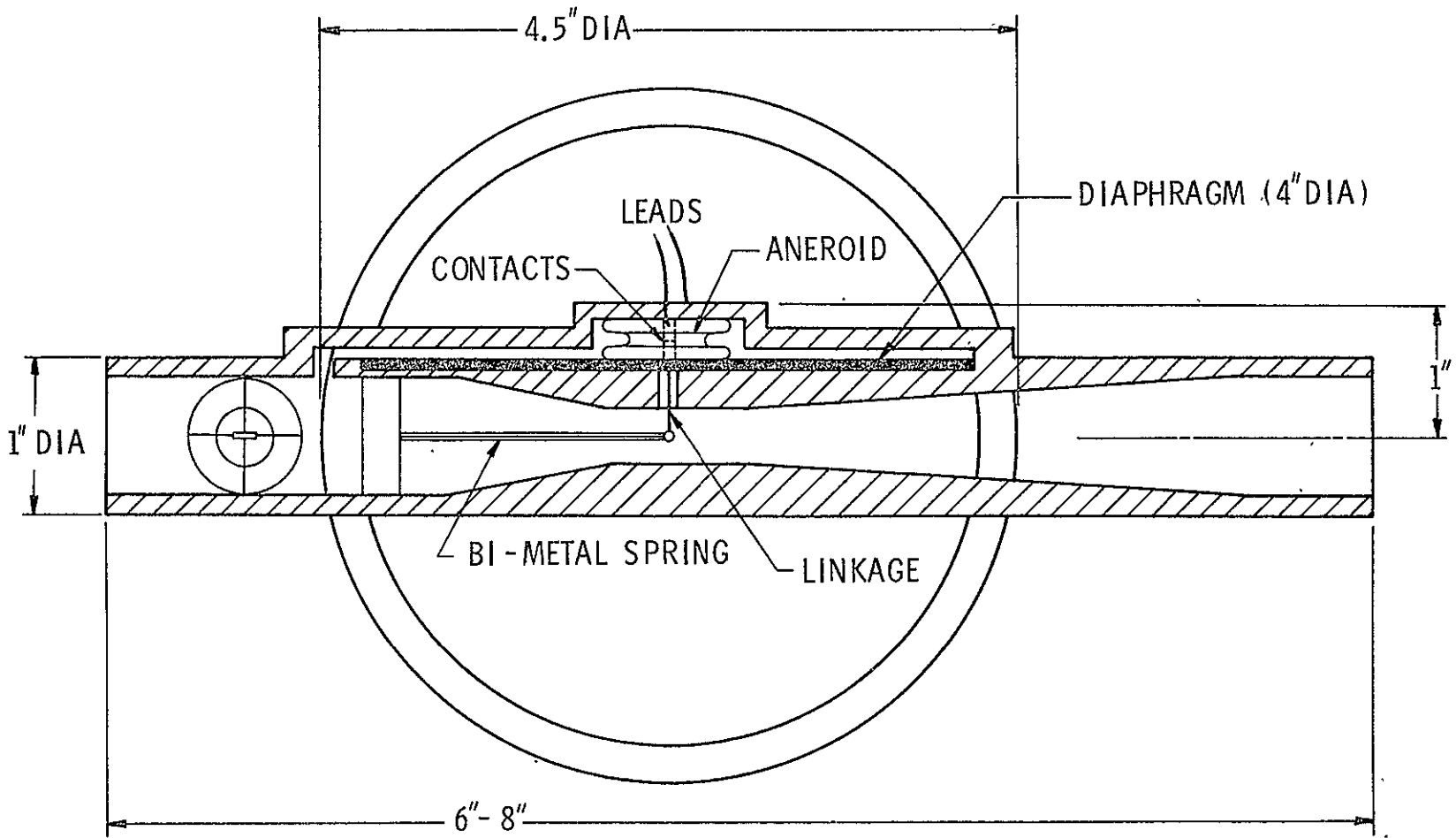
$$Re = \frac{4Q}{\pi \nu d}$$

Figure D-9. Mechanically Compensated Venturi Meter

In terms of the diameter ratio, β, the expression for Re becomes

$$Re = \frac{4Q}{\pi \nu \beta D}$$

Thus for the fixed critical flow defined above the Re is primarily a function of β. The differential pressure has been calculated at these conditions as a function of β and is presented in Figure D-10.

If the venturi expansion and contraction sections are designed to ASME standards, the maximum total GFI pressure loss will be a small percentage of the developed differential pressure ΔP_m between the inlet and throat. Figure D-11 presents the overall pressure loss as % ΔP_m versus β. By combining this data with Figure D-10, the maximum overall pressure loss vs. β at the critical conditions were calculated and also plotted in Figure D-10. Note that the minimum value for β that produces a total GFI pressure loss = 0.25" H_2O is $\beta = .442$. By selecting $\beta = .450$, the sensor is within the design specifications and yet produces a relatively large differential pressure which will be more easily sensed, requiring less sophisticated and expensive pressure instrumentation.

The developed ΔP which is to be sensed is also shown in Figure D-10 for the range of actuation conditions expected. The minimum and maximum actuation ΔP's are .982 and 10.07" H_2O, respectively.

The dimensions in Figure D-7 are adequate for the electronically compensated venturi GFI. The total length is approximately 7 inches and the inlet and exit diameters are .75 inches. The ends may be either threaded or flanged to attach to the supply line. The volume of the complete system, including the pressure transducers and electronic circuit is estimated to be 40 in^3. This could be made to fit in a box 4" x 3" x 8" or 96 in^3.

The weight is the sum of the venturi weight, transducer weights, and the electronic circuit weight. The Venturi weight is approximated by assuming it to consist of a seven inch long cylinder, with an internal diameter of .750 inches and a wall thickness equal to .125". The material will be aluminum to provide as light a GFI as possible.

$$\text{Total Weight} = W_{\text{venturi}} + W_{\text{transducers}} + W_{\text{electronics}}$$
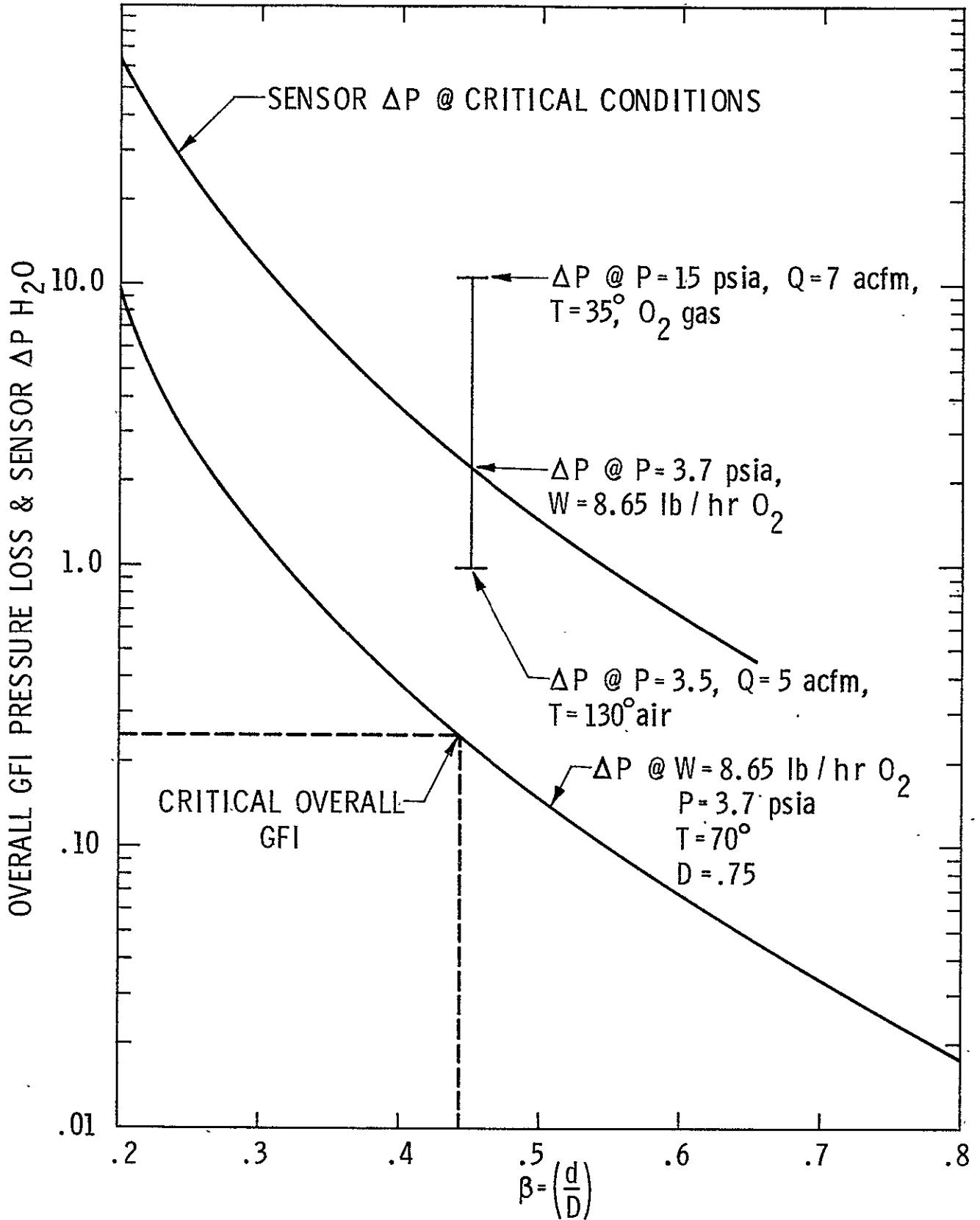
where
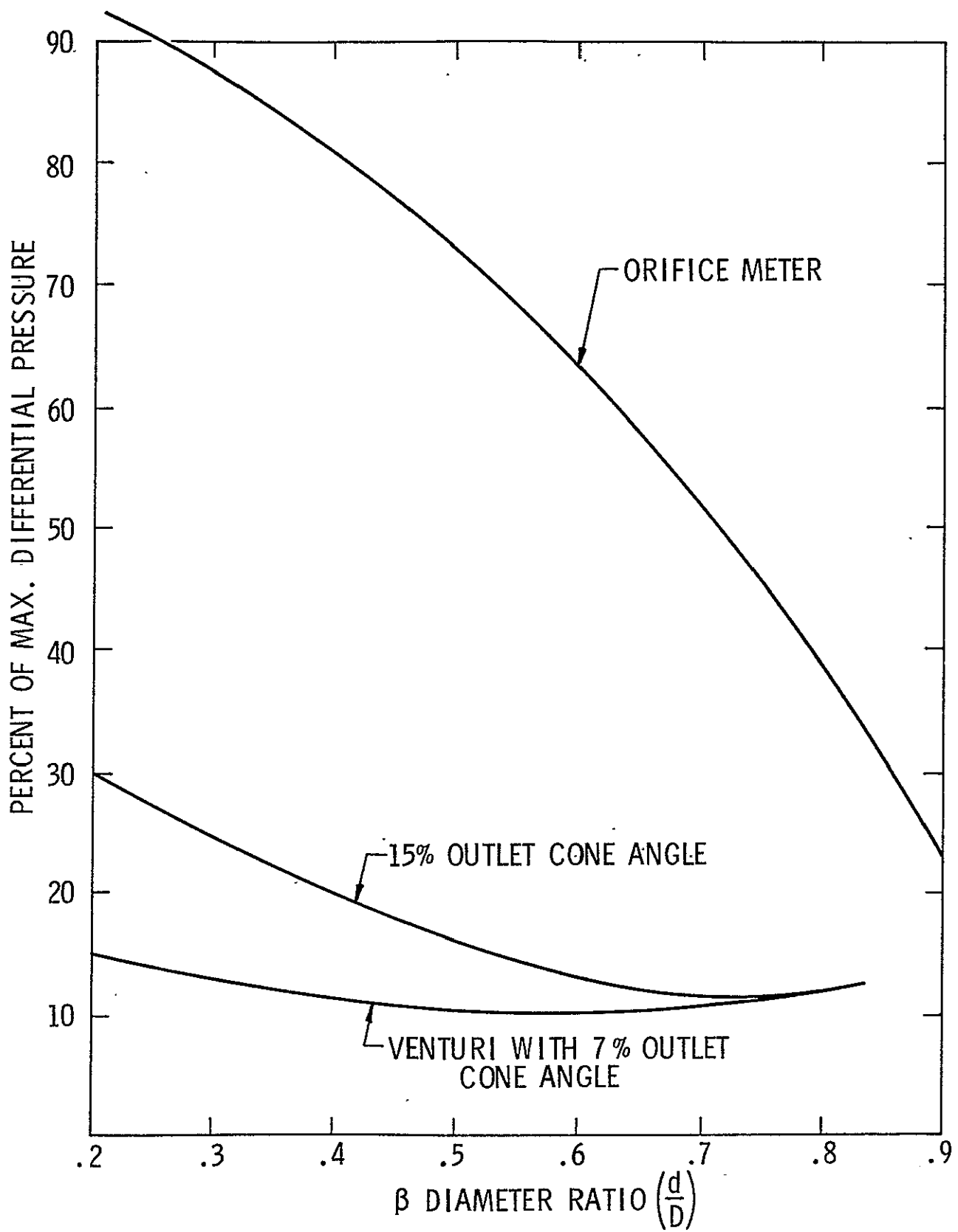
Figure D-10. Venturi Pressure Drop Characteristics

Figure D-11. Total Pressure Loss vs. Diameter Ratio

$$W_{venturi} = \frac{\rho\, L\, \pi}{4} \left(d_2{}^2 - d_1{}^2 \right) = .235 \text{ lbs}$$

$$W_{transducers} = .875 + .031 = .906 \text{ lbs}$$

$$W_{electronics} = .250 \text{ lbs}$$

and

Total Weight $= 1.391$ lbs

The total pressure drop for this type GFI was estimated at the critical or specified flow conditions outlined in the statement of work. In fact, the venturi design was based on using the total $\Delta P = .25$ inches H_2O in order to maximize the differential pressure generated by the venturi.

The weight and volume of the uncompensated and mechanically compensated GFI is less than the electronically compensated unit since the transducer and electronics weight and volume will be greater than the additional mechanical parts of the other two methods.

Improvements Over Apollo Ventilation Flow Sensor

The uncompensated venturi GFI would be quite similar to the Apollo Ventilation Flow Sensor, except that the alarm actuation would be accomplished directly by the mechanical movement of the pressure switch diaphram. Therefore, the sensitivity to moisture of the current capacitance transducer would be eliminated.

Both the electronically and mechanically compensated models offer a vast improvement in the GFI performance. The compensation techniques can eliminate all effects of temperature and pressure variations. In addition, the problems created in the Apollo sensor by humidity would be reduced in both compensation schemes. The differential pressure transducer selected for use in the GFI will be unaffected by damp air since all the electronic components are isolated from the moisture. The mechanical version will be fabricated from materials which are resistant to corrosion. The fully compensated model GFI venturi can be operated at any temperature and pressure while correctly sensing the flow rate within the specified limits of $5 \pm .3$ acfm.

Differential Pressure Concept Final Evaluations

The three differential pressure GFI concepts have been evaluated on the basis of thirteen different characteristics and the results are

tabulated on the GFI evaluation chart in Chapter II. For the venturi meter GFI concept, actual implementation of the sensor can be provided by three separate means. If the operating static pressure is known in advance to within $\pm 3\%$, and if the gas temperature is always $50° < T < 80°F$, then the sensor can be quite simple, requiring only a pressure switch which can be present to actuate the alarm by closing when the sensed differential pressure falls below a level corresponding to $Q = 5 \pm$ acfm. This method is referred to as the uncompensated version and is probably the most inexpensive and maintenance free of all concepts. However, due to the imposed temperature range and pressure limits, this concept will have different operational characteristics outside the design limits.

A second type venturi meter for GFI is an electronically compensated version where the differential pressure required to actuate the alarm is compensated by sensing the static pressure and gas temperature. This concept rates high in operational characteristics, as well as mechanical complexity; however, the electronic complexity rates low as well as the power requirements. Due to the small differential pressures which must be sensed, the differential pressure transducer required must have a relatively large diaphram and hence higher weight and volume.

A third method of implementing the venturi meter system as a GFI sensor is through complete mechanical compensation. This scheme appears to be the best overall of the three venturi methods. The electronic complexity and power requirements are nil, and the operational characteristics should be quite high. Since this system requires considerable detailed design work, the development lead and risk are somewhat higher than the uncompensated technique.

The orifice meter and pitot-static concepts for GFI application have also been rated and in general, the operational characteristics and reliability of these techniques are somewhat less than the venturi system. These elements may also be electronically or mechanically compensated similar to the venturi meter concept.

APPENDIX E

TURBINE METER EVALUATION

E. 1   Introduction

A turbine meter built by Quantum Dynamics was constructed for NASA under a previous contract, to monitor astronauts' respiratory oxygen flow. Since this meter had the potential of being modified to meet the GFI specifications, NASA furnished SwRI with a QD turbine meter to evaluate.

E. 2   Electronic Circuit Evaluation

The QD turbine meter electronic circuitry was evaluated with respect to the GFI specifications. Only a small portion (one of the detector circuits) of the electronic circuitry used with the respiratory QD turbine meter is required for the GFI application. The power consumption of this detector circuit was measured at 0.8 watts. Additional power will be required to convert from the backpack supply voltage to the required ± 10 volts for the detector circuitry and to power the GFI alarm triggering circuit. In view of this it was concluded that the total power requirements for the turbine meter GFI would exceed the required 1 watt. The electronics package could be made relatively small, however, such that volume would be minimal.

E. 3   Turbine Meter Flow Tests

The Quantum Dynamics turbine meter was flow-tested with air over a pressure range from 3 to 15 psia to obtain frequency versus flow rate characteristics as a function of flow static pressure. The recorded data were compared to previously published Quantum Dynamics flow calibrations. Figure F-1 shows SwRI data superimposed on a QD calibration plot for $P \cong 15$ psia. Excellent agreement is observed between the SwRI calibration and the calibration reported by QD. Figure F-2 compares SwRI to the QD calibration at 5 psia. At the higher flow rates, a slight increase in output frequency is observed for the SwRI calibration. This could possibly result from data obtained with different meters or a calibration shift with meter usage. Figure F-3 shows the calibration shift with pressure for tests over the required pressure range ($3 \leq P \leq 15$ psia). The results show that the maximum deviation in output frequency at the alarm flow rate (5 acfm) for a pressure change from 3 to 15 psia remains within acceptable alarm triggering accuracy. For example, if the set point is chosen at 725 Hz, which corresponds to 5 acfm at 3 psia, then at atmospheric pressure the meter would trigger at 5.3 acfm. On the other hand, if some mid-pressure range set point was chosen, for example 705 Hz, then the alarm would trigger at 4.9 and 5.2 acfm at pressure levels of 3 and 15 psia, respectively. This indicated that the meter output characteristics were sufficient to provide appropriate alarm triggering over the required

I ATM. GAS FLOW CALIBRATION

SwRI

Volumetric Flow, actual ft³/min.

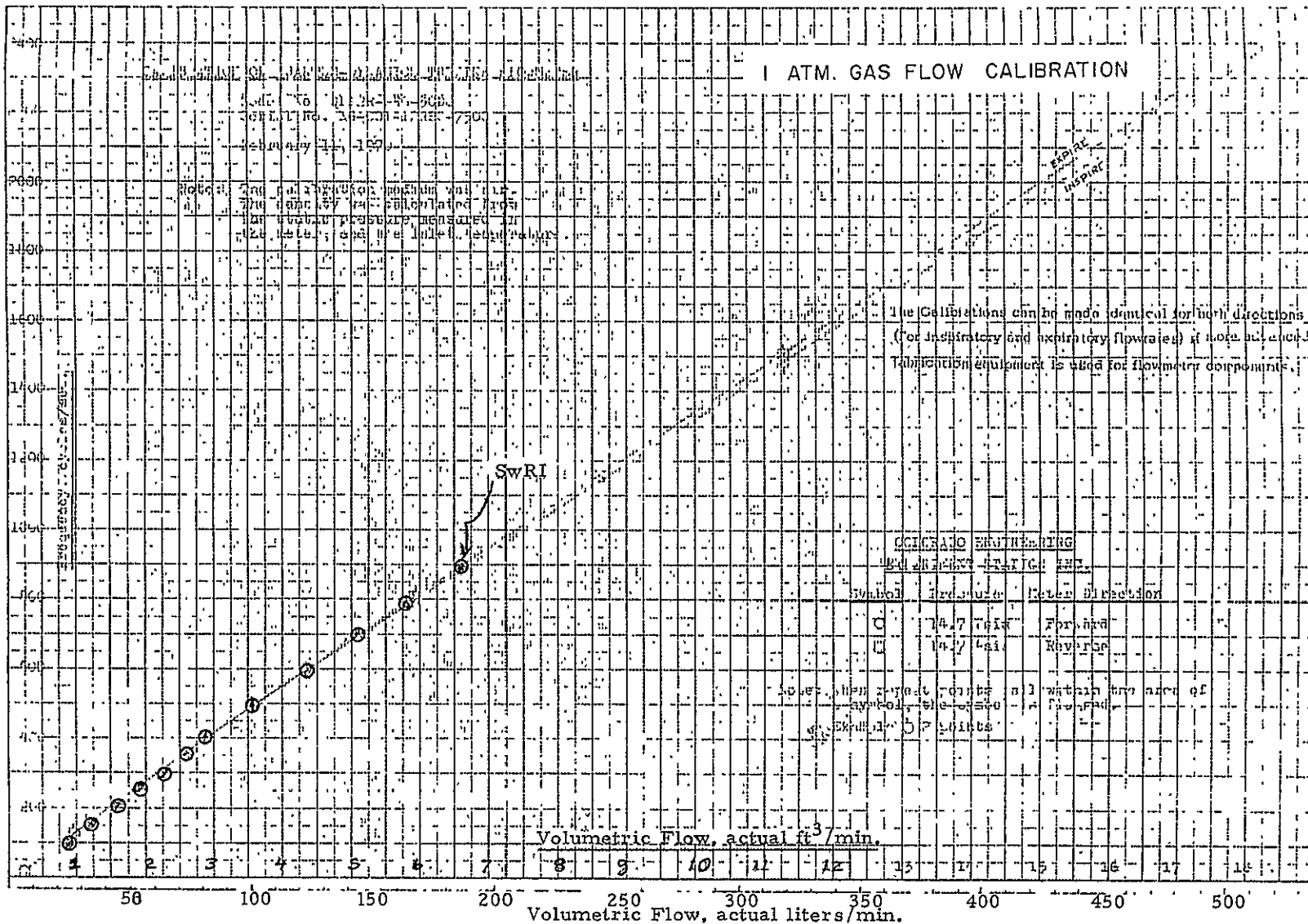Volumetric Flow, actual liters/min.
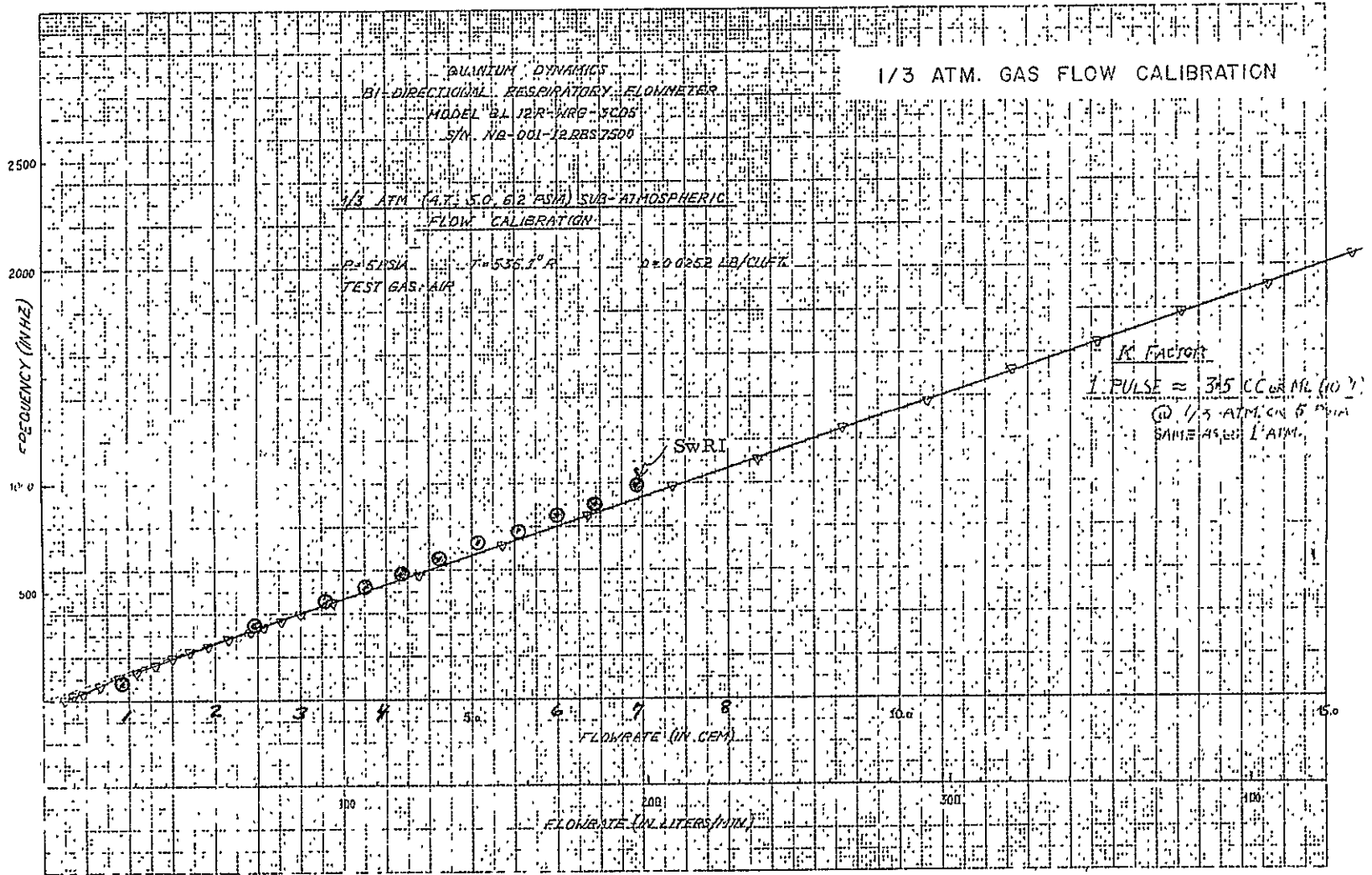
Figure E-1. 1 Atm. Gas Flow Calibration

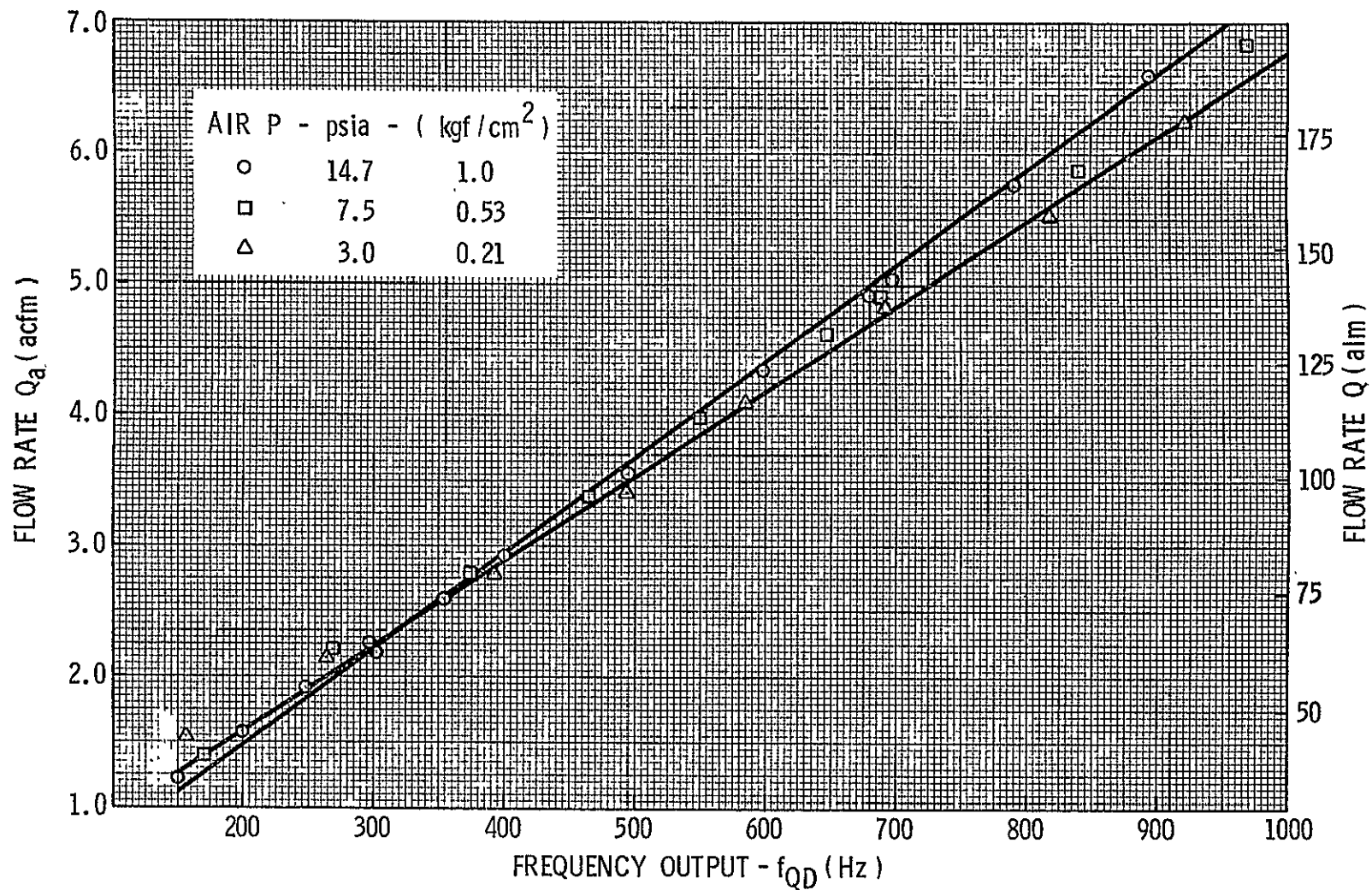Figure E-2. 1/3 Atm. Gas Flow Calibration

Figure E-3. Turbine Meter Calibration for $3 \leq P \leq 15$ psia (0.27 to 1.0 kgf/cm^2) - Air

static pressure range. In addition, the repeatability of the output charac-teristics at a given pressure, based on the limited test data, was also good. Tests were not conducted to determine if the meter's calibration or repeatability was affected by moisture. The turbine meter pressure drop at $P = 3.8$ psia, $Q = 6.3$ acfm is 0.12" H_2O, compared to the specified maximum loss of 0.30" H_2O.

During the initial QD flow meter calibration tests, a small piece of rubber (about the size of the tip of a pencil point) flaked off the inside wall of the upstream hose leading to the meter. This piece became wedged between the turbine meter wheel and the wall rendering the meter inoperative. Although a filter in the PLSS flow loop would have removed particulate matter this size, this occurrence indicates that a small piece of material inadvertently finding its way into the meter could cause the meter to fail. It is unlikely that a piece of matter this size would have affected the venturi GFI design.

APPENDIX F

G FI TEST FACILITY

F.1   GFI Test Facility

Figure F-1 shows a schematic of the GFI test facility. The primary components of this facility are (1) an oxygen supply source, (2) a calibrated flow meter, (3) a humidifier, (4) a large vacuum storage tank, and (5) a vacuum pump. The flow meter, a Dwyer RMC-104, is calibrated for both air and oxygen at atmospheric pressure. The flow meter is located at the entrance to the test loop piping where the flow static pressure is atmospheric. The humidifier is a water-filled reservoir where gas enters from the bottom, is bubbled up through the water and out at the top, just upstream of the GFI. This provides 100% humidity gas for moisture testing. The large vacuum storage tank located just downstream from the GFI is utilized to damp flow pulsations from the vacuum pump to ensure steady flow conditions.

For a given test condition, either air or oxygen flow is established by proper setting of Valves 1 and 5. The required GFI flow rate and static pressure levels are obtained by adjusting Valves 2 and 3 which are located just upstream and downstream of the GFI, respectively. The actual volume flow rate at the GFI is determined from the flow meter reading as follows:

$$(\rho Q)_{meter} = (\rho Q)_{GFI}$$

Solving for $\dot{Q}_{GFI}$ yields

$$Q_{GFI} = Q_{meter} \frac{\rho_{meter}}{\rho_{GFI}}$$

or

$$Q_{GFI} = Q_{meter} \frac{P_{meter} T_{GFI}}{P_{GFI} T_{meter}}$$

Since the temperature at the flow meter and the GFI are equal and the meter is at atmospheric pressure (P_{atm}) the actual GFI flow rate is

$$Q_{GFI} = Q_{meter} \frac{P_{atm}}{P_{GFI}}$$

When oxygen is utilized in the testing, Valve 4 is opened to allow room air to be drawn in through the vacuum pump to insure a safe operation.

F.2   GFI Test Configuration

Figure F-2 shows the instrumentation and test configuration utilized for testing both the breadboard and prototype GFI's. Two differential pressure gauges are utilized to establish GFI pressure loss (P_1-P_3) and GFI
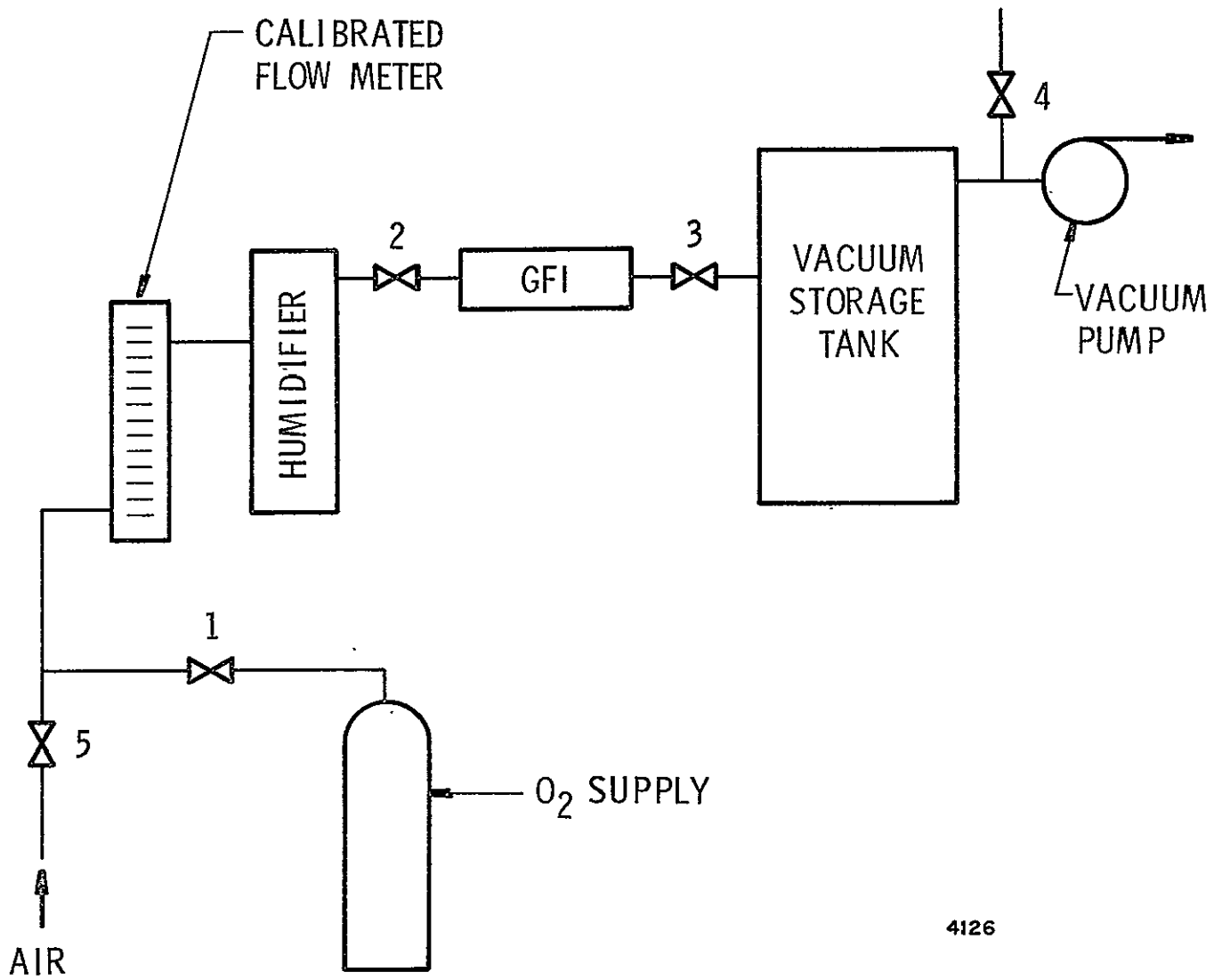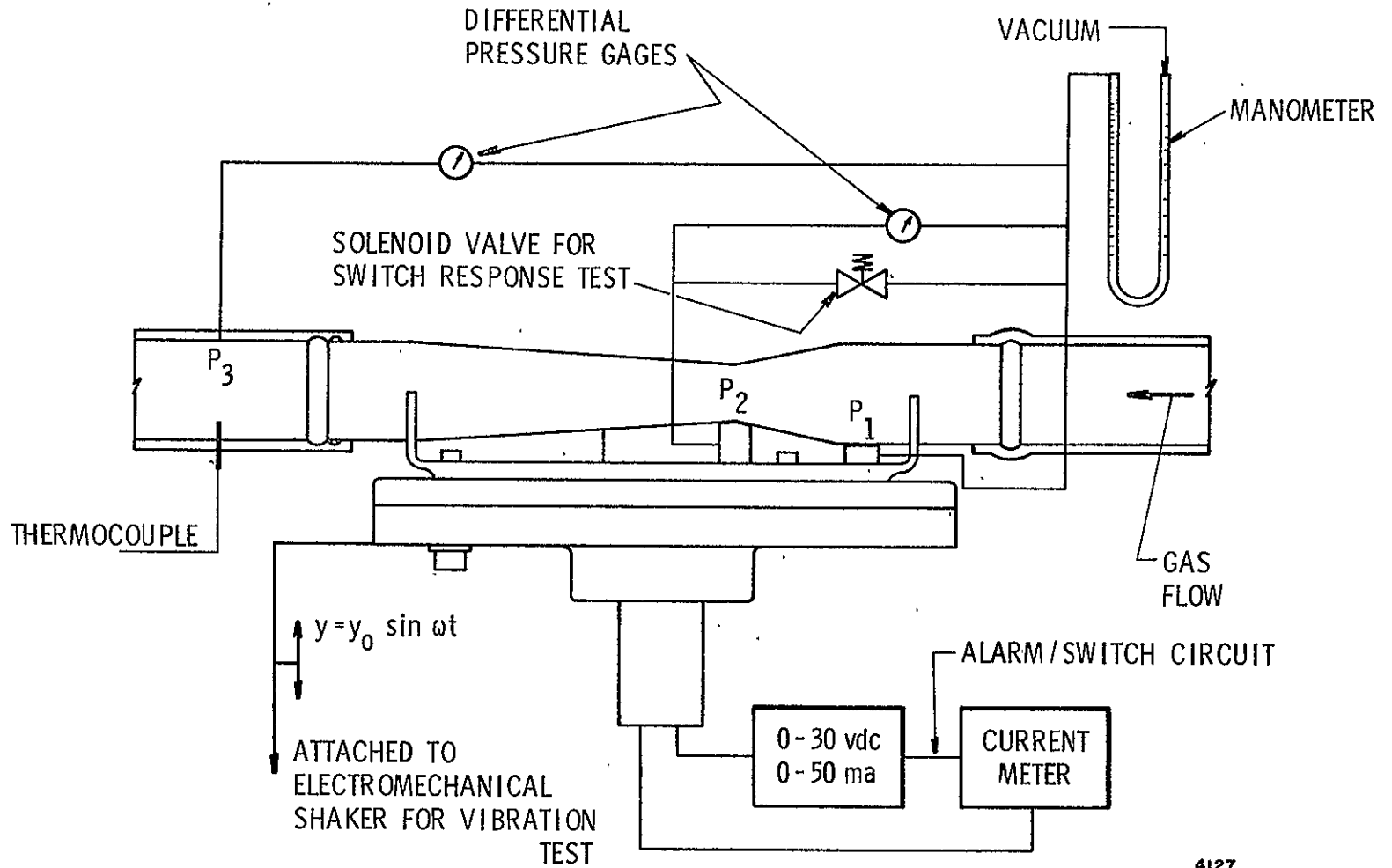
Figure F-1. GFI Test Loop Schematic

4126

Figure F-2. GFI Test Configuration

pressure drop (P_1-P_2). In addition, a mercury manometer, with one leg at $P=0$, is attached to venturi Port 1 to record absolute flow static pressure, P_1. A thermocouple is located just downstream of the venturi exit to record flow temperature, T.

The GFI switch circuit consists of a zero to 30 volt DC power supply and current meter. The switch triggering point is established by observing the flow condition where current flow is initiated on the current meter. The majority of the testing is conducted at the specified GFI current and voltage · of 25 milliamps and 16.8 volts DC, respectively. Other combinations of current and voltage within the ranges shown on Figure F-2 are also possible for other testing.

A solenoid valve is located between Pressure Ports 1 and 2. This valve is utilized to establish switch response to step changes in flow rate. It is also utilized for life cycling testing of the switch-diaphragm assembly. Triggering of the solenoid valve causes the pressure between Ports 1 and 2 to be suddenly equalized. This is representative of a sudden drop from finite to zero flow. By recording the time from the triggering of the solenoid valve to current flow in the alarm switch circuit, the switch-diaphragm response is established. By alternately opening and closing the solenoid valve for the required number of cycles, the GFI switch cycling tests are performed.

An electromechanical shaker can also be attached to the GFI to establish meter performance at various vibration levels. The shaker is attached to the compensator housing with the meter in the test loop with gas flowing. Thus, vibration tests are accomplished under gas flow conditions.